

2020-01-01

Impact Of Interface Condition On Performance Of Thin Asphalt Overlays

Cheng Zhu
University of Texas at El Paso

Follow this and additional works at: https://scholarworks.utep.edu/open_etd



Part of the [Civil Engineering Commons](#)

Recommended Citation

Zhu, Cheng, "Impact Of Interface Condition On Performance Of Thin Asphalt Overlays" (2020). *Open Access Theses & Dissertations*. 3065.
https://scholarworks.utep.edu/open_etd/3065

This is brought to you for free and open access by ScholarWorks@UTEP. It has been accepted for inclusion in Open Access Theses & Dissertations by an authorized administrator of ScholarWorks@UTEP. For more information, please contact lweber@utep.edu.

IMPACT OF INTERFACE CONDITION ON PERFORMANCE OF THIN
ASPHALT OVERLAYS

CHENG ZHU

Doctoral Program in Civil Engineering

APPROVED:

Carlos Ferregut, Ph.D., Chair

Cesar Carrasco, Ph.D.

Cesar Tirado, Ph.D.

Heidi Taboada Jimenez, Ph.D.

Stephen Crites, Ph.D.
Dean of the Graduate School

Copyright ©

by

Cheng Zhu

2020

Dedication

To the Lord,
To my parents, sisters,
To my wife-Xianxian Li.
For their constant support and love.

IMPACT OF INTERFACE CONDITION ON PERFORMANCE OF THIN
ASPHALT OVERLAYS

by

CHENG ZHU, MS

DISSERTATION

Presented to the Faculty of the Graduate School of
The University of Texas at El Paso
in Partial Fulfillment
of the Requirements
for the Degree of

DOCTOR OF PHILOSOPHY

Department of Civil Engineering
THE UNIVERSITY OF TEXAS AT EL PASO

May 2020

Acknowledgements

First of all, I would like to express my sincere thanks to my advisor, Professor Carlos Ferregut and Professor Vivek Tandon, for supporting me to finish this graduate study.

My sincere thanks also goes to my committee members: Professor Nazarian, Professor Carrasco, Dr. Tirado, and Dr. Taboada for their encouragement and input on this study.

It is acknowledged that the former research assistants (Aliasghar Dormohammadi and Sadeer Mustafa) conducted some of the modified direct shear tests. Thanks for allowing me to use the data in this study.

I would like to thank you my colleagues and friends at The University of Texas at El Paso. The names of my colleagues are not limited to Dr. Sundeep Inti, Dr. Megha Sharma, Aliasghar Dormohammadi, Jorge Navarrete, Anjuman Ara Akhter, Angel A. Rodarte, Sofia Martin, and Maria I. Morales. I appreciate their help and sharing of the knowledge during my study. Friends are always important to our life. I am grateful that Honglun Xu, Yuxin Wen, Jinliang Wang, Fathi Aria, Mohammad Rashidi, Matt Vehione, and Okan Gurbuz could be my friends and their friendship are the meaningful gift from the God.

I also would like to express my thank you to the Center for Transportation Infrastructure System (CTIS) and the High Performance Computer (HPC) administration center for allowing me to access the laboratory equipment and ABAQUS software to finish this study. Special thanks should due to Dr. Imad Abdallah and Jose Garibay for their assistance in laboratory for CEE 3336 class and research, and Marc T. Hertlein from HPC center for his tremendous help on the ABAQUS modeling. Professor Jack Chessa also gave me some constructive advice on the ABAQUS modeling, thanks to him.

Last but not least, I want to thank you to my parents, parents' in-law, wife and kids for their unconditional support and love. I love you so much!

Abstract

Asphalt overlay has been widely used in the United States as a cost-effective maintenance approach to keep the pavement in a satisfactory condition. In recent years, many studies have been conducted to investigate the overlay asphalt mix design, overlay pavement design, and quality control/quality assurance for the asphalt overlay pavement. In Texas, thin overlays (lift thickness less than 2 in.) and ultra-thin overlays (lift thickness of 0.5 in. to 0.75 in.) seem to be more beneficial than conventional asphalt overlays. For this type of overlay, the bonding condition between the overlay and existing AC layer is crucial for the pavement to exhibit a long-lasting performance. However, the importance of tack coat to the performance of thin overlays is still not emphasized. Each state highway agency has its own selection procedure for determining which tack coat material is appropriate for a specific area. The related standard and specifications for quality control of tack coat is still under development. Therefore, there is a need to understand fully the performance of different tack coat materials.

This study was trying to make an effort to answer some of these questions. There are three parts in this research including the laboratory study with tack coat materials, the numerical modeling of overlay pavement in consideration of bonding condition, and LTPP case study on evaluation of performance of asphalt overlay pavement in Texas.

The results of laboratory study indicated that the modified direct shear test could be applied to differentiate the quality of different tack coat materials. The new product of tack coat, such as Trackless and Ultrafuse, exhibit greater shear strength than conventional tack coat. The Christensen-Anderson-Marasteanu (CAM) model is also suitable to characterize the dynamic modulus of tack coat material. The Multiple Stress Creep Recovery (MSCR) test results indicated that all the investigated tack coat materials have low rutting susceptibility. The low temperature property of tack coat material should be addressed in the standard to achieve a material with a balanced performance.

ABAQUS was used to simulate the asphalt overlay pavement's response under static traffic load. The results indicated that a good bonding condition between the asphalt overlay layer and existing AC layer is crucial to asphalt overlay pavement's integrated performance.

The LTPP case study results indicated that the calculated life gain of these experimental sections was not consistent with the life gain based on the Pavement Condition Rating (PCR) curves. There is a rough trend that the service life of the overlay pavement has a reverse relationship with the annual traffic volume. The field performance of overlays is affected by many factors, such as the climate, the over-loading vehicles, and the accuracy of pavement condition survey. These factors were not investigated at the time of writing this report.

This study proved that a good quality of asphalt overlay pavement's interface is important to the pavement for retaining a long-term satisfactory performance. More in-depth research is needed in the future.

Table of Contents

Acknowledgements	v
Abstract	vi
Table of Contents	viii
List of Tables	x
List of Figures	xi
Chapter 1: Introduction	1
1.1 Problem Statement	1
1.2 Structure of Report	6
Chapter 2: Literature Review	8
2.1 Tack Coat	8
2.2 Abaqus Modeling of Asphalt Overlay Pavement	10
2.3 LTPP Program	14
Chapter 3: Study Plan	19
3.1 Laboratory Tests with Tack Coat Materials	19
3.1.1 Material	19
3.1.2 Laboratory Tests	20
3.2 ABAQUS Modeling with Asphalt Overlay Pavement	24
3.3 Analysis Method with LTPP Database	28
Chapter 4: Laboratory Study of Tack Coat	33
4.1 Modified Direct Shear Test Results	33
4.2 DSR Tests	41
4.3 Elastic Recovery Tests	44
5.1 ABAQUS Output	46
5.2 Data Analysis	51
5.2.1 Pavement Layer Thickness	51
5.2.2 Pavement Layer Elastic Modulus	58
5.2.3 Bonding Condition on Interface Response	61

Chapter 6: Case Study: Taxes Thin Asphalt Overlay from LTPP	65
6.1 LTPP Overlay Case Study	65
6.2 ABAQUS Modeling of Sections 1087 and 6079	70
Chapter 7: Conclusion and Recommendation.....	72
7.1 Conclusion	72
7.2 Recommendation	73
References	74
Appendix.....	80
Appendix A-ABAQUS Modeling Results.....	81
Appendix B-Plots of ltp case study results.	86
Vita.....	112

List of Tables

Table 2.1: Several Types of Tack Coat Material	8
Table 2.3: List of SPS Experiments [57]	16
Table 3.1: Laboratory Tests with Tack Coat Materials	22
Table 3.2: The Pavement Structure Combination for ABAQUS Modeling	26
Table 3.3a: The Input Parameters for LTPP Case 1 and 2 ABAQUS Modeling.....	26
Table 3.3b: The Input Parameters for LTPP Sections ABAQUS Modeling	26
Table 3.5: Distress Summary [68]	29
Table 4.1: Test Results for Different Application Rates and 1.5 psi of Compaction Pressure (without clamping).....	34
Table 4.2: Test Results with 0.03 gal/yd ² Application Rate and Different Compaction Pressures.	34
Table 4.3: Elastic Recovery Test Results	44
Table 6.1: LTPP Asphalt Overlay Construction, Location, and Traffic Volume Information of Texas Experimental Sections.....	66
Table 6.2 Structural Information and Pavement Performance of LTPP Sections	69
Table 6.3: ABAQUS Modeling of LTPP Sections 1087 and 6079 and PCR Results	71

List of Figures

Figure 1.1: Typical Asphalt Pavement Structure [1]	1
Figure 1.2: Surface Layer Slippage Due to Debonding [3]	2
Figure 1.3: The Stress State of Pavement Interface under Wheel Loading [4]	2
Figure 1.4: ABAQUS/CAE Screen-User Interface [8]	4
Figure 1.5: Influence of Interface on the Shear Stress Distribution [12]	5
Figure 2.1: Modules in ABAQUS software [26]	10
Figure 3.1: Scheme of Laboratory Testing with Different Tack Coat Materials	19
Figure 3.2 Curing Conditions for Direct Shear Test Specimens	20
Figure 3.3: Example of Direct Shear Test Result	21
Figure 3.4: The Simplified Shear Strength Model for Tack Coat-Ultrafuse	21
Figure 3.5: Example of the Results of Direct Shear Test with PG70-22	22
Figure 3.6: Example of Dynamic Modulus of PG70-22 at Reference Temperature of 25°C	23
Figure 3.7: Example of Correlation between Shear Viscosity and $J_{nr3.2}$	23
Figure 3.8: Example of Correlation between Low Shear Viscosity and Elastic Recovery.	24
Figure 3.9: ABAQUS Modeling with Asphalt Thin-overlay Pavement	25
Figure 3.10: Traffic Loading Simulation and Critical Response Locations	25
Figure 3.11: Example of the Shear Stress over Depth of 1-inch Asphalt Overlay Pavement	27
Figure 3.12: Example of the Vertical Stress over Depth of 1-inch Asphalt Overlay Pavement ..	27
Figure 3.13: Pavement Experiment Sections Selected in Texas from LTPP	29
Figure 3.13: PCR Curve of Section 1068 over Time	31
Figure 3.14: PCR Drop Rate over Time of Section 1068	32
Figure 4.1: Failure envelopes for 1.5 psi of compaction pressure under Normal Loading of 18, 36 and 72 lbs.	35
Figure 4.2: Failure envelopes for 1.5 psi of compaction pressure under Normal Loading of 18, 36 and 72 lbs.	35
Figure 4.3: Failure envelopes for application rate of 0.03 gal/yd ² under Normal Loading of 18, 36 and 72 lbs.	36
Figure 4.4: Failure envelopes for application rate of 0.03 gal/yd ² under Normal Loading of 18, 36 and 72 lbs.	36
Figure 4.5: Trackless B and C tack coat test results with 0.03 gal/yd ² rate of application under Normal Loading of 18, 36 and 72 lbs.	38
Figure 4.6: K Parameters of Tack Coat Materials.	39
Figure 4.7: Fracture Energy of Tack Coat under Different Curing Condition.	39
Figure 4.8: Critical Strain of Tack Coat in Direct Shear Test.	40
Figure 4.9: Maximum Shear Stress of Tack Coat Materials	40
Figure 4.10: Shear Complex Modulus Master Curves of Tack Coat Materials	42
Figure 4.11: Correlation between J_{nrs} at Different Loading Level	43
Figure 4.12: Correlation between J_{nr} , 3.2 with Recovery Strain	44
Figure 5.1: Example of ABAQUS Output	47
Figure 5.2: Typical Variation in Horizontal Stress with Depth	48
Figure 5.3: Typical Variation in Vertical Stress with Depth	48
Figure 5.4: Typical Variation in Shear Stress with Depth	49
Figure 5.5: Tensile Strain of 4051 over Depth	49
Figure 5.6: Vertical Strain of 4051 over Depth	50

Figure 5.7: Shear Strain of 4051 over Depth	50
Figure 5.8: Tensile Stress at bottom of Existing AC Layer under Fully-bonded Condition	52
Figure 5.9: Tensile Stress at bottom of Existing AC Layer under Partially-bonded Condition ...	52
Figure 5.10: Tensile Stress at bottom of Existing AC Layer under Non-bonded Condition.....	53
Figure 5.11: Vertical Strain at top of Subgrade Layer under Fully-bonded Condition	53
Figure 5.12: Vertical Strain at top of Subgrade Layer under Partially-bonded Condition	54
Figure 5.13: Vertical Strain at top of Subgrade Layer under Non-bonded Condition.....	55
Figure 5.14: Vertical Deformation of Asphalt Overlay Pavement under Fully-bonded Condition	55
Figure 5.15: Vertical Deformation of Asphalt Overlay Pavement under Partially-bonded Condition.....	55
Figure 5.16: Vertical Deformation of Asphalt Overlay Pavement under Non-bonded Condition	56
Figure 5.17: Maximum Shear Stress of AC Layer under Fully-bonded Condition.....	56
Figure 5.18: Maximum Shear Stress of AC Layer under Partially-bonded Condition.....	57
Figure 5.19: Maximum Shear Stress of AC Layer under Non-bonded Condition	57
Figure 5.20: Tensile Stress at bottom of AC Layer	58
Figure 5.21: Tensile Strain at bottom of AC Layer	59
Figure 5.22: Maximum Shear Stress at AC layer	59
Figure 5.23: Vertical Strain at top of Subgrade	60
Figure 5.24: Vertical Deformation.....	61
Figure 5.25: Shear Stress at the Interface under Full-bonding Condition	61
Figure 5.26: Shear Strain at the Interface under Full-bonding Condition	62
Figure 5.27: Shear Stress at the Interface under Partial-bonding Condition	62
Figure 5.28: Shear Strain at the Interface under Partial-bonding Condition	63
Figure 5.29: Shear Stress at the Interface under Non-bonding Condition.....	63
Figure 5.30: Shear Strain at the Interface under Non-bonding Condition.....	64
Figure 6.1: The Relation between Cost Rate of Treatment and Pavement Condition [79]	65
Figure 6.2: PCR Curve of Section 1068 over Time.....	67
Figure 6.3: Pavement Condition Deterioration Rate of Section 1068 after Overlay	68
Figure 6.4: Life Gain after Overlay Treatment	70
Figure 6.5: Correlation between Life Gain and Traffic Volume	70

Chapter 1: Introduction

1.1 PROBLEM STATEMENT

Asphalt pavement is a multi-layer structure consisting of surface layer, base layer, subbase layer if necessary, and a subgrade layer, see Figure 1.1 [1]. A bonding material of sufficient strength is usually applied between each layer to ensure that the pavement structure can respond to the traffic load as a uniform system. A prime coat can penetrate the surface to function as a waterproofing membrane. Typically, this is applied before spraying the bonding material, called as tack coat. Therefore, the pavement interface can be defined as the thin layer bonding the two pavement layers as an integrated structure.

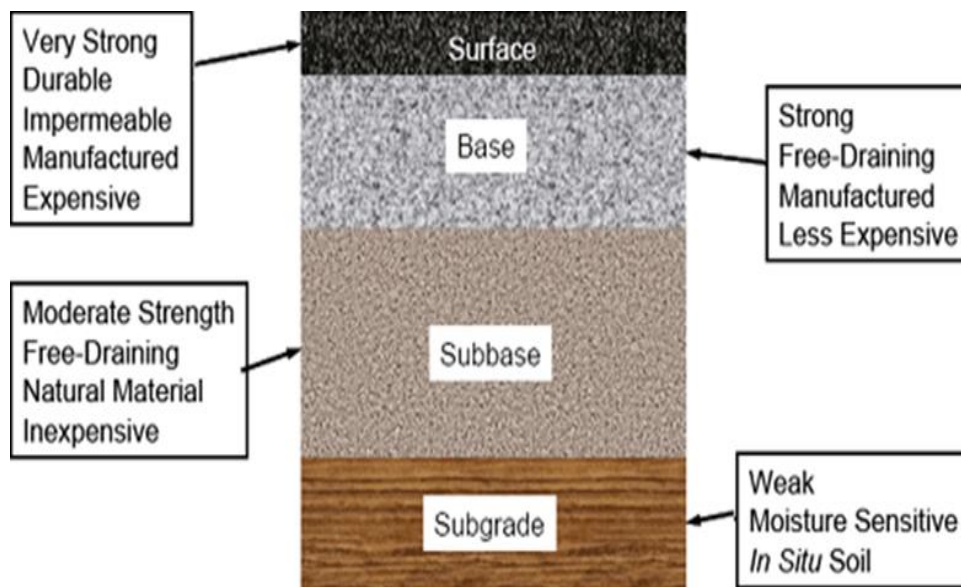


Figure 1.1: Typical Asphalt Pavement Structure [1]

Although the interface between the overlay and existing layer is relatively thin when compared with other pavement structural elements, such as the surface layer or base layer; in engineering practice the importance of a good bonded interface is under-addressed. The premature failure caused by deficient interface bonding condition is common [2]. For instance, the slippage of overlay from existing layer can lead to premature failure, as shown in Figure 1.2 [3]. The

separation between these two layers not only reduces the efficiency of load transfer, but also introduces the ingress of moisture, resulting in significantly expediting pavement deterioration. It is essential to understand the change of stress state when investigating the mechanism of debonding in asphalt overlay pavement. As shown in Figure 1.3, the stress state through the pavement structure changes with the traffic load over time [4].



Figure 1.2: Surface Layer Slippage Due to Debonding [3]

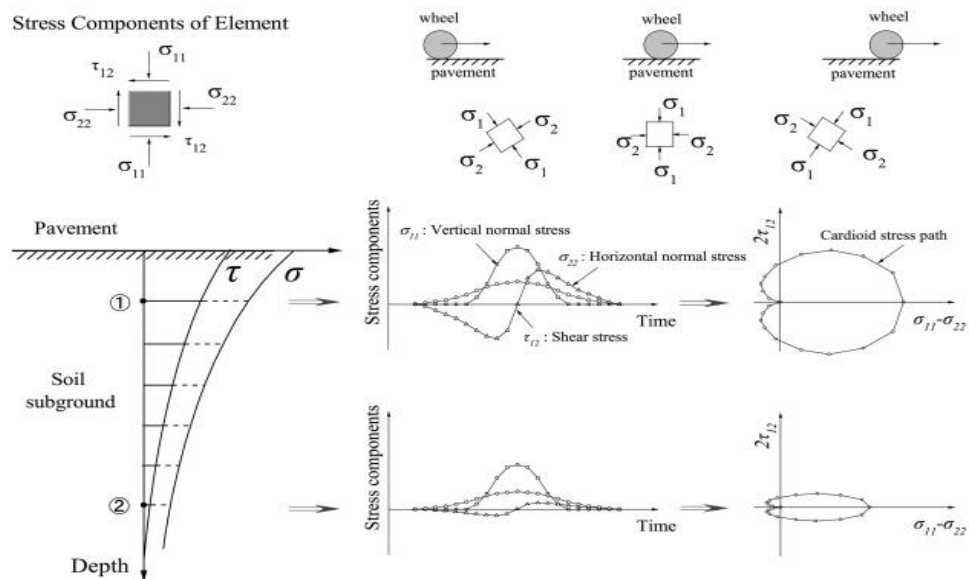


Figure 1.3: The Stress State of Pavement Interface under Wheel Loading [4]

In recent decades, thin or ultra-thin asphalt overlay has been widely applied to pavement in routine maintenance practices. Some of the reasons for using these types of overlay are: i) a thin asphalt overlay is cheaper than conventional hot mix asphalt (HMA) layer; ii) thin asphalt overlay is feasible and effective in the correction of distresses in the asphalt pavement; and iii) the technology and guidelines for thin asphalt overlay application are developed, with successful field practice [5, 6, 7]. Generally, the compacted thickness of the overlay ranges from 1 inch to 2 inches, while the “thin overlay” is thinner than 1.5 inches and the “ultra-thin overlay” is thinner than 1 inch [8].

For thin or ultra-thin asphalt overlay pavement, the quality requirement for interface bonding condition is stricter than that for the regular overlay because the interface is closer to the loading surface, resulting in higher stress or strain. The literature review showed that the primary research conducted with thin or ultra-thin asphalt overlay was focused on the mix design procedure, with locally available paving materials and construction technology, such as usage of recycling material, and lift thickness control [9, 10, 11]. However, the specifications on tack coat quality has not been fully studied, so the physical parameters influencing the performance of the interface of overlay pavement must be investigated.

When investigating the mechanism of how does the interface of thin asphalt overlay pavement affect the field performance, several potential approaches are available. For instance, the chemical and physical properties of bonding materials has been extensively investigated in laboratory experiments [2, 3]. In addition, numerical modeling has been widely applied to simulate response of composite structure under complex loading condition, i.e., ABAQUS program. Other available sources, including several programs sponsored by Federal or local agencies, can provide valuable data for the study of pavement performance.

ABAQUS is robust in performing finite element modeling (FEM) or finite element analysis (FEA) in pavement engineering. The software allows modeling of elastic as well as visco-elastic materials under different interface conditions. A typical example of an ABAQUS simulation being used to study pavement’s response under truck tires is shown in Figure 1.4. As discussed in the

literature review, ABAQUS is widely used in pavement engineering to numerically simulate the response of pavement under real loading conditions, including PCC pavement slab internal stress state under changing temperature and moisture condition, the effect of dowel bar on the loading transition between two PCC slabs, cracking propagation in asphalt pavement, and the stress distribution in pavement interface, among others [8].

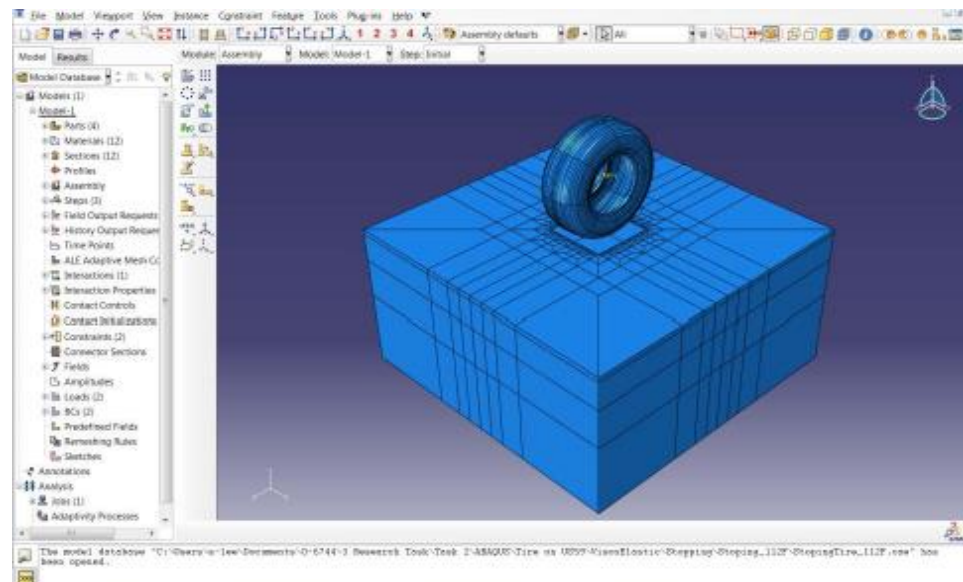


Figure 1.4: ABAQUS/CAE Screen-User Interface [8]

A study conducted by Su et al. on the influence of bonding conditions on the pavement stress distribution identified high stress areas in both fully-bonded and unbonded pavements, as shown in Figure 1.5 [12]. The authors indicated that the high stress concentrated more significantly for the area under unbonded condition than under the bonded condition. For thin or ultra-thin asphalt overlay pavements, the validity of this result is not tested, and more research on bonding conditions' effect on the durability is needed.

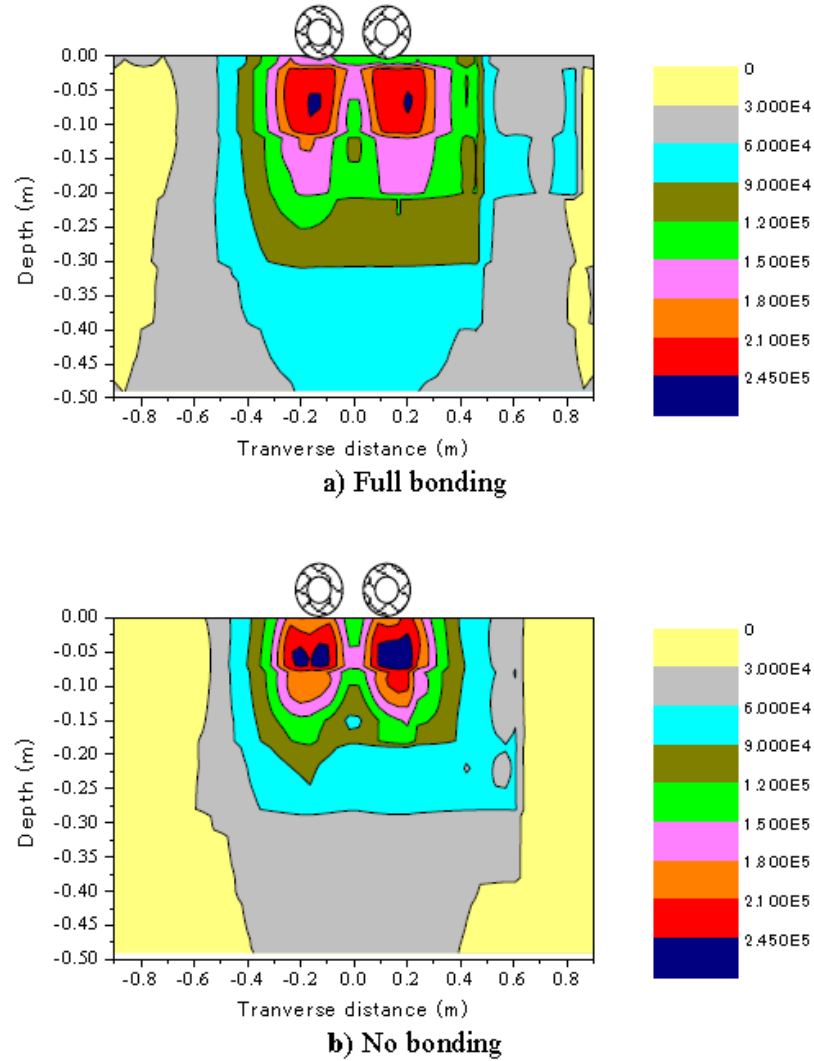


Figure 1.5: Influence of Interface on the Shear Stress Distribution [12]

The mechanism of interface bonding is complicated by the fact that each layer's surface is uneven, which makes it difficult to quantify the level of frictional resistance offered by mixture texture.

The Long-Term Pavement Performance Program (LTPP) database, a research program sponsored by the Federal Highway Administration (FHWA), provides extensive information for specific interest studies. The LTPP program includes data on more than 2,500 pavement sections. These sections are divided into general pavement sections (GPS) and specific pavement sections (SPS). The database includes information on the construction history, material properties, site

location, structure, climate, traffic, and field performance, etc. Experimental sections designated as GPS-6 and SPS-10 represent AC overlay on AC pavement and warm mix asphalt overlay on asphalt pavement, respectively.

The LTPP database contains information about several modes of pavement distress, such as alligator cracking, block cracking, longitudinal cracking, transverse cracking, and rutting for each section. Information about the international roughness index (IRI) and the transverse profile of the pavement is also available.

This research investigates the performance of thin asphalt overlays by conducting an experimental laboratory study with a different type of tack coat material. The study method includes numerical modeling by using ABAQUS program, as well as an evaluation of field asphalt overlay performance by analyzing the available LTPP sections within the state of Texas.

1.2 STRUCTURE OF REPORT

This study mainly includes seven chapters:

- Chapter 1, Introduction, introduces the pavement structure and function of tack coat material, then the main problem that this study proposed to solve;
- Chapter 2, Literature Review, describes the relevant research work conducted and the future needs;
- Chapter 3, Study Plan, mainly discusses the methodologies which will be applied in this study;
- Chapter 4, Laboratory Study of Tack Coat, presents the results of laboratory testing conducted with different types of tack coat materials;
- Chapter 5, Numerical Modeling of Thin Asphalt Overlay Pavement, discusses the results of ABAQUS modeling of thin asphalt overlaid pavements;
- Chapter 6, LTPP Case Study, Texas Thin Asphalt Overlay from LTPP, presents the results of the performance of Texas thin asphalt overlays from the LTPP database by using the Pavement Condition Rating (PCR) model.

- Chapter 7, Conclusion, summarizes the main findings based on this study and future research needs.

Chapter 2: Literature Review

2.1 TACK COAT

Tack coat is a type of bituminous material that can be applied on the existing pavement layers to bond the upper layers together. ASTM D8, *Standard Terminology Relating to Materials for Roads and Pavements*, stated, “Tack coat (bond coat) is an application of bituminous material to an existing relatively non-absorptive surface to provide a thorough bond between the old and new surfacing” [13]. Table 2.1 lists several types of tack coat material that are commonly used in the United States. Several types of tack coat materials, such as regular asphalt binder, emulsion, and cutback, are commercially available. Due to the environmental concerns, cutback asphalt (manufactured by adding controlled amounts of petroleum distillates such as kerosene) has not been widely applied in practice.

Table 2.1: Several Types of Tack Coat Material

Tack Coat Types			
Regular Asphalt Binder	Emulsion	Cutback	Solid Asphalt Binder
PG 64-22	SS-1, SS-1h, SS-1HH, SS-1S, CSS-1, CSS-1h, CSS-1HH,	Slow Curing Cutback	Ultrafuse
PG 64-28	CSS-1S, RS-1, RS-2, RS-1H, RS-1HH,	Medium Curing Cutback	Ultratack
PG 58-28	CRS-1, CRS-2, CRS-2P, CRS-2L	Rapid Curing Cutback	NTSS-1HM
PG 70-22		EPR-1 Prime	AE-NT Trackless
		AEP Prime	EM-50-TT

Recent research on tack coat generally includes the original material evaluation, the diluted emulsion technology, recovery of emulsion to obtain the residual asphalt binder, tack coat storage condition, and breaking time, and so on; however, the quality control and quality assurance on tack coat application are not totally addressed. If tack coat is of poor quality, it can cause surface course delamination due to bonding failure, especially at the intersections where vehicles suddenly stop and accelerate. In addition, poor-quality tack coats can result in cracking caused by the shear stress concentration, slippage, or premature fatigue [2]. One research study concluded that the lift thickness of HMA can be decreased by 0.5 in. and the pavement life can be increased by 21%

when the bonding is increased from 25% to 75% [14]. Thickness reduction of 0.75 inches is feasible when the layers have bonding ratios of 85% or more, while more than 5 inches of additional HMA are needed when the bonding ratio is 25% or less [14]. The next part of this section briefly describes past studies and ongoing research on tack coat materials.

The earliest research conducted on tack coat dates back to 1919. Bowman [15] carried out a study titled “Europe Moves to Modified Binders” in support of using heavy tack coats. *Transportation Research Circulars* E-C102, E-C122 and E-C182 thoroughly summarized the latest development in asphalt emulsion technology [16, 17, 18]. NCHRP 9-40 studied the optimization of tack coat for HMA placement and evaluated the effects of emulsified tack coat type, application rate, dust and wetness [2]. NCHRP 9-50 studied emulsion performance grade (EPG) specifications that directly related the asphalt material properties to field performance [19]. The International Union of Testing and Research Laboratories for Materials and Structures (RILEM) held a symposium on tack coats’ performance under tension and torsional shear type tests [20]. Generally, the shear strength of interface combines two parts including chemical strength provided by tack coat, and mechanical strength supplied by the surface texture’s friction. It was found that the pavement surface texture’s effect is more influential than the chemical materials [21, 22, 23].

Trackless tack is a popular paving material applied to avoid pick-up of the bituminous material (which happens when it adheres to tires during paving operations) without compromising their performance. The Texas Department of Transportation (TxDOT) sponsored a study to develop specifications on performance evaluation for trackless tack [24]. The track-free time test (ASTM D711) and dynamic shear rheometer (DSR) tackiness test were selected to evaluate the tracking resistance of trackless tack and conventional tack. The authors recommended that those two tests be adopted. A study conducted to evaluate the effects of trackless tack interface on pavement top-down cracking performance concluded that the trackless tack performed better in terms of shear strength and top-down cracking resistance than conventional tack [25].

Another study for TxDOT evaluated the design and construction challenges of thin HMA overlay [7]. It recommended the shear strength test as a measure of the interlayer bonding strength. The results showed that the effect of mix type and compaction effort was more impactful on the bonding strength than the tack coat material and tack rate. The authors also concluded that the tack coat type and rate were essential to obtain adequate bonding strength between pavement layers.

ABAQUS is a suite of powerful engineering simulation programs based on the finite element method [26]. As shown in Figure 2.1, ABAQUS is a robust software with well-developed modules that can assist the numerical analysis either internally or externally with other third-party software, such as Auto-CAD, ADMAS. The following section reviews the literature on ABAQUS's applications for simulating asphalt pavement response.

Figure 2.1: Modules in ABAQUS software [26]

backcalculated nonlinear moduli showed consistency with FWD deflections measured on an asphalt pavement site. The ABAQUS special-purpose gap elements were used to simulate longitudinal and transverse cracks in the pavement surface layer. The results showed that dynamic deflections are 17% higher for a pavement with longitudinal cracks when compared with an uncracked pavement.

Masad et al. [28] studied the strain distribution in asphalt mixes by using ABAQUS plane strain finite-element models. The results from the models were consistent with those measured in experimental tests. This study emphasized the significant influence of the base layer's stiffness on the strain distribution within the mastic, and the asphalt binder.

In one study, a three-dimensional finite element (FE) model with the HMA viscoelastic properties obtained from laboratory test was used in a study to simulate pavement's responses at different temperatures and traffic speeds [29]. The results from that modeling were compared with the field-measured pavement responses. It was found that the elastic theory underpredicted the pavement response to vehicular loading at intermediate and high temperatures. The FE viscoelastic model could simulate the HMA's retardation response in transverse direction and relaxation in the longitudinal direction with promising accuracy.

Dai et al. [30] conducted a study predicting the creep stiffness of asphalt mixtures with micromechanical finite-element and discrete-element models. The ABAQUS FE model was integrated with a user-defined material model (UMAT) that combined continuum elements with viscoelastic properties for the effective asphalt mastic and rigid body elements. In addition, discrete-element models were developed and compared with the FE model to predict the mixture's creep stiffness. The results showed that both models produced results that were consistent with the laboratory testing results.

A study was performed with ABAQUS FE modeling and experimental tests to simulate the microstructure of asphalt materials [31]; it found that the load carrying behavior of an asphalt mixture depended on the local load transfer among aggregate particles. An ABAQUS model was developed to simulate the micromechanical response of the aggregate-binder structure. Video

imaging and computer analyses were applied in the experimental verification phase. The model simulation generated results similar to those produced by the laboratory tests.

Abbas et al. [32, 33] carried out linear and nonlinear viscoelastic analyses of the microstructure of asphalt concrete. They used ABAQUS along with two-dimensional imaging techniques to capture the microstructure of asphalt concrete at different strain levels to obtain the viscoelastic property of the binder. Then, they used asphalt concrete shear modulus G^* to compare the consistency of the results obtained by prediction model against those obtained by laboratory testing.

In another study [34], ABAQUS was used to simulate the viscoelastic-viscoplastic property of asphalt concrete and to verify the experimental test on asphalt mixture at multiple stress levels and temperatures. A three-dimensional FE model of ABAQUS was used to simulate the response of three-layer pavement structure under traffic loading at different temperatures. The results showed that tensile viscoplastic strain accumulated at the pavement surface, which might be the potential cause of cracking. This study also found that at pavement temperatures as high as 40°C, tensile viscoplastic strain will be the main problem at the vehicle tire edge because of the asphalt mixture heave (permanent deformation and dilation).

A rate-dependent cohesive zone model was integrated into ABAQUS to characterize the fracture behavior (heterogeneous and viscoelastic behavior) of asphalt mixtures [35]. That model could simulate the initiation and propagation of discrete cracks taking place in the microstructure of the asphalt mixtures. The results indicated that this type of model could yield results that are consistent with the experimental test results.

A 3D finite element analysis with ABAQUS was used to simulate the response of an asphalt pavement structure containing a transverse top-down crack under traffic loading [36]. The stress intensity factors and T-stress (fracture toughness) were calculated for different locations between the crack and the vehicle wheels. They found that the crack modes (I, II, and III) were present, depending on the loading position in relation to the crack plane.

A study used ABAQUS with a micromechanical finite element model to investigate the influence of material properties on moisture-induced damage in asphalt mixtures [37]. The maximum total resistant force provided by the asphalt mixture microstructure was used as an indicator of its susceptibility to moisture damage. The results showed that the diffusion coefficient of the asphalt matrix and aggregate, as well as the bond strength of the aggregate-matrix interface, had the most influence on the asphalt mixtures' moisture susceptibility.

Hadi and Bodhinayake [38] conducted nonlinear and linear finite element analyses on flexible pavements with realistic material properties of pavement layers under moving traffic loads. The results indicated that the displacements under cyclic loading with non-linear material behavior were consistent with the field measured deflections.

Huang et al. [39] used ABAQUS to simulate the responses of asphalt pavements at the Louisiana Transportation Research Facility's accelerated loading facility. A rate-dependent viscoplastic model and a creep model were incorporated into the 3D finite element procedure. The results indicated that the 3D FE model could simulate the response of pavement structure under various traffic and environmental conditions with reasonable accuracy.

Another research study investigated a new creep test, Partial Triaxial Test (PTT), to characterize the permanent deformation of asphalt mixture [40]. The results from the PTT were compared with the triaxial repeated load permanent deformation tests and with the rutting depth simulated by ABAQUS modeling. The PTT method produced more accurate prediction on the rutting behavior.

In another study, the Indiana Department of Transportation and Purdue University [41] studied the effects of factors including the pavement geometry, boundary conditions, materials, loads, test conditions, and construction variables, on the pavement field performance. A creep model was applied in ABAQUS program to simulate the time dependent behavior of asphalt mixtures. The results indicated that the creep model could effectively predict the in-service pavement performance.

Elseifi et al. [42] modeled the semi-circular bend (SCB) test with 3D FE with cohesive elements to simulate the propagation of damage during testing. Their proposed modeling approach was consistent with the measured test results for all asphalt mixtures.

Dave et al. [43] studied the reflective and thermal cracking of asphalt overlays. They used a bi-linear cohesive zone model to simulate three field pavement sections to provide new insight about cracking mechanism in asphalt overlay systems under thermal and traffic loads. They proposed an overlay design process that accounted for the initiation and propagation of cracks in overlays.

Dormohammadi [44] used ABAQUS to study the impact of overlay thickness on pavement structural characteristics. The results showed that the overlay thickness of less than 2 inches contributed minimally to the pavement's structural capacity. Overlays with the thickness less than 1 inch significantly influenced the stress levels at the interface. The paper also concluded that the bonding condition played an important role in the performance of overlay pavement systems.

Ai-Qadi and his colleagues [45-55] have used ABAQUS to study phenomena such as the viscoelastic properties of asphalt mixtures, tire-pavement interaction, static and dynamic traffic loading, reflective cracking, tire braking, and wide-base tires, etc.

2.3 LTPP PROGRAM

The Long-Term Pavement Performance Program (LTPP) database provides useful and valuable information for pavement engineering studies. LTPP, which was initiated by the Transportation Research Board (TRB) of the National Research Council (NRC) in the early 1980s, is a research program sponsored by Federal Highway Administration (FHWA) to collect and analyze pavement structural and functional performance in the United States and Canada. LTPP database has the most comprehensive information on more than 2500 pavement sections [56]. Table 2.2 and 2.3 list the experiments in the LTPP database, including General Pavement Studies (GPS) and Specific Pavement Studies (SPS).

Elkins et al. [57] authored an FHWA report titled *Long-Term Pavement Performance Information Management System Pavement Performance Database User Guide* to aid in understanding and using the LTPP pavement performance database.

Malla and Joshi [58] the LTPP database to propose a generalized constitutive model to predict the resilient modulus (M_R) that considered the effects of bulk stress and octahedral shear stress of subgrade soils as the influencing variables.

Table 2.2: List of GPS Experiments [57]

Experiment	Experiment Title
GPS-1	Asphalt Concrete (AC) Pavement on Granular Base
GPS-2	AC Pavement on Bound Base
GPS-3	Jointed Plain Concrete Pavement (JPCP)
GPS-4	Jointed Reinforced Concrete Pavement (JRCP)
GPS-5	Continuously Reinforced Concrete Pavement (CRCP)
GPS-6A	Existing AC Overlay of AC Pavement (existing at the state of the program)
GPS-6B	AC Overlay Using Conventional Asphalt of AC Pavement-No Milling
GPS-6C	AC Overlay Using Modified Asphalt of AC Pavement-No Milling
GPS-6D	AC Overlay on Previously Overlaid AC Pavement Using Conventional Asphalt
GPS-6S	AC Overlay of Milled AC Pavement Using Conventional or Modified Asphalt
GPS-7A	Existing AC Overlay on PCC Pavement
GPS-7B	AC Overlay Using Conventional Asphalt on PCC Pavement
GPS-7C	AC Overlay Using Modified Asphalt on PCC Pavement
GPS-7D	AC Overlay on Previously Overlaid PCC Pavement Using Conventional Asphalt
GPS-7F	AC Overlay Using Conventional or Modified Asphalt on Fractured PCC Pavement
GPS-7R	Concrete Pavement Restoration Treatments with No Overlay
GPS-7S	Second AC Overlay, Which Includes Milling or Geotextile Application, on PCC Pavement With Previous AC Overlay
GPS-9	Unbounded PCC Overlay on PCC Pavement

Table 2.3: List of SPS Experiments [57]

Category	Experiment	Title
Pavement	SPS-1	Strategic Study of Structural Factors for Flexible Pavements
Structure Factors	SPS-2	Strategic Study of Structural Factors for Rigid Pavements
Pavement	SPS-3	Preventive Maintenance Effectiveness of Flexible Pavements
Maintenance	SPS-4	Preventive Maintenance Effectiveness of Rigid Pavements
Pavement	SPS-5	Rehabilitation of AC Pavements
Rehabilitation	SPS-6	Rehabilitation of Jointed Portland Cement Concrete (JPCC)
	SPS-7	Bounded PCC Overlays of Concrete Pavements
Environmental Effects	SPS-8	Study of Environmental Effects in the Absence of Heavy Loads
Asphalt	SPS-9P	Validation and Refinements of Superpave Asphalt Specifications and Mix Design Process
Aggregate		
Mixture	SPS-9A	Superpave Asphalt Binder Study
Specification		

A study was conducted utilizing LTPP data to evaluate the effectiveness and cost-effectiveness of asphalt pavement rehabilitations [59]. It used multiple regression to evaluate the influence of overlay thickness, existing pavement thickness, traffic volume, and pre-overlay pavement conditions on the pavement performance. The parameter of international roughness index (IRI) was selected to evaluate pavement performance. The findings indicated thin-overlay, high traffic level, and poor pre-rehabilitation pavement condition increased the deterioration rate of new overlay.

Dong and Huang [60] conducted a parametric survival analysis on the LTPP data to evaluate the effect of factors including overlay thickness, total pavement thickness, pretreatment pavement serviceability, traffic volume, freeze index, mixture, and milling treatment, on crack initiation in resurfaced asphalt pavements. They used the Weibull hazard function to analyze the data obtained from five LTPP SPS experiments. They considered four types of cracking including alligator crack, longitudinal crack on wheel/non-wheel path, and transverse crack. The results indicated that traffic level had a significant impact on the development of those four cracks. Thick overlays delayed the initiation of cracking, except for the non-wheel path longitudinal cracking. A

30% of reclaimed asphalt pavement (RAP) in overlay accelerated the initiation of early-age fatigue cracking, although it did not cause severe fatigue cracking in the long term. Severe freeze-thaw conditions were attributed to the non-wheel path longitudinal and transverse cracking; the milling before overlay construction can retard the initiation of these two types of cracks.

A study sponsored by FHWA [61] investigated the feasibility of a backcalculation method in determining layer parameters for flexible and rigid pavements from LTPP database. They presented the procedures and steps to back-calculate the layered elastic properties, such as Young's modulus, the coefficient and exponent of the nonlinear constitutive equation, from the available deflection basin measurements in the LTPP test sections.

Another study that drew data from the LTPP program evaluated the joint and crack load transfer within rigid pavements [62]. Representative load transfer efficiency (LTE) indices and joint stiffness were calculated for all GPS, SPS, and Seasonal Monitoring Program (SMP) rigid test sections. A trend analysis was conducted to investigate the effects of design features and site conditions on LTE. They concluded that LTPP database was useful in understanding the factors affecting LTE, such as the plate position of FWD, steel reinforced or non-reinforced, and testing time.

An FHWA sponsored study [63] investigated the existing methods of predicting the dynamic modulus of HMA. The primary factors used included the binder, volumetric, and resilient material properties obtained from the LTPP database. The authors used artificial neural networks to predict the dynamic modulus from those data.

Hall et al. [64] assessed the relative performance of different maintenance and rehabilitation treatments, including the influence of pretreatment conditions on treatment effectiveness, using LTPP SPS-3, SPS-5, and GPS-6B (flexible pavement rehabilitation), and SPS-6 and GPS-7B (rigid pavement rehabilitation) studies. Roughness, rutting and fatigue cracking were selected as the three distress modes to evaluate the effectiveness of different maintenance treatment. The results indicated that the thin overlay treatment is the most effective method in the SPS-3 core experiment. In the SPS-5 experiment, the overlay thickness and pre-overlay roughness

level were the two factors that most influenced the performance of asphalt overlays. They found that most of the rutting that occurred in the asphalt overlays took place in the first twelve years after the overlay was applied.

A methodology to help determine the most appropriate time to apply a thin overlay treatment based on the condition of the existing pavement was proposed in the LTPP SPS-3 and SPS-5 studies [65]. These studies evaluated the effects of climate, traffic, existing asphalt concrete (AC) layer thickness, and overlay thickness on the life of pavement after a new thin overlay treatment. Threshold triggers based on rutting severity and longitudinal cracking in the wheel path were selected to determine the best time to apply thin overlay. The study concluded that the traffic level and existing AC-layer thickness significantly affected the life extension produced by the application of a thin overlay treatment.

The above literature review enables a primary understanding of the scope and objective of relevant research studies conducted with the LTPP database. The present study will focus on evaluating the performance of asphalt overlay pavements in Texas based on the LTPP database.

Chapter 3: Study Plan

3.1 LABORATORY TESTS WITH TACK COAT MATERIALS

Many research studies have been conducted on the laboratory testing with tack coat material in recent years, including the chemical and physical property of tack coat materials and the mechanical performance of pavement layers [2]. Figure 3.1 shows the scope of laboratory tests with tack coat materials. Several laboratory tests were carried out to evaluate the pure shear strength and rheology performance of the tack coat under investigation.

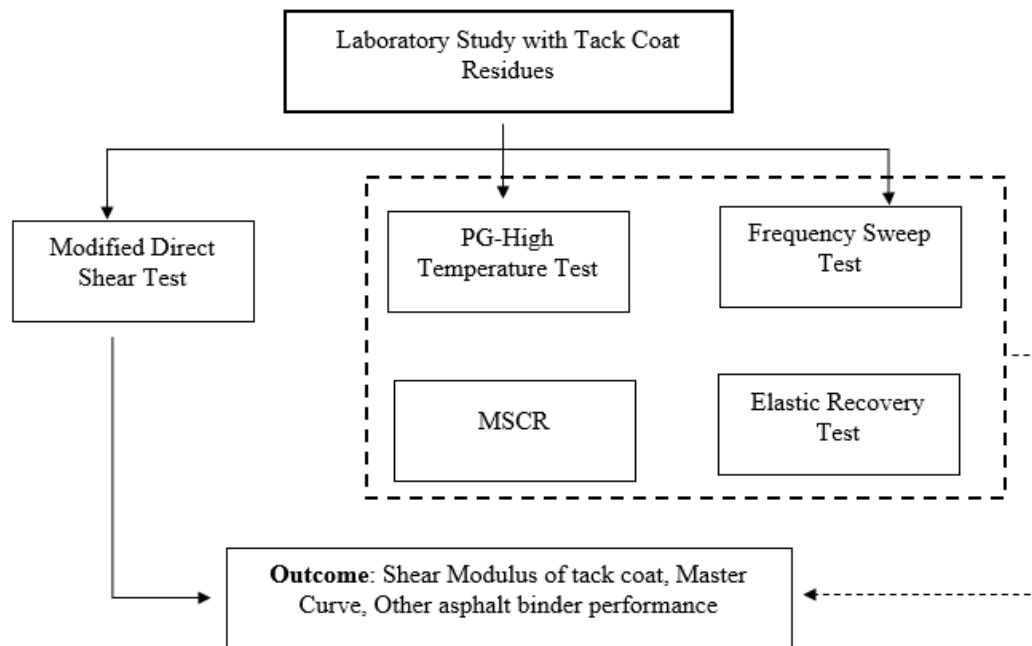


Figure 3.1: Scheme of Laboratory Testing with Different Tack Coat Materials

3.1.1 Material

Seven tack coat materials were investigated in this study. These materials included two emulsions (SS-1H, CRS-2), two performance-graded asphalt binders (PG64-22, PG70-22) and three trackless tacks (Trackless A, B, and C). Trackless A was a brown to black color emulsion with a pH of 2.1-4. Trackless B was an anionic Blacklidge Emulsion product having a 0-20 penetration base asphalt. Trackless C was a blend of a stiff base binder with specialized additives

and polymers. The emulsion SS-1H, CRS-2, Trackless A and Trackless B were recovered by following AASHTO T59 (ASTM D6934).

3.1.2 Laboratory Tests

A typical direct shear test (DST) device commonly used by geotechnical engineers to obtain soil shear strength was modified for use in this study. The detailed modification of DST can be found in Hajj et al. [66]. During the direct shear test, circular solid synthetic cylindrical specimens of 4 in. (101.6 mm) diameter and 2 in. (50.8 mm) thickness, which have frictionless surfaces, were used for evaluating tack coat quality. The specimens were prepared with a residue application rate of 0.3 gal/yd². As shown in Figure 3.2, each tack coat was cured at two levels of applied pressures either by placing a 20 lbs weight on them or by applying 300 lbs of clamping load for three days at room temperature (77°F). The normal loading amounts applied in the direct shear test were 18 lbs, 36 lbs and 72 lbs, individually. For each normal loading level, three replicate specimens were tested to verify repeatability. Figure 3.3 shows an example of typical results obtained from the direct shear test, and Figure 3.4 depicts the simplified shear strength model.



(a) 20 lbs Curing Loading



(b) 300 lbs Clamping Curing Loading

Figure 3.2 Curing Conditions for Direct Shear Test Specimens

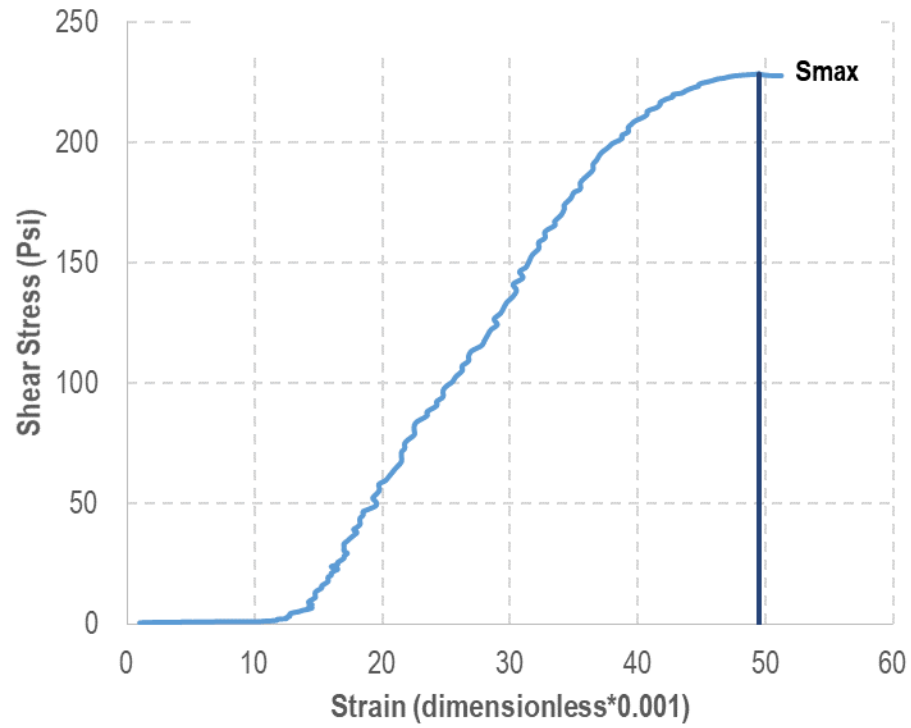


Figure 3.3: Example of Direct Shear Test Result

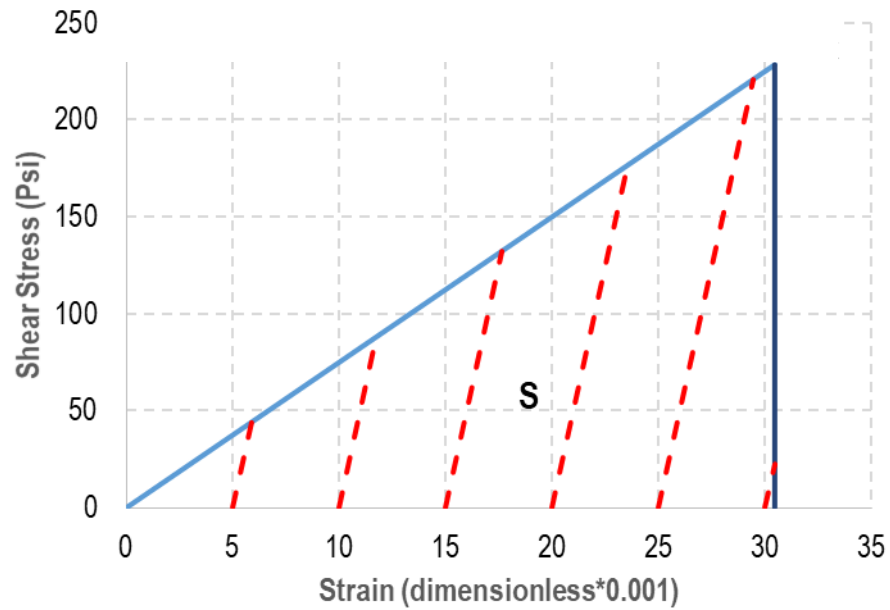


Figure 3.4: The Simplified Shear Strength Model for Tack Coat-Ultrafuse

As shown in Table 3.1, a number of tests were carried out on the recovered residue and other tacks to evaluate their rheological properties.

Table 3.1: Laboratory Tests with Tack Coat Materials

Laboratory Test	Specification(Equip. ^a)	Test Condition	Output
Recovery	AASHTO T59/ASTM D6934 (Oven, Beaker, Balance)	50 g emulsion in 600 mm beaker, oven 163°C for 2 hours.	Residue
Frequency Sweep Test	AASHTO TP101 (DSR)	4, 28, 46, 60, 80°C; 0.0159-15.9 rad/s, strain level-0.1%.	Shear complex modulus master curve, rheological indicators-LSV, G^* , G-R
MSCR ^b	AASHTO TP70/ASTM D7405 (DSR)	PG-high temperature, DSR, 0.1 kPa and 3.2 kPa loading levels.	J_{nr} , %Recovery
Elastic Recovery	Tex-539-C (Ductilometer)	10°C, 20 cm for 5 min., cut and measure after 1 hour.	%Recovery

Note: a-Equip. represents equipment;
b-MSCR-multiple stress creep recovery test.

Figure 3.5 shows the result of direct shear tests with PG70-22 at different application rates and under different normal curing loads. Figure 3.6 plots the dynamic modulus curve, which is shifted based on results from the frequency sweep tests.

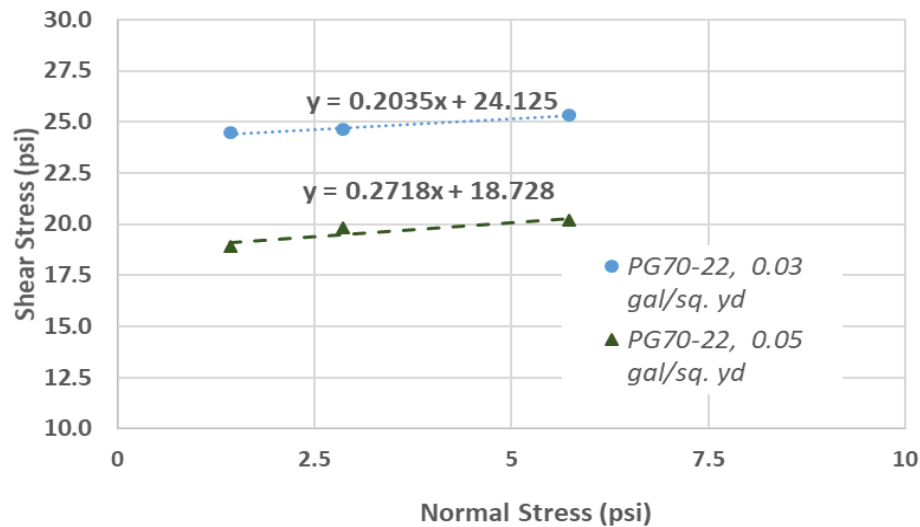


Figure 3.5: Example of the Results of Direct Shear Test with PG70-22

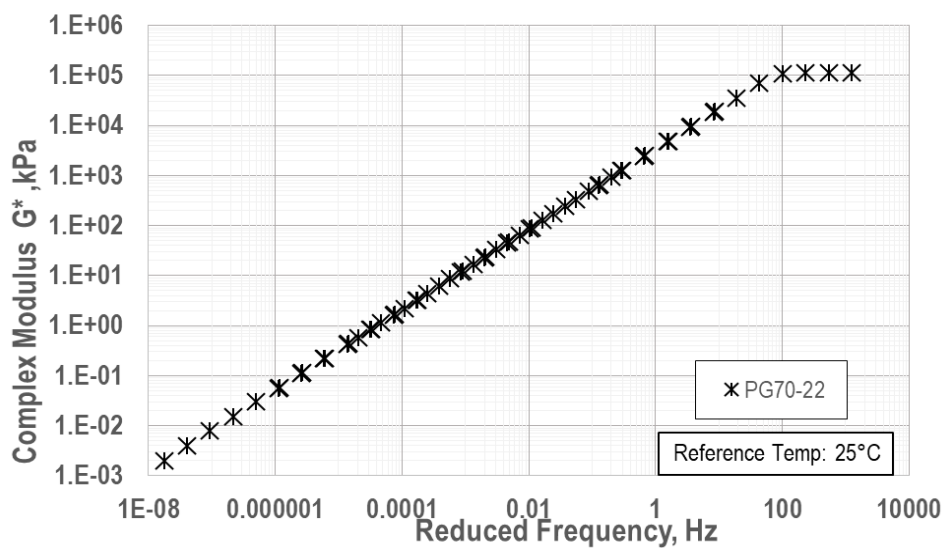


Figure 3.6: Example of Dynamic Modulus of PG70-22 at Reference Temperature of 25°C

Figure 3.7 shows a strong correlation between shear viscosity and $J_{nr3.2}$, and Figure 3.8 depicts the correlation between low shear viscosity and elastic recovery.

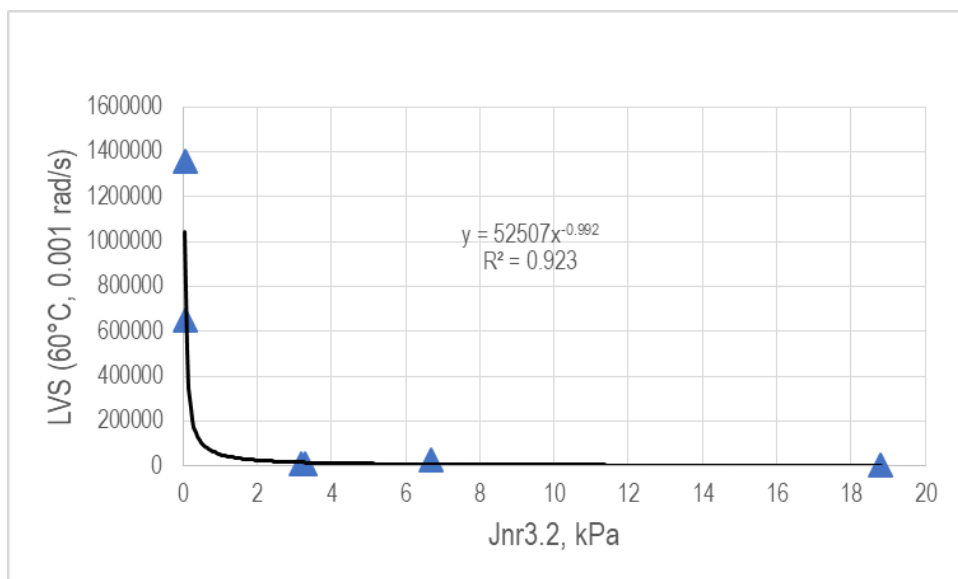


Figure 3.7: Example of Correlation between Shear Viscosity and $J_{nr3.2}$.

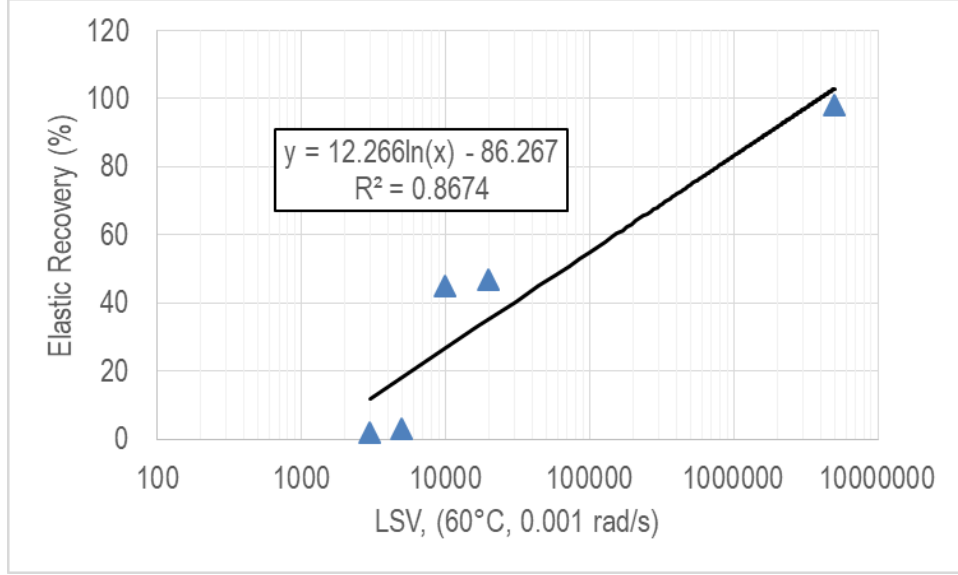


Figure 3.8: Example of Correlation between Low Shear Viscosity and Elastic Recovery.

3.2 ABAQUS MODELING WITH ASPHALT OVERLAY PAVEMENT

In this study, ABAQUS was used to model the responses of different thin overlay pavement structures under static traffic loading. A matrix study considering several factors, including pavement layers property (such as overlay thickness, material Poisson ratio, HMA elastic property, and interface cohesive behavior), as well as traffic loading, is proposed. In total, are 60 cases were studied to investigate the factors affecting the performance of thin overlay pavement structures.

Figure 3.9 shows the ABAQUS modeling flowchart with the consideration of different variables. Two existing pavement structures were modeled with different thin-overlay thickness, as shown in Table 3.2. The overlay layer thickness varied between 0.5 to 2 inches. In addition, two LTPP pavement sections simulated by ABAQUS. Figure 3.10 indicates the traffic loading scheme which consisted of two tires. Each tire was subjected to 80 psi of static pressure.

Further analysis was conducted with the results based on the fatigue model to investigate the fatigue life of these asphalt overlay pavements [67]. In this study, the general form of the number of load repetitions can be used as shown in equation 3.1 as below:

$$N_f = Ck_1 \left(\frac{1}{\varepsilon_t} \right)^{k_2} \left(\frac{1}{E} \right)^{k_3} \quad (3.1)$$

where N_f = Number of repetitions to fatigue cracking, ϵ_c = Tensile strain at the critical location. E = Stiffness of the material, k_1, k_2, k_3 = Laboratory regression coefficients and C = Laboratory to field adjustment factor.

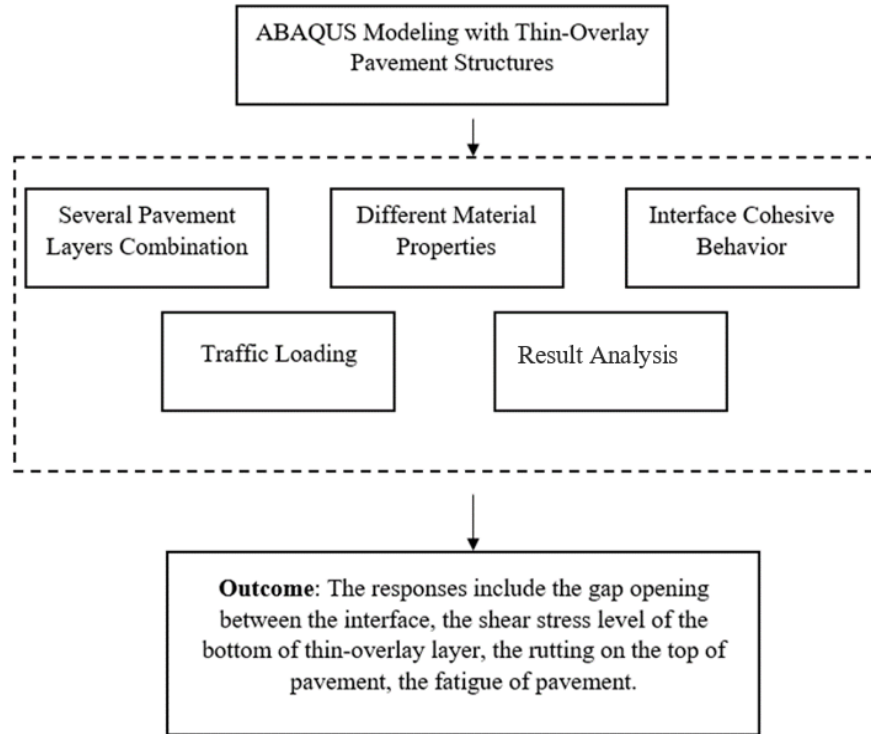


Figure 3.9: ABAQUS Modeling with Asphalt Thin-overlay Pavement

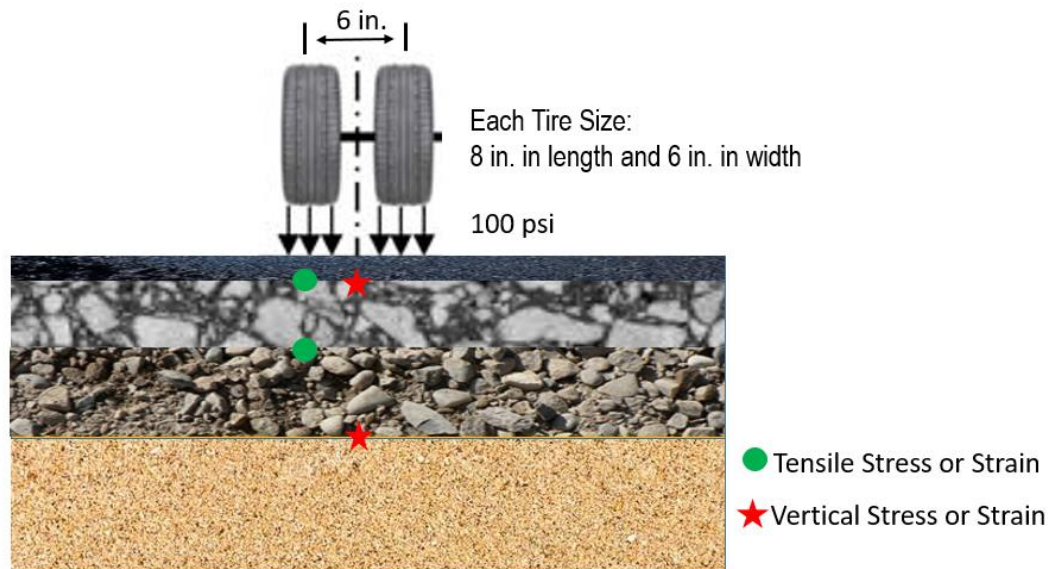


Figure 3.10: Traffic Loading Simulation and Critical Response Locations

Table 3.2: The Pavement Structure Combination for ABAQUS Modeling

Pavement Structure	Case 1	Case 2	FEM1087	FEM6079
Overlay Layer (in.)	0.5, 1.5, 2	0.5, 1	1	2
HMA Layer (in.)	4	5	7	7
Base Layer (in.)	6	6	7	5
Subgrade Layer (in.)	12	12	12	12

Table 3.3a shows the parameters of the material properties used in the ABAQUS modeling. The main parameters include the density, elastic modulus, Poisson ratio, and modulus of cohesive behavior. Table 3.3b presents the parameters for LTPP cases 1087 and 6079. These parameters were obtained from the LTPP database. Figures 3.11 and 3.12 are output examples of ABAQUS modeling of depth at critical locations.

Table 3.3a: The Input Parameters for LTPP Case 1 and 2 ABAQUS Modeling

Material	Density (lb/in. ³)	Elastic Parameters	
		Elastic Modulus (psi)	Poisson's Ratio
Thin Asphalt Overlay	0.087	500000/ 250000	0.30
Existing AC Layer	0.087	500000/ 250000	0.30
Base Layer	0.063	15000/ 30000	0.35
Subgrade	0.058	7000	0.4

Table 3.3b: The Input Parameters for LTPP Sections ABAQUS Modeling

Material	Density (lb/in. ³)	Elastic Parameters	
		Elastic Modulus (psi)	Poisson's Ratio
Thin Asphalt Overlay	0.079	500000	0.30
Existing AC Layer	0.079	500000/ 850000	0.30
Base Layer	0.097	25000	0.35
Subgrade	0.090	11900/7860	0.4

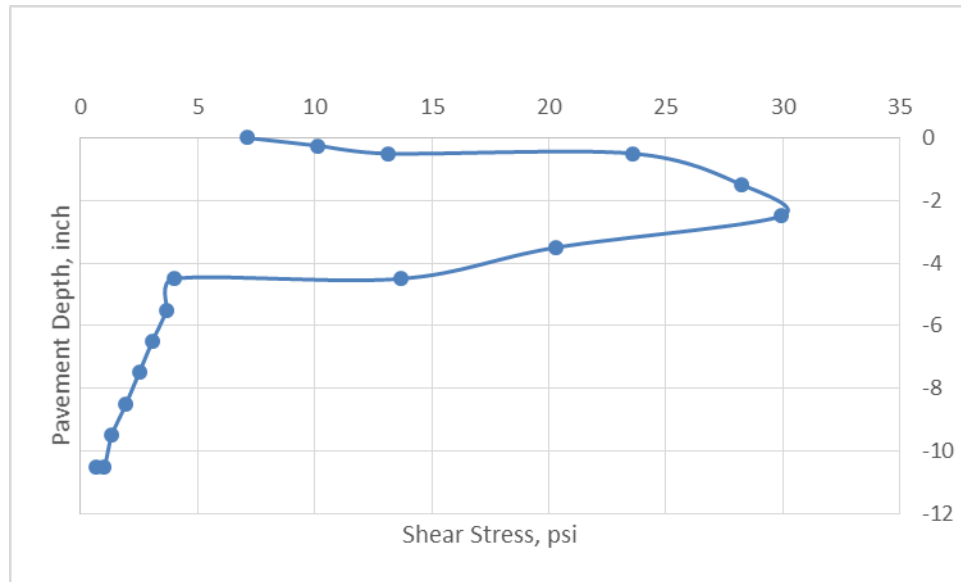


Figure 3.11: Example of the Shear Stress over Depth of 1-inch Asphalt Overlay Pavement

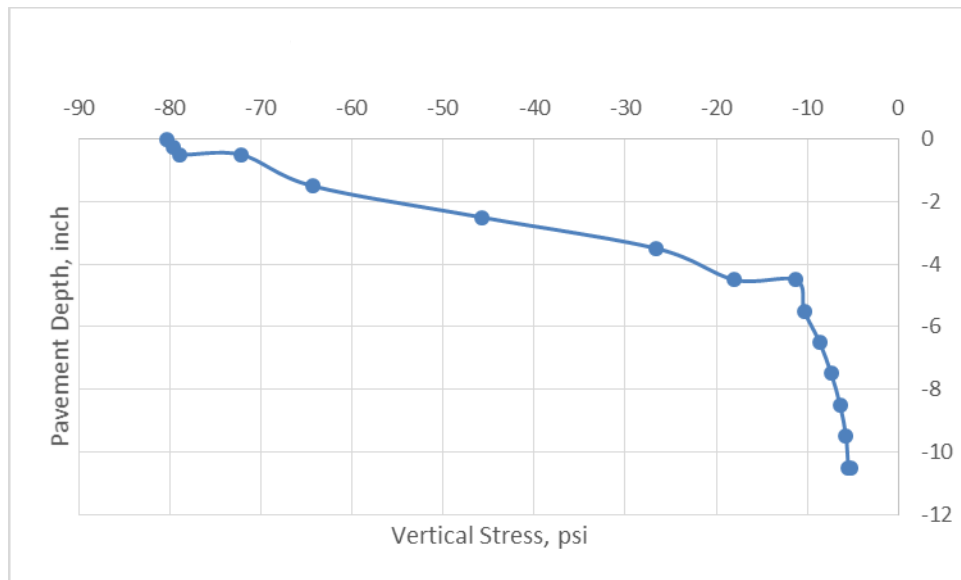


Figure 3.12: Example of the Vertical Stress over Depth of 1-inch Asphalt Overlay Pavement

As shown in below Table 3.4, an ID number is assigned to each of ABAQUS case study to characterize the case's representative information. For example, "4051" indicates "the ABAQUS modeling of overlay pavement with the features that it has AC layer of 4-inch in thickness and overlay of 0.5 inch, and layers' properties as 500,000 psi of AC layer, 30,000 psi of Base layer, and 70,000 psi/inch of interface (fully-bonded)." The fully-bonded cases should have last digit as

1, 4, 7, or 9. If the last digit is 2, 5, 8, or 11, the bonding condition is partially-bonded. If the last digit is 3, 6, 9, or 12, the bonding condition is non-bonded. All the cases of ABAQUS modeling in this study follow this ID pattern. Chapter 5 will present and discuss the results of ABAQUS modeling study.

Table 3.4: Case ID of Numerical Modeling Study

Properties		AC 4-inch			AC 5-inch	
AC M_E (psi)	Base M_E (psi)	Cohesive Behavior	0.5 Overlay	1.5 Overlay	2 Overlay	0.5 Overlay 1 Overlay
500,000	30,000	70,000	4051	4151	4201	5051 5101
	30,000	7,000	4052	4152	4202	5052 5102
	30,000	500	4053	4153	4203	5053 5103
500,000	15,000	70000	4054	4154	4204	5054 5104
	15,000	7000	4055	4155	4205	5055 5105
	15,000	500	4056	4156	4206	5056 5106
250,000	30,000	70,000	4057	4157	4207	5057 5107
	30,000	7,000	4058	4158	4208	5058 5108
	30,000	500	4059	4159	4209	5059 5109
250,000	15,000	70000	40510	41510	42010	50510 51010
	15,000	7000	40511	41511	42011	50511 51011
	15,000	500	40512	41512	42012	50512 51012

3.3 ANALYSIS METHOD WITH LTPP DATABASE

The objective of the LTPP study was to evaluate the asphalt pavement performance that resulted from the asphalt overlay treatment in Texas, using findings based on the available experiment sections. The criteria used to select the pavement experiment sections from the LTPP database included the following items: (a) existing pavement type should be flexible pavement; (b) the location of the test sections is limited to Texas; and (c) the treatment should be asphalt overlay. Based on these requirements, 30 sections were selected for the future analysis study, as shown in Figure 3.13.

The main pavement distress inventory drawn from the LTPP database included transverse cracks, longitudinal cracks, alligator cracks, patching/potholes, rutting, and roughness according to the International Roughness Index (IRI). The information about transverse cracks, longitudinal

cracks, alligator cracks, and patching/potholes was obtained from digital video images, and roughness (IRI) data were measured by the FHWA's automatic road analyzer (ARAN), as shown in Table 3.5.

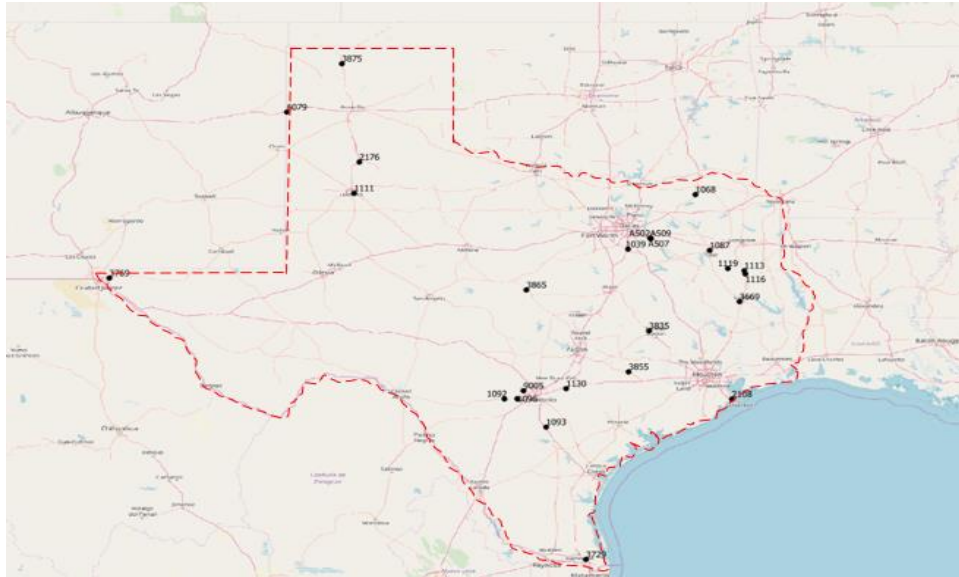


Figure 3.13: Pavement Experiment Sections Selected in Texas from LTPP

Table 3.5: Distress Summary [68]

Asphalt-Surfaced Pavement Distress Types with Rutting and Roughness				
Distress Type	Unit of Measure	Converted To	Defined Severity Levels?	Measured By
Alligator Cracking	Square Feet	Percent of Lane Per 0.02 Mile	Yes	Contractor (Video Analysis)
Transverse Cracking	Linear Feet	Number of Cracks Per 0.02 Mile	Yes	Contractor (Video Analysis)
Longitudinal Cracking	Linear Feet	Percent of Lane Length Per 0.02 Mile	Yes	Contractor (Video Analysis)
Patching/Potholes	Square Feet	Percent of Lane Per 0.02 Mile	No	Contractor (Video Analysis)
Rutting	Inches	Rut Depth Per 0.02 Mile	Yes	FHWA (Data Collection Vehicle)
Roughness	IRI	RCI	No	FHWA (Data Collection Vehicle)

In this study, the pavement condition evaluation was conducted by following the document titled “*Pavement Distress Identification Manual for the NPS Road Inventory Program*” [68]. That manual was developed based on the “*Distress Identification Manual for the Long-Term Pavement Performance Program*” [69]. Each surface distress was classified with one of several severity levels, low, medium, or high based on the criteria listed. Table 3.5 indicates the distress type and related features. The Surface Condition Rating (SCR) was calculated using the surface distress data which covers the distress type, severity, and other information. An IRI rating was assigned to compute the Roughness Condition Index (RCI). The overall Pavement Condition Rating (PCR) was computed based on the combination of RCI and SCR using

$$PCR = (0.60 * SCR) + (0.40 * RCI) \quad (3.2)$$

The following formulas describe the calculation of each distress index, roughness index, and SCR:

Alligator Crack Index (AC-INDEX)

$$AC_INDEX = 100 - 40 * [(\%LOW/70) + (\%MED/30) + (\%HI/10)] \quad (3.3)$$

Longitudinal Crack Index (LC-INDEX)

$$LC_INDEX = 100 - 40 * [(\%LOW/350) + (\%MED/200) + (\%HI/75)] \quad (3.4)$$

Transverse Crack Index (TC-INDEX)

$$TC_INDEX = 100 - \{ [20 * ((LOW/15.1) + (MED/7.5))] + [40 * (HI/1.9)] \} \quad (3.5)$$

Patching Index

$$PATCH_INDEX = 100 - 40 * (\%PATCHING/80) \quad (3.6)$$

Rutting Index

$$RUT_INDEX = 100 - 40 * [(\%LOW/160) + (\%MED/80) + (\%HI/40)] \quad (3.7)$$

Roughness Condition Index (RCI)

$$RCI = 32 * [5 * (2.718282 ^ {(-0.0041 * AVG\ IRI)})] \quad (3.8)$$

Surface Condition Rating Index (SCR)

$$SCR = 100 - [(100 - AC_INDEX) + (100 - LC_INDEX) + (100 - TC_INDEX) + (100 - PATCH_INDEX) + (100 - RUT_INDEX)] \quad (3.9)$$

In above equation LOW, MED and HI refer to the corresponding intensity of a specific distresses as defined in Reference [68]. For all indices, a higher value indicates a better road conditions, and vice versa. Under certain conditions, these index values calculated may be less than 0 or greater than 100. In those instances, index values of <0 default to 0, and index values >100 default to 100.

Figure 3.13 shows the result of PCR curve for the pavement performance of section 1068 over time using the relevant distress data from the LTPP database. The asphalt overlay treatment was applied in the year of approximately 1993, when the pavement condition was poor. Figure 3.14 indicates the pavement performance (PCR curve) from the time of conducting an overlay treatment to the time of implementing next maintenance or rehabilitation activity, and a linear function can be applied to characterize the pavement performance's deterioration rate.

The service life gain is calculated based on the rate parameter of the above curve. Considering an index of 60 as the condition to overlay, the life gain from applying asphalt overlay to section 1068 is $(100-60)/0.7962 = 50.6$ months = 4.2 years. This methodology also will be applied to analyze other sections.

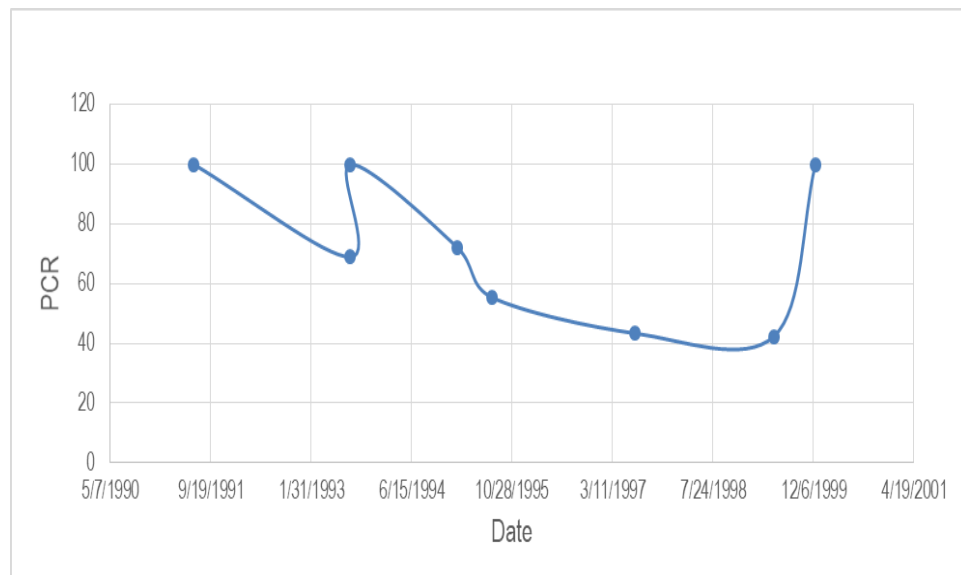


Figure 3.13: PCR Curve of Section 1068 over Time

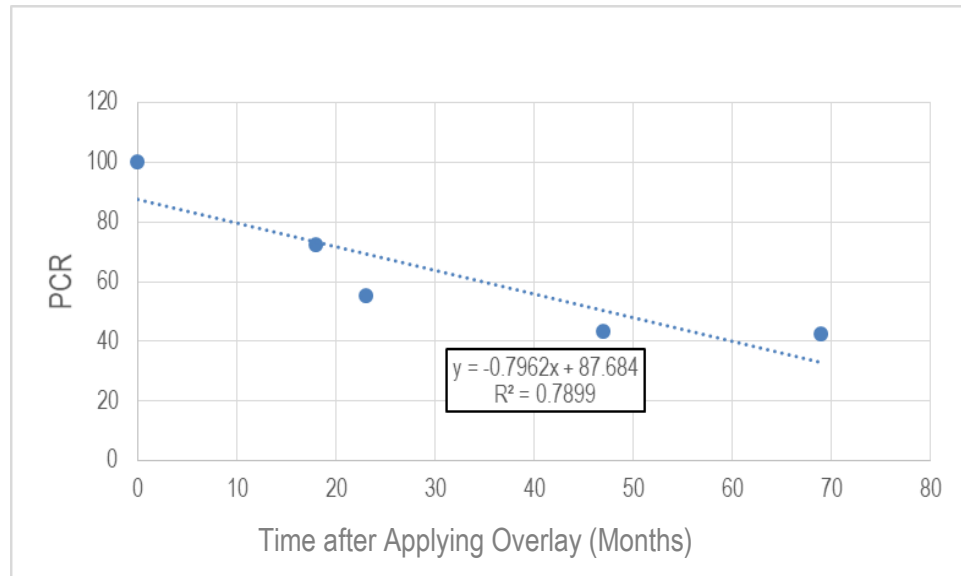


Figure 3.14: PCR Drop Rate over Time of Section 1068

In addition, sections 1087 and 6079, which have similar pavement structures as the numerical study cases, were simulated with the previously developed ABAQUS model. The fatigue life was calculated to compare with the field service life of asphalt overlay as shown by the LTPP database.

Chapter 4: Laboratory Study of Tack Coat

This chapter describes the analysis and results of several laboratory tests that studied the tack coat materials.

4.1 MODIFIED DIRECT SHEAR TEST RESULTS

Direct Shear tests are typically performed by varying the normal loads (18, 36 and 72 lbs in this study), and Mohr-Coulomb failure criterion is used to obtain shear strength (ASTM D3080). For each increment of normal stress, the peak shear strength is recorded. To identify the cohesion as well as frictional resistance component of the shear strength, the following equation is used:

$$\tau = c + \sigma \tan \phi \quad (4.1)$$

where τ is the shear strength, c is cohesion, σ is normal stresses and ϕ is the angle of friction. In the case of tack coat testing, c is the cohesive strength of applied tack and $\tan \phi$ is the frictional resistance offered by the two layers.

The test results on various tack coat types, application rates, and compaction efforts are included in Tables 4.1 and 4.2. It highly acknowledges that part of the direct shear tests on SS-1H, PG64-22, and PG70-22 were conducted by former research assistants. The test results for compaction pressure of 1.5 psi are included in Table 4.1 for different application rates while Table 4.2 includes influence of different compaction pressures at only one application rate of 0.03 gal/yd². The increase in compaction effort enhances the shear strength and increase in application rate reduces the shear strength with relative soft emulsion residue material. The loss in strength at the application rate of 0.05 gal/yd² can be attributed to creation of a thin film that acts as a lubricant between the specimens. Also, since the synthetic specimens are impervious, they do not allow the infiltration of emulsion as one would expect in the field due to porosity inherently present in the asphalt concrete mixtures.

The test results presented in Table 4.1 also indicate that the CRS-2 has the lowest shear strength in comparison to other tack coat types while Trackless C has the highest shear strength. The main reason for causing these performance difference would be that each type of tack coat

material were developed by using different raw materials, different refining or emulsion techniques, as well as different storage conditions. The test results also indicate that the cohesion values varied from 1.5 psi (for CRS-2) to 207 (for Trackless C) while friction angle varied from 2.7 (for CRS-2) to 36.4 (Trackless B) degrees. Although there is a change in the friction angle, the influence of friction angle is minimal on the measured shear strength.

Table 4.1: Test Results for Different Application Rates and 1.5 psi of Compaction Pressure (without clamping).

Tack Coat	0.05 gal/yd ²		0.03 gal/yd ²	
	Cohesion (psi)	ϕ (°)	Cohesion (psi)	ϕ (°)
SS-1H	5.0	7.0	8.1	3.0
CRS-2	1.5	2.9	2.4	2.7
PG64-22	11.0	13.0	15.4	17.0
PG70-22	18.7	15.0	24.1	12.0
Trackless A	13.3	1.0	16.4	8.0
Trackless B	Not Tested	Not Tested	123.32	36.4
Trackless C	Not Tested	Not Tested	206.76	32.2

Table 4.2: Test Results with 0.03 gal/yd² Application Rate and Different Compaction Pressures.

Tack Coat	Without Clamping (1.5 psi)		Clamping (20 psi)	
	Cohesion (psi)	ϕ (°)	Cohesion (psi)	ϕ (°)
SS-1H	8.1	3.0	13.7	7.0
CRS-2	2.4	2.7	4.9	11.0
PG64-22	15.4	17.0	22.7	15.0
PG70-22	24.1	12.0	24.0	7.0
Trackless A	16.4	8.0	26.0	15.0
Trackless B	123.3	36.4	128.4	35.6
Trackless C	206.8	32.2	217.5	29.5

The test results in Figures 4.1 through 4.5 better explain the influence of application rates and compaction pressure on the shear strength for each tack coat. Since Trackless B and C had significantly higher shear strength, the test results are separately presented in Figure 4.5. As expected, the cohesion provided by the asphalt binder (PG 64 and PG 70) is higher than the emulsions (CRS-2 and SS-1). The only emulsion Trackless A provided cohesive strengths similar

to that of PG 64-22. Further exploration of the Trackless A, identified the tack coat to be trackless tack coat.

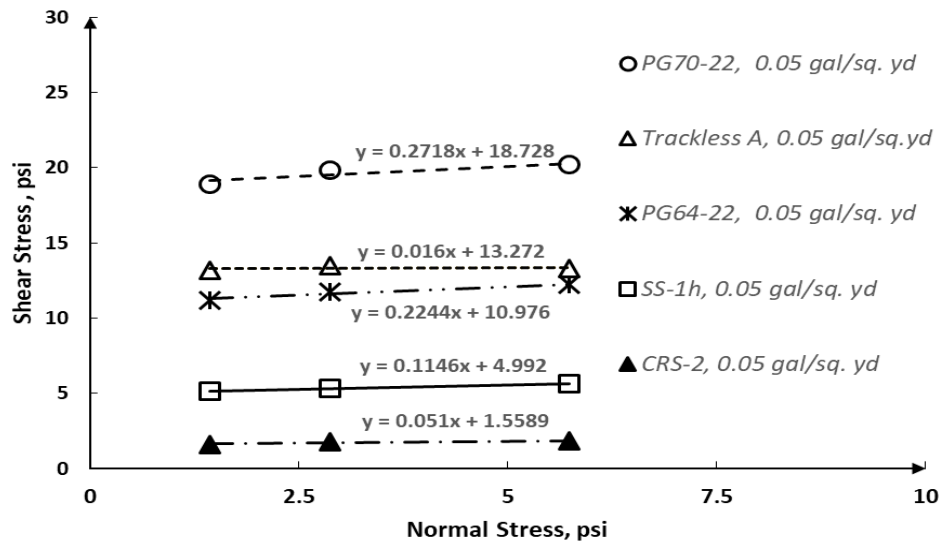


Figure 4.1: Failure envelopes for 1.5 psi of compaction pressure under Normal Loading of 18, 36 and 72 lbs.

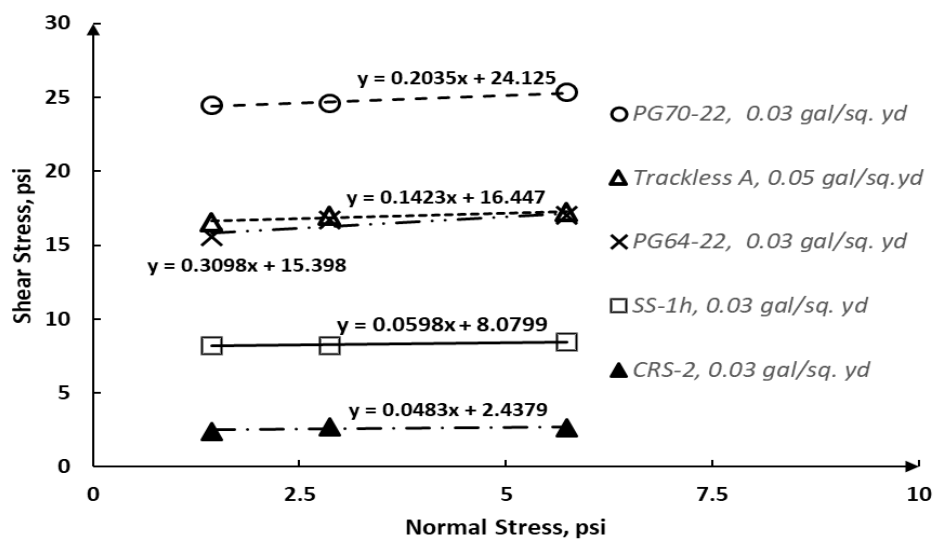


Figure 4.2: Failure envelopes for 1.5 psi of compaction pressure under Normal Loading of 18, 36 and 72 lbs.

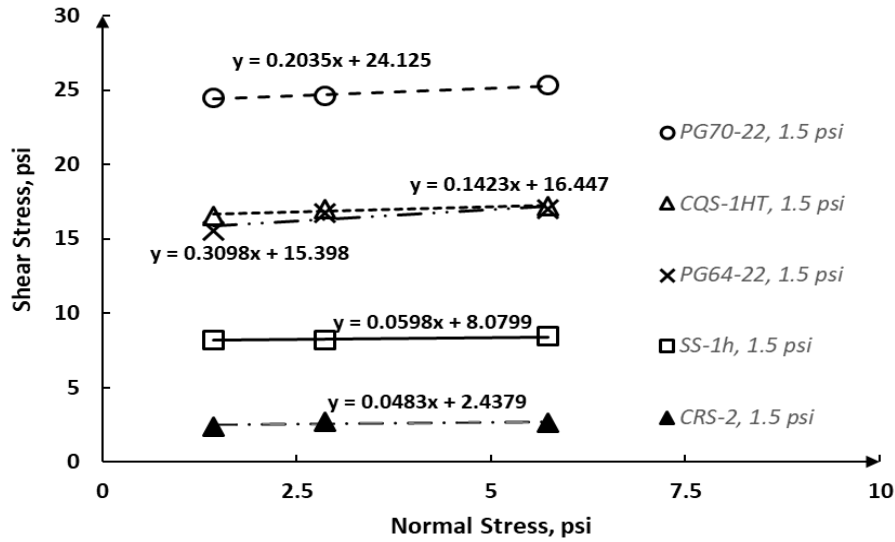


Figure 4.3: Failure envelopes for application rate of 0.03 gal/yd² under Normal Loading of 18, 36 and 72 lbs.

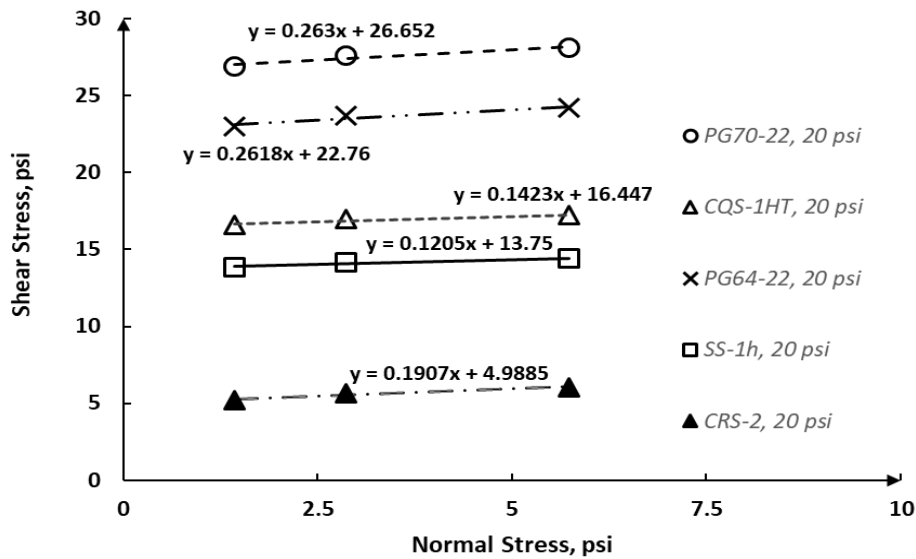


Figure 4.4: Failure envelopes for application rate of 0.03 gal/yd² under Normal Loading of 18, 36 and 72 lbs.

On comparing the influence of the application rate (Figures 4.1 and 4.2), the higher application rate negatively influenced shear or cohesive strength for all tack coat types. Since synthetic specimens were used, there are no pores that can be filled by the tack coat. Therefore, only the application rate of 0.03 gal/yd² was used for evaluating the quality of tack coat.

As shown in Figures 4.3 and 4.4, the second set of tests was performed by increasing the compression pressure from 1.5 psi to 20 psi. Effect of compaction on the cohesion value is significant for the weaker tack coats (tack coats with cohesion values less than 5 psi). For instance, CRS-2 cohesive strength increased from 1.5 psi to 5 psi (more than 3 times) with increase in the pressure from 1.5 psi to 20 psi. However, the similar influence was not found in tack coats with cohesion greater than 15 psi. For instance, the cohesive strength of the PG 70-22 tack coat (24 psi) remained the same at the two pressure levels. On the other hand, the improvement for PG6 4-22, and Trackless A are 50%, and 45%, respectively. This means that compaction plays an important role on the final characteristics of the interface layer, especially when the cohesion value of the tack coat material is low. The enhancement in the shear strength provided by compaction effort is minimal for good quality tack coats and significant for weak tack coats.

The Trackless B and C tack coats test results are included in Figures 4.5. These two tack coats performed significantly different than the others. The Trackless C tack coat exhibited shear strengths more than 200 psi while Trackless B exhibited strength in excess 120 psi. Additionally, the strength exhibited by Trackless C may have been even higher because a failure in terms of peak shear strength was not observed when the test was stopped. The test was stopped after horizontal deformation reached 0.12 in.

The shear strength of Trackless C tack coat is between 5 to 10 times greater than the shear strengths of the other tack coat types. The increase in shear strength occurred both in the cohesion and frictional components. Friction angles of more than 30° were measured for Trackless B and C tack coats. Although the frictional component increased, the magnitude of friction component is less than 5 psi (for 30° frictional angle and normal load of 72 lbs) in comparison to cohesion component of 120 or 200 psi. Since Trackless B and C tack coats are proprietary materials, the reasons for increase in frictional components could not be identified.

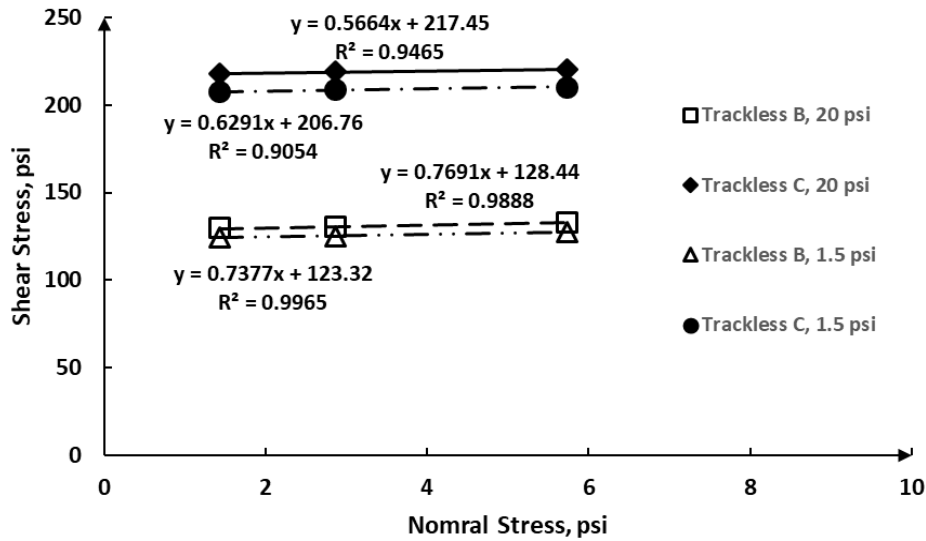


Figure 4.5: Trackless B and C tack coat test results with 0.03 gal/yd² rate of application under Normal Loading of 18, 36 and 72 lbs.

Figure 4.6 shows the variation in the K parameter representing the shear resistant modulus. The K parameter is sensitive to the type of tack coat and the curing condition. Generally, the clamping of 300 lbs resulted in higher shear modulus than the 20-lb curing loading except for Trackless A. Trackless B and C had higher K values than SS-1H, CRS-2, PG64-22, PG70-22 and trackless C. The effects of curing loading was less pronounced for the materials with higher shear moduli. CRS-2 had the lowest K value in comparison with other tacks.

Figures 4.7 and 4.8 demonstrate the variations in the fracture energy and critical strain. The fracture energy and critical strain followed a similar trend pattern: the trackless tack coats exhibited higher fatigue energy and critical strain than regular binders, followed by emulsions of SS and CRS. Generally, the clamping loading during the curing process can contribute the development of bonding strength. The fracture energy of tack coat in decreasing order were Trackless C, Trackless B, PG70-22, PG64-22, Trackless A, SS-1H and CRS-2. The decreasing order of critical strain with clamping was same with the fracture energy cases, and the scenario of without clamping by decreasing order were Trackless C, Trackless B, PG70-22, PG64-22, SS-1H, Trackless A and

CRS-2. Trackless C has critical strain as high as 4.8%, and CRS-2 failed at the strain level around 1%. Trackless tacks have superior shear strength than conventional tacks except trackless A.

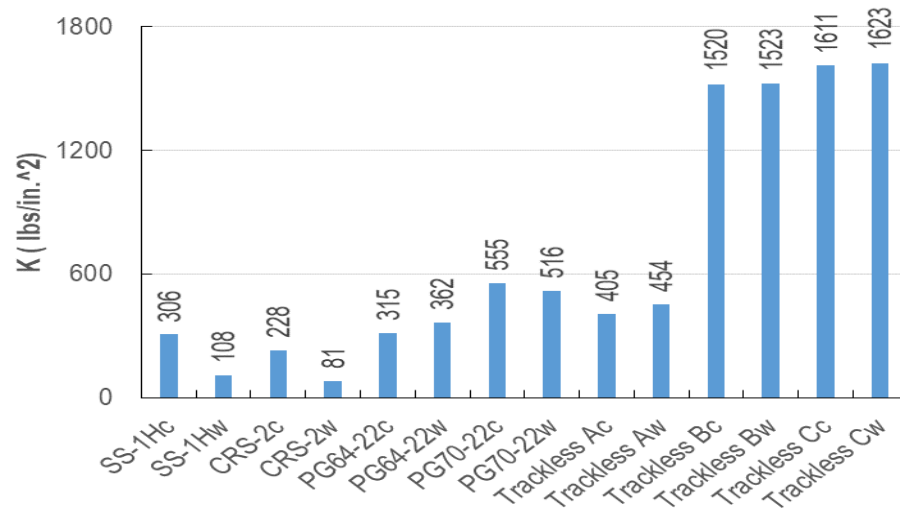


Figure 4.6: K Parameters of Tack Coat Materials.

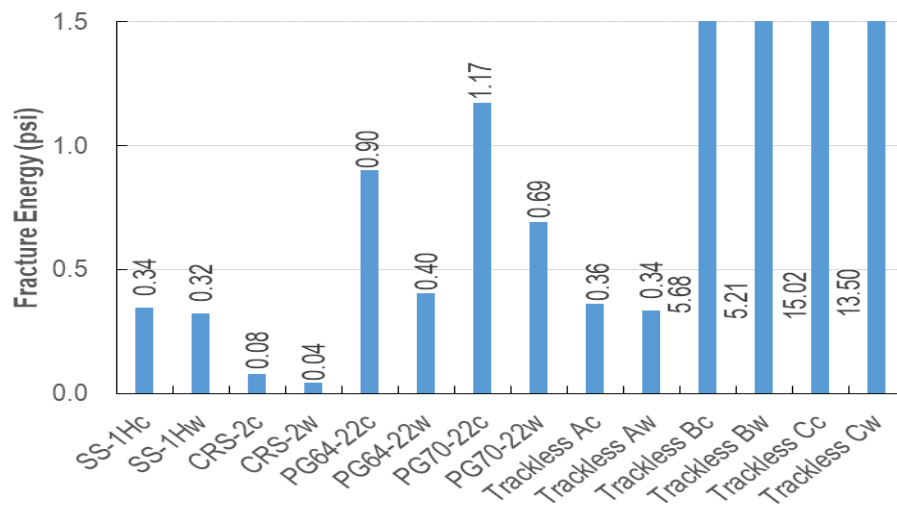


Figure 4.7: Fracture Energy of Tack Coat under Different Curing Condition.

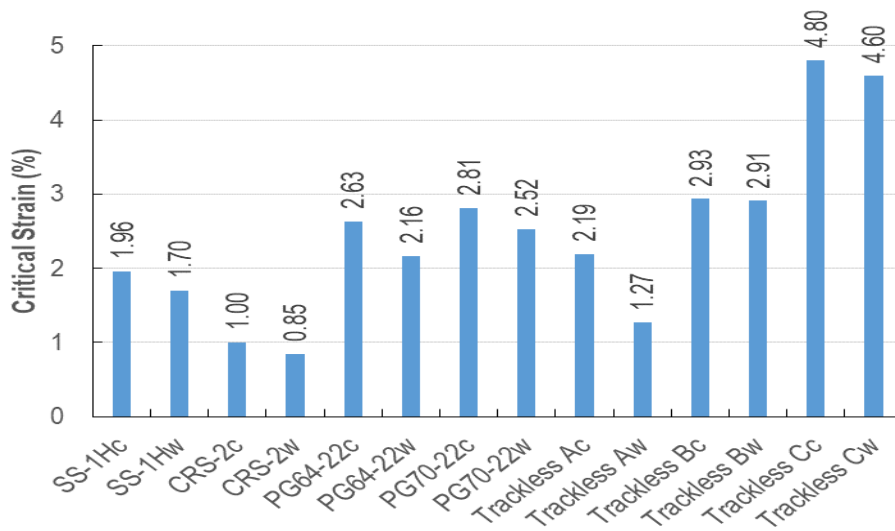


Figure 4.8: Critical Strain of Tack Coat in Direct Shear Test.

Figure 4.9 depicts the maximum shear strength of each tack coat. The shear strengths followed a similar order trend pattern with the fracture energies as shown in Figure 4.7. Overall, the direct shear test can successfully evaluate the bonding strength contributed by the chemical mechanics in terms of distinguishing different tack coat materials. Due to the complexity of shear strength mechanism between the pavement interfaces, it is crucial to qualify and quantify the shear resistant performance of tack coats under different application rate and curing condition.

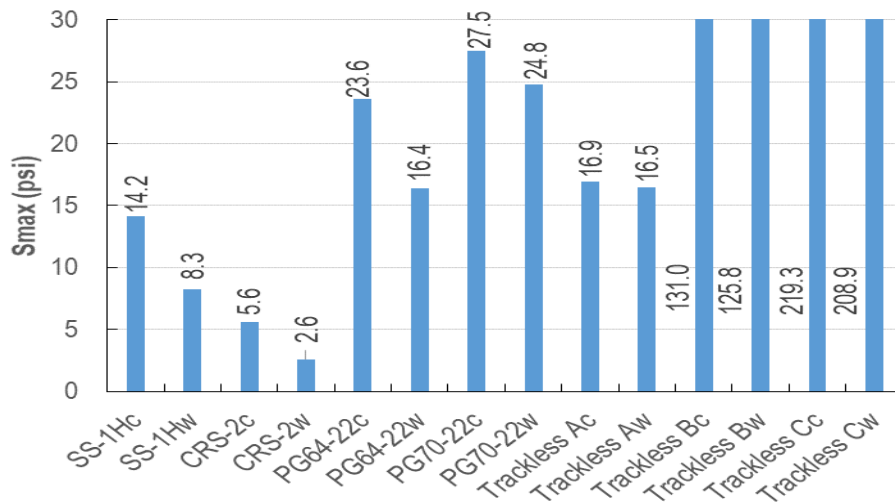


Figure 4.9: Maximum Shear Stress of Tack Coat Materials.

In addition to the direct shear tests, the laboratory study also included other physical tests, such as Dynamic Shear Rheometer (DSR) tests and Ductilometer test, to evaluate the rheological performance of these subject tack coat materials.

4.2 DSR TESTS

DSR test is commonly used for evaluating the Performance Grading (PG) of binder cement material. Nowadays, dynamic modulus is an essential parameter to indicate the binder's physical property under the conditions of different temperatures and loading frequencies.

The frequency sweep tests were carried out on the Bohlin CVO dynamic shear rheometer (DSR). A 25 mm plate with a gap of 1mm was used at the testing temperatures of 60°C, 80°C, and an 8 mm plate with a gap of 2 mm was selected for the rest of the testing temperatures. The time temperature superposition principle (TTSP) was applied in shifting a single curve of each temperature to a smooth master curve at the reduced frequency at a specified reference temperature. Among many existing models [70, 71, 72, 73], the Christensen-Anderson-Marasteanu (CAM) model, as shown in Equation 4.2, was used for the master curve construction.

$$G^* = G_e^* + \frac{G_g^* - G_e^*}{[1 + (\frac{f_c}{f})^k]^{m_e/k}} \quad (4.2)$$

where, G_g^* = the glassy modulus of asphalt binder; G_e^* = the equilibrium modulus representing the minimum modulus; f_c = the crossover frequency according to the phase angle at 45° and k and m_e = shape parameters.

Equation 4.3 is the function that models the phase angle at a specific temperature to the reference temperature.

$$\delta = \delta_m \left\{ 1 + \left[\frac{\lg(\frac{f_t}{f})}{R_d} \right]^2 \right\}^{-m_d/2} \quad (4.3)$$

where δ_m = the peak value of phase angle or the maximum value of the phase angle, R_d and m_d = shape parameters, and f_t = the frequency corresponding to the highest point of the phase angle.

A modified Kealble shift function, as shown in Equation 4.4, was implemented to determine the shift factor from the specific temperature to the reference temperature.

$$\log a_T = -c_1 \left(\frac{T - T_d}{c_2 + |T - T_d|} - \frac{T_r - T_d}{c_2 + |T_r - T_d|} \right) \quad (4.4)$$

where a_T = shift factor as a function of temperature T , c_1 , c_2 = fitting coefficients, T = test temperature of interest, °C or °K; T_g = glassy transition temperature; T_d = defining temperature, sets the location of the inflection point in the shift function.

Figure 4.10 demonstrates the result of the dynamic modulus master curve of each tack coat. The analysis showed that the CAM model is feasible for constructing the master curve for tack coat materials, including emulsion, regular PG binder, and trackless tack. Trackless A had a narrow range of shear complex modulus, which means it behaves more elastically. The residue of SS-1H had a similar dynamic modulus to PG64-22. A plateau in the master curve occurred at the high frequencies, where Trackless C had the highest shear modulus. The rheological performance indicators, such as the low shear viscosity (LSV), crossover modulus (G_c^*), and the Glover-Rowe (G-R) parameter, can be extracted from the dynamic modulus master curve under specific conditions [74].

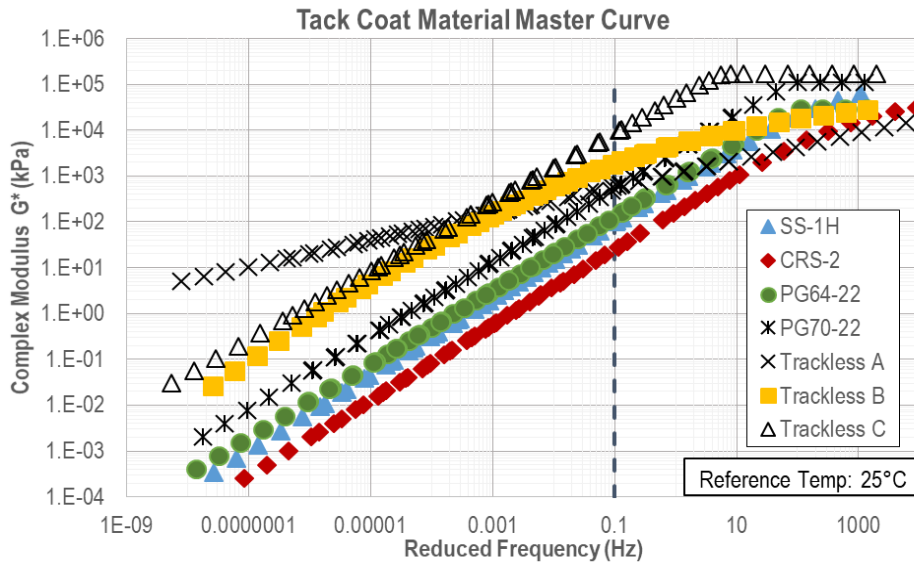


Figure 4.10: Shear Complex Modulus Master Curves of Tack Coat Materials

Comparing the master curves in Figure 4.10 with the results of the direct shear test in Figure 4.9, the shear complex modulus at a frequency of around 0.1 Hz yields a similar order with the maximum shear strength, while this observation was affected by the reference temperature and loading frequency.

Multiple Stress Creep Recovery (MSCR) tests were conducted as per AASHTO TP70 on the tack coats without the aging process; this was because performing rolling thin film ovens (RTFO) test with trackless tack, which has an exceptionally high modulus, is not practical due to the limitations of the equipment. The testing temperature selected for SS-1H and PG64-22 was 64°C, and for the other tack coats was 70°C. Figures 4.11 and 4.12 show the results of the MSCR tests. The results of non-recovery creep compliance for these two different loading levels (0.1 kPa and 3.2 kPa) were strongly correlated. Figure 4.11 also shows that CRS-2 had the highest J_{nr} in comparison with other tacks and the trackless tacks had the lowest J_{nr} which was close to zero, indicating these materials behave elastically at the loading level of 3.2 kPa. Figure 4.12 indicates that the recovery percentage has an exponential functional relationship with J_{nr} at 3.2 kPa, which is consistent with the findings of several other research studies [75, 76].

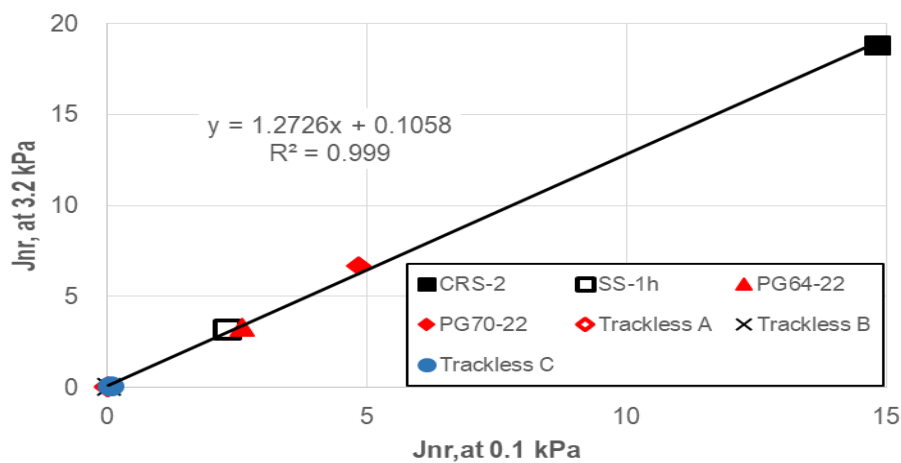


Figure 4.11: Correlation between Jnrs at Different Loading Level

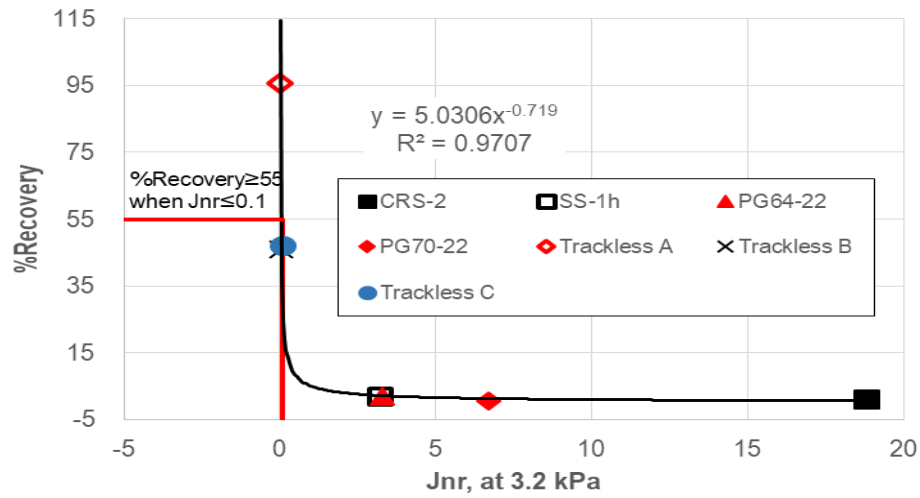


Figure 4.12: Correlation between Jnr, 3.2 with Recovery Strain

4.3 ELASTIC RECOVERY TESTS

Ductilometer test was initially developed to evaluate the ductility performance on asphalt binder material. The specifically molded binder sample was extending under a constant rate in a stainless steel insulated water bath which the temperature can be controlled.

The elastic recovery test was performed based on the specifications of Tex-539-C, which specifies a testing temperature of 10°C (50°F). As shown in Table 4.3, the results of this test were not promising according to the TxDOT specification (Item 300). One reason might be that the quality of the tack coat material became deficient during the storage process.

Table 4.3: Elastic Recovery Test Results

Tack coat	Test Temp (°C)	Rep1 (cm)	Rep2 (cm)	Rep3 (cm)	Recovery (%)
CRS-2	10	2.5	2.5	3	Fail
SS-1h	10	9.8	10	10	Fail
PG64-22	10	17.5	17.2	17	14
PG70-22	10	16.8	17	17	15
Trackless A	10	13.5	14	-	Fail
Trackless B	10	2.5	3	-	Fail
Trackless C	10	0	0	0	Fail

The scope of this study is limited that it lacked field information about the performance of tack coat materials. The correlation between laboratory tests and field performance should be established so that it is possible to better update the guidance on selecting high-quality tack coat material.

The following conclusions can be drawn from this study:

- ✓ The methodology used in this study can identify the quality of different tack coat materials in terms of shear strength without the influence of texture friction.
- ✓ The Mohr-Coulomb failure criterion can be adopted to characterize the relationship between tack coat's shear strength and normal load.
- ✓ Trackless tack has superior strength performance in comparison to conventional tack coats.
- ✓ The cohesion characteristics of the tack coats significantly influence their bond strengths.

Chapter 5: Numerical Modeling of Pavements with Thin Asphalt Overlays

This study applied the ABAQUS program to simulate the response of asphalt overlay pavements under traffic loading. A parametric study was carried out to evaluate the sensitivity of several factors in the response of overlay pavement over depth. These factors included the interface bonding condition, HMA property, base modulus, existing AC layer thickness, and overlay thickness. The parameters extracted from the output file for each case included the tensile stress, tensile strain, shear stress, shear strain, vertical strain, and vertical deformation.

5.1 ABAQUS OUTPUT

Figure 5.1 shows typical output results from the ABAQUS viewer. The location of the critical stress or strain was determined by the output results. The Case 1 pavement structure in Table 3.4 is used to demonstrate the typical results. That pavement structure consists a 4-in.-thick existing AC layer, a 0.5-in.-thick overlay both with elastic modulus of 500,000 psi, a 6-in.-thick base layer with a modulus of 30,000 psi with a fully-bonded interface condition; over a subgrade with a modulus of 7,000 psi.

Figures 5.2 to 5.8 depict several critical stresses and strains with depth for the example demonstration. All the cases were simulated under same traffic loading. This study was to investigate the influence of structural layer thickness, layer properties, and layer interface cohesive behavior on the response of combined overlay pavements. The critical tensile stress is located at the center of the tire. Figure 5.2 indicates that the horizontal stress changes from around -104 psi in compressive state to 67 psi in tensile state over the depth of the overlay and AC layer. The maximum tensile stress is at the bottom of the existing AC layer.

Figure 5.3 shows the result of vertical stress over depth, indicating the vertical stress is decreasing from the pavement surface to subgrade. As shown in Figure 5.4, the shear stress increases from 7 psi at the pavement surface to around 30 psi at the depth of around 2.25 in. which is located at the middle of the asphalt layer. Then, it gradually decreases with depth.

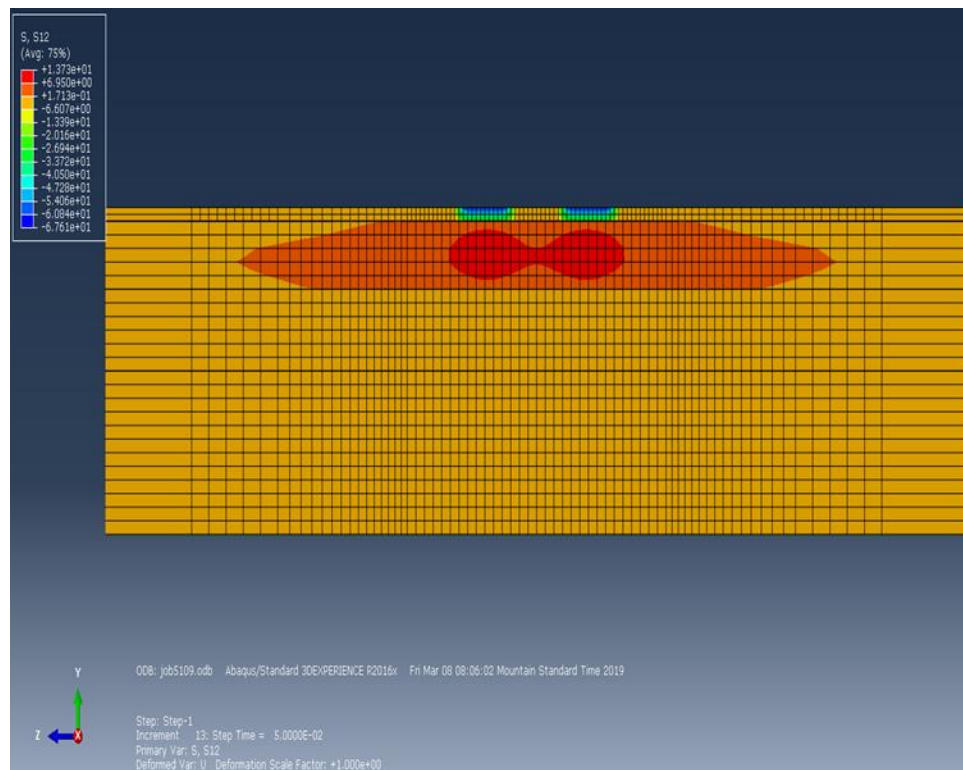
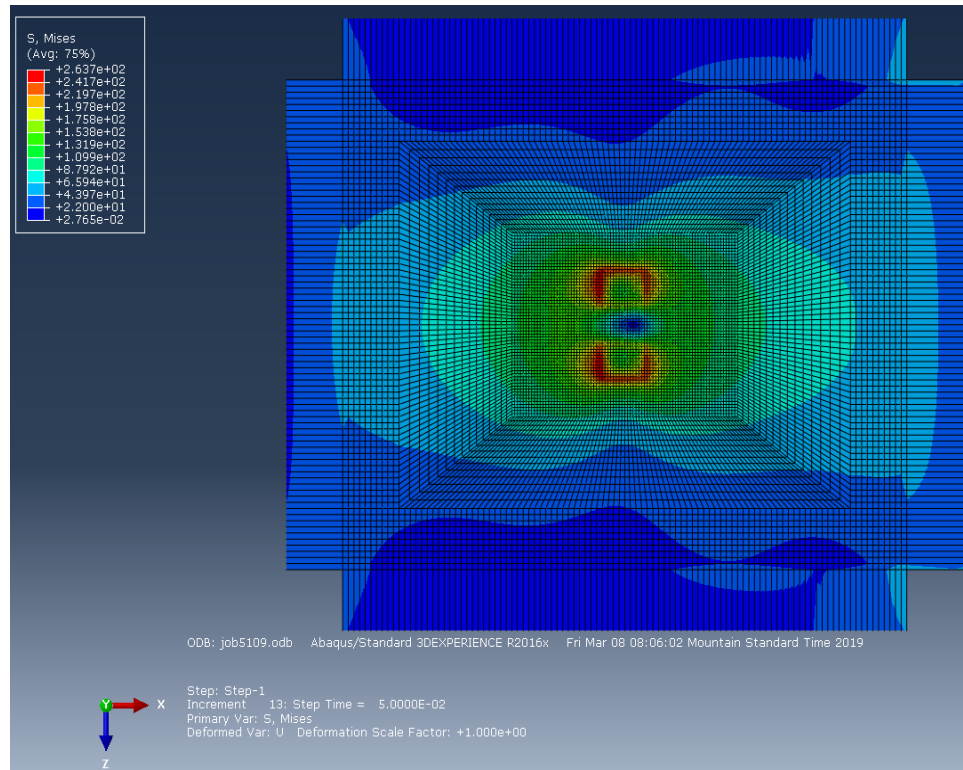


Figure 5.1: Example of ABAQUS Output

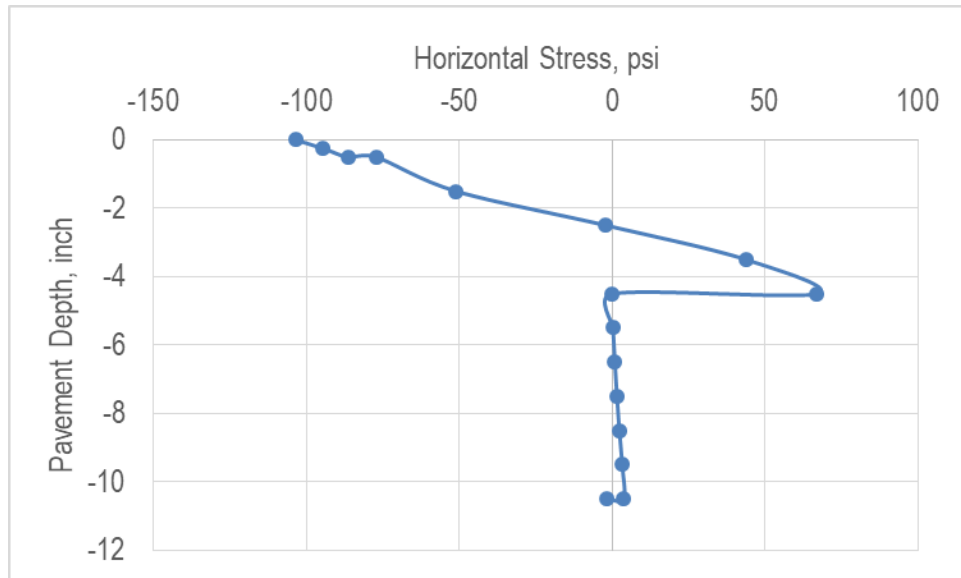


Figure 5.2: Typical Variation in Horizontal Stress with Depth

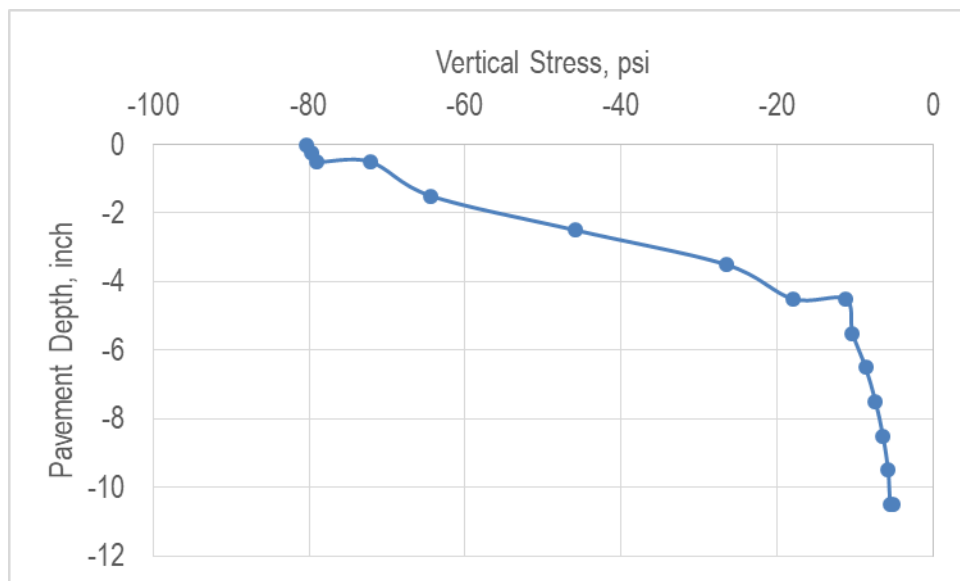


Figure 5.3: Typical Variation in Vertical Stress with Depth

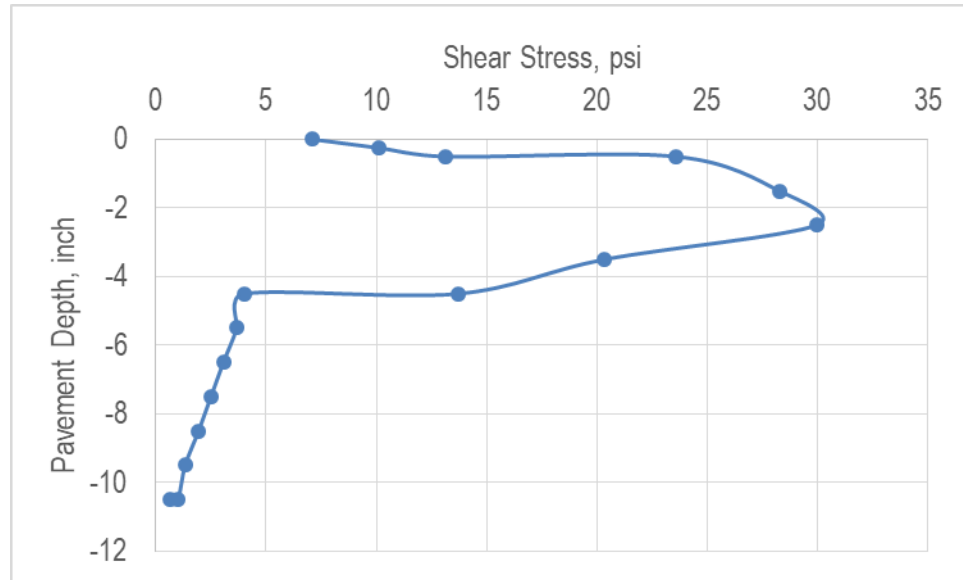


Figure 5.4: Typical Variation in Shear Stress with Depth

Figure 5.5 shows the variation in horizontal strain with depth. The strains are in compressive state within the overlay and it changes to tensile state at the middle of the asphalt layer. The strain reaches its maximum at the bottom of the existing AC layer. The comparison of the bonding condition's effects on horizontal strain will be discussed later.

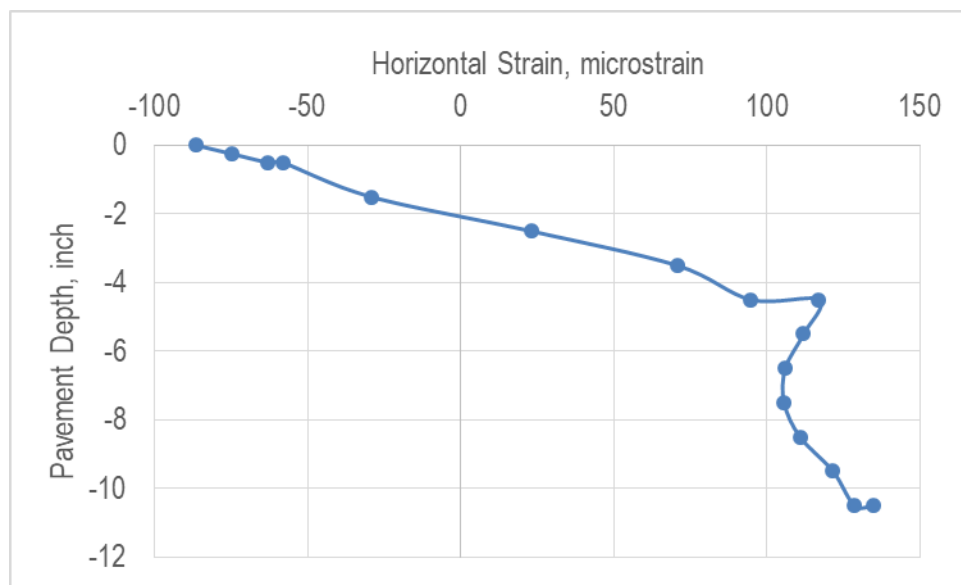


Figure 5.5: Tensile Strain of 4051 over Depth

Figure 5.6 shows the variation in vertical strain with depth. The maximum strain is reached at the top of the subgrade. The change in the rate of strain is related to the elastic modulus of each layer.

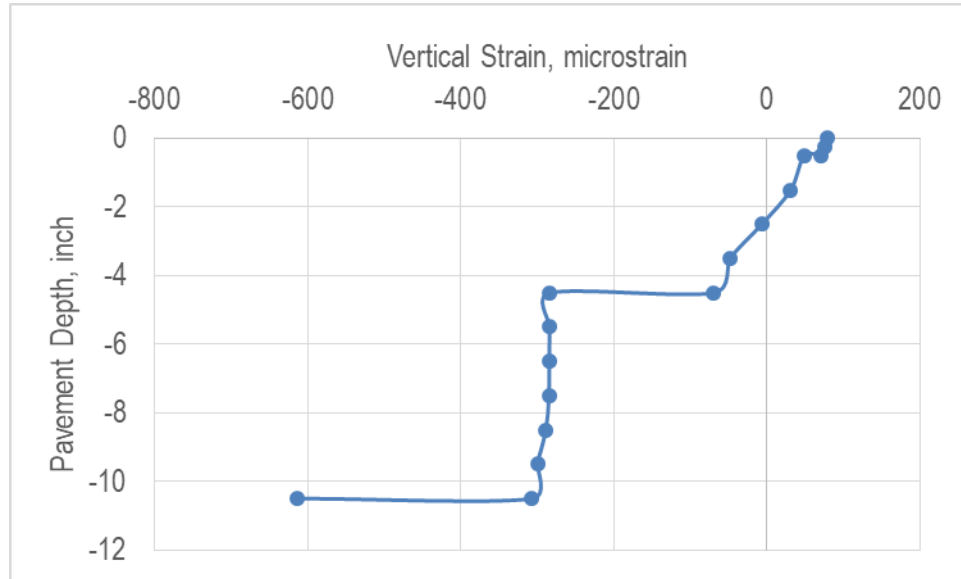


Figure 5.6: Vertical Strain of 4051 over Depth

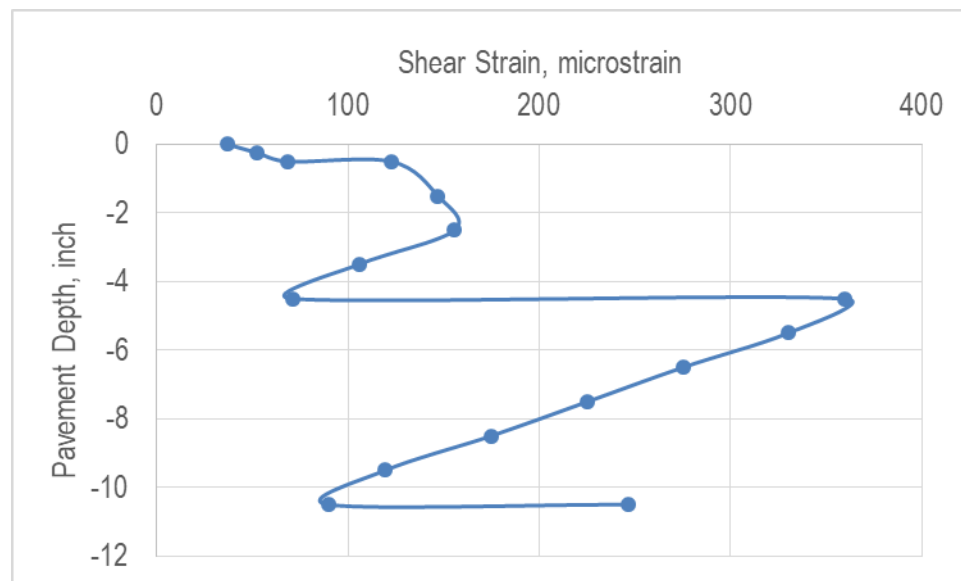


Figure 5.7: Shear Strain of 4051 over Depth

Figure 5.7 shows the variation in the shear strain with depth. The shear strain increases from 37 micro-strains ($\mu\epsilon$) at the pavement surface to 155 $\mu\epsilon$ at the middle of the asphalt layer, then drops to around 71 $\mu\epsilon$ at the bottom of the AC layer.

Sixty cases of ABAQUS were executed to evaluate the influences of the asphalt overlay pavements' properties on their responses to traffic loading, as discussed below.

5.2 DATA ANALYSIS

A matrix comparison study factored in potential pavement layer thickness, material modulus, and bonding condition, evaluating the influence of these on the asphalt overlay pavement performance in respect to shear stress, tensile stress, vertical stress, and fatigue life. The following subsections provide the results of the ABAQUS modeling, and relevant discussion.

5.2.1 Pavement Layer Thickness

Figures 5.8 to 5.11 show the results of tensile stress at the bottom of existing asphalt pavement layers for different pavement structures, with different overlay and AC layer thicknesses, different layer properties, and different interface conditions (including fully-bonded, partially-bonded, and unbonded conditions).

Figure 5.8 shows that the tensile stress level is decreasing with increasing the thickness of the overlay and the AC layer. Interestingly, when the overlay interface has fully-bonded condition, AC4inO1.5in and AC5inO0.5in, AC4inO2in and AC5inO1in, which have the same HMA thicknesses, also have close tensile stress levels at the bottom of the AC layer. Increasing the AC layer can reduce the tensile stress level. These trends are consistent with the theory described in Reference [78].

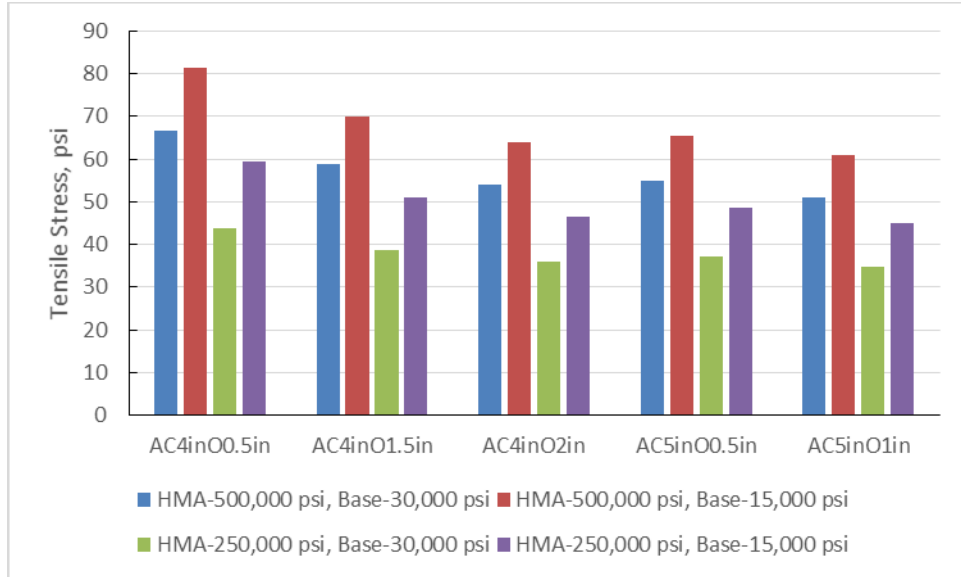


Figure 5.8: Tensile Stress at bottom of Existing AC Layer under Fully-bonded Condition

Figures 5.9 and 5.10 show similar trends in fully-bonded asphalt overlay pavement. While with deficient interface bonding condition, the stress state at the interface is more complicated, the tensile stress level at the bottom of AC layer is increasing, and the influence of the existing AC layer thickness is more significant than the overlay layer thickness.

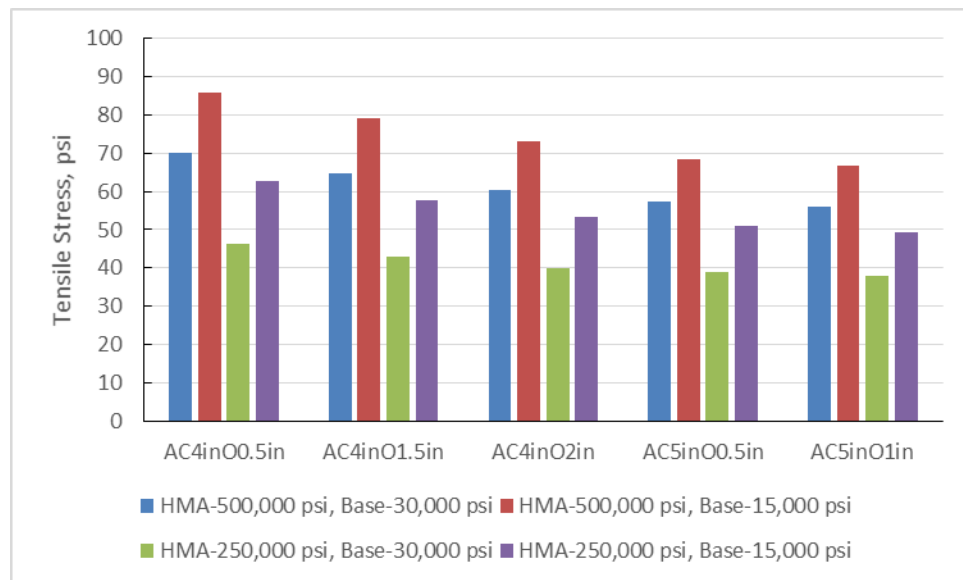


Figure 5.9: Tensile Stress at bottom of Existing AC Layer under Partially-bonded Condition

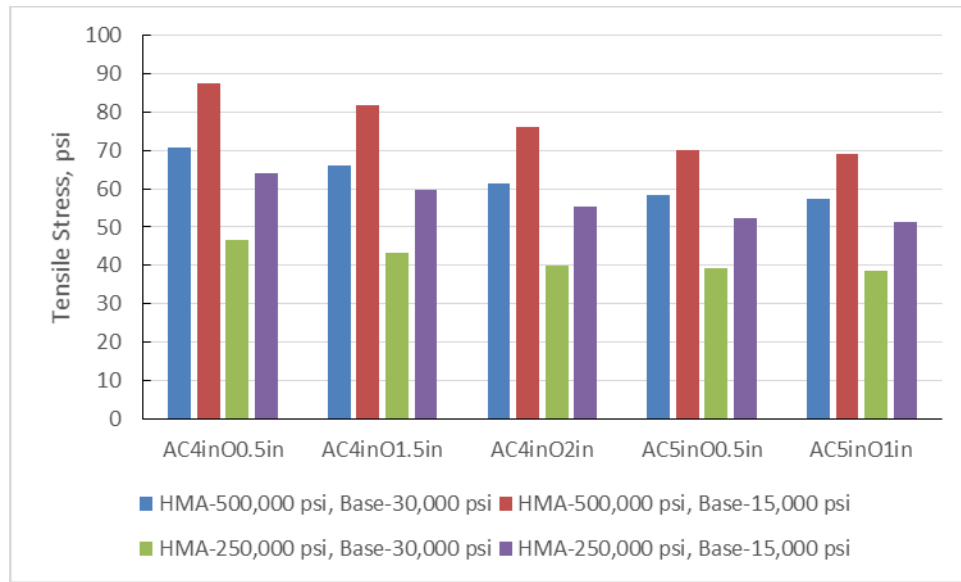


Figure 5.10: Tensile Stress at bottom of Existing AC Layer under Non-bonded Condition

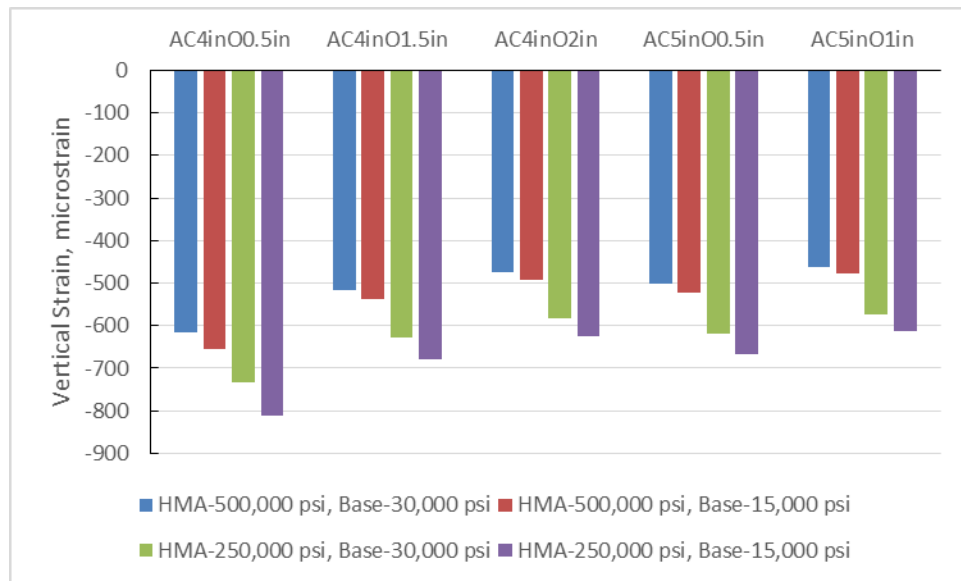


Figure 5.11: Vertical Strain at top of Subgrade Layer under Fully-bonded Condition

Here in Figures 5.11 to 5.13 we see that the whole HMA layer thickness affects the vertical strain distribution of asphalt overlay pavement over depth. The vertical strain decreases with increasing HMA thickness. AC4inO1.5in (Existing AC layer with thickness of 4 inches and overlay thickness of 1.5 inches), AC5inO0.5in, AC4inO2in and AC5inO1in which have same total

thickness also have same level of vertical strain at the top of the subgrade. Under partially-bonded and non-bonded conditions, the vertical strain increases when compared with fully-bonded condition. The thicker existing AC layer has a little lower vertical strain. It should be noted that in Figure 5.14, the effect of asphalt overlay on the vertical strain at the top of subgrade is minimized, and the existing AC layer governs the level of vertical strain.

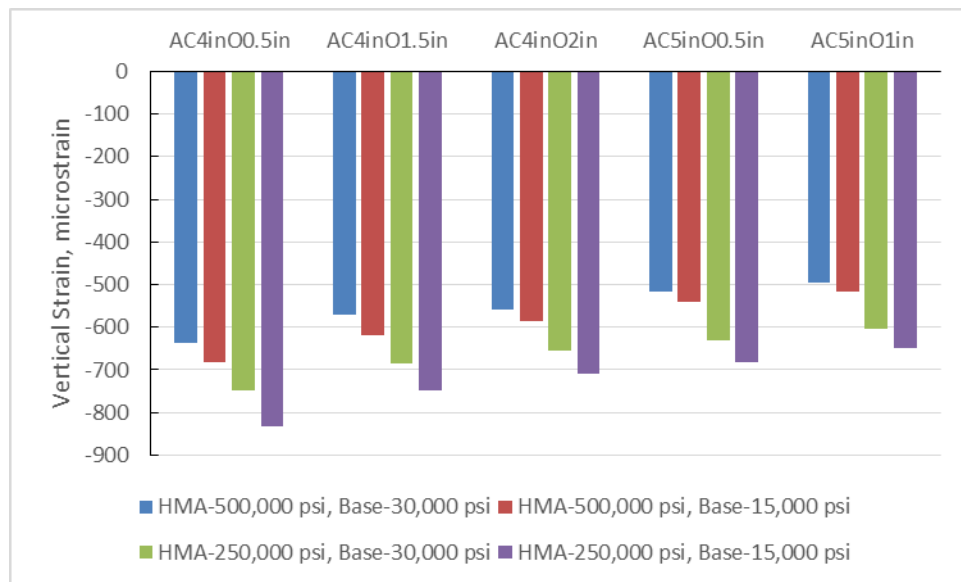


Figure 5.12: Vertical Strain at top of Subgrade Layer under Partially-bonded Condition

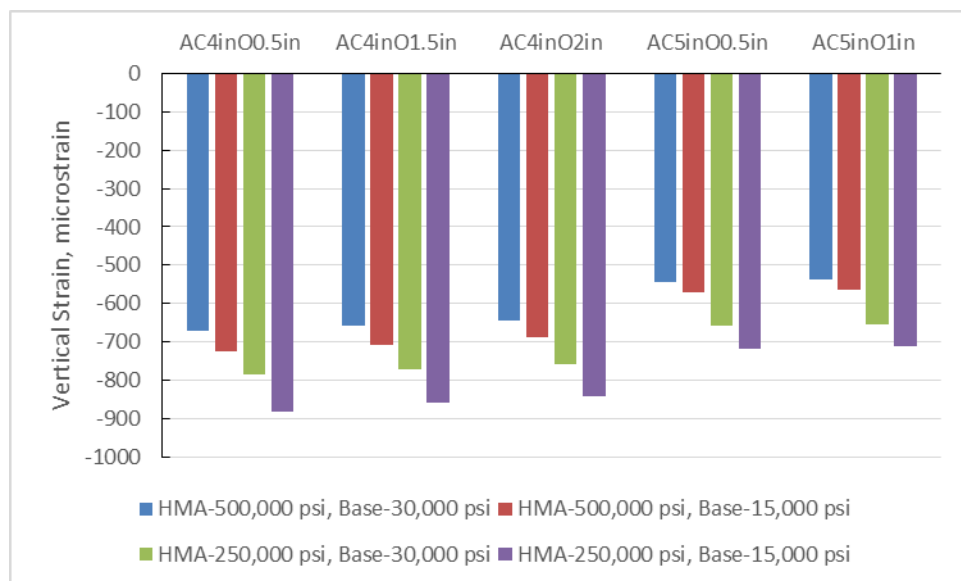


Figure 5.13: Vertical Strain at top of Subgrade Layer under Non-bonded Condition

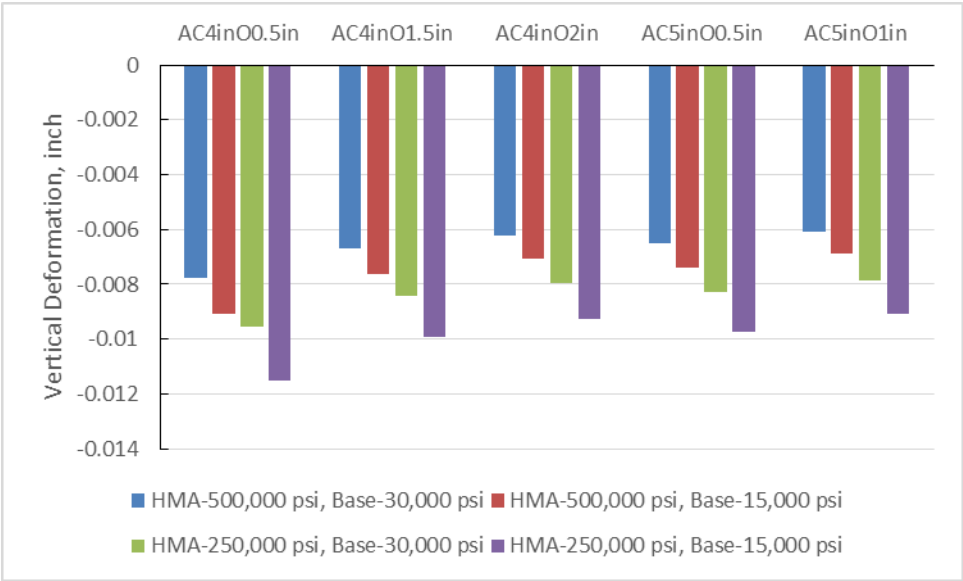


Figure 5.14: Vertical Deformation of Asphalt Overlay Pavement under Fully-bonded Condition

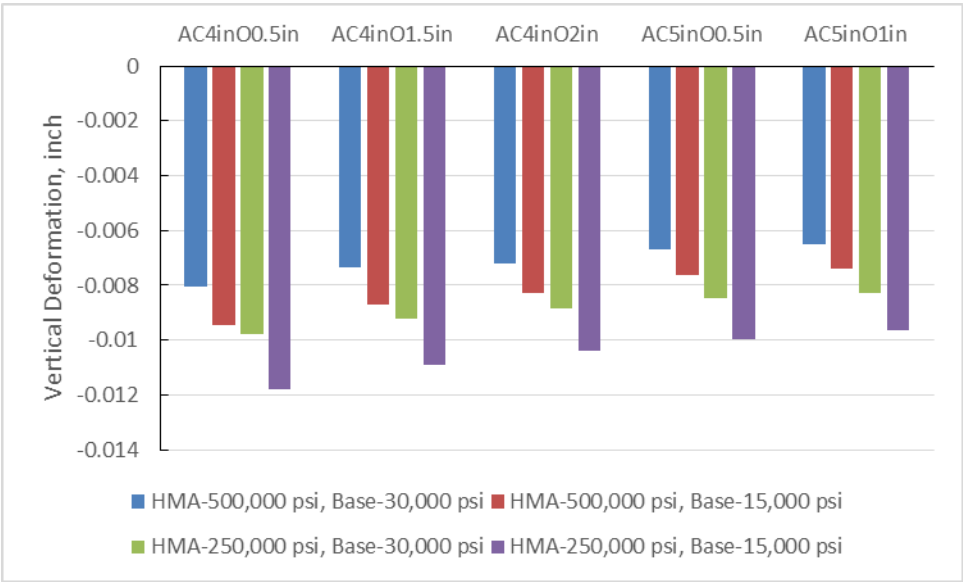


Figure 5.15: Vertical Deformation of Asphalt Overlay Pavement under Partially-bonded Condition

The Figures 5.14 to 5.16 show vertical deformation of ABAQUS modeling with pavement properties and different interface conditions over depth. This trend is similar to the vertical strain. This makes it clear that the combination of the overlay thickness and the interface bonding

condition determines the vertical deformation level. Figure 5.15 (above) shows that under the no-bonding condition, the vertical deformation is determined by the thickness of the existing AC layer. However, all these analysis were conducted for asphalt overlay pavements, which have the same properties.

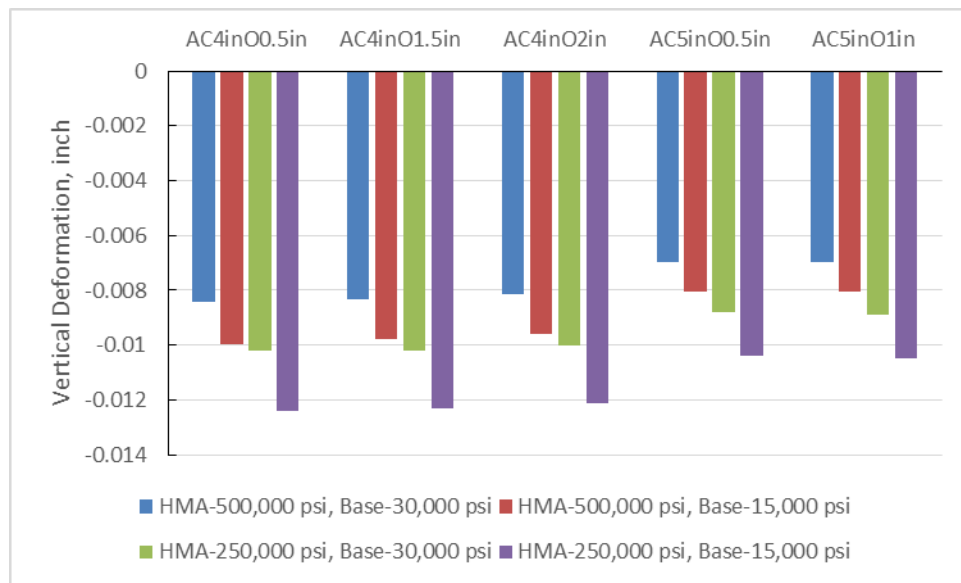


Figure 5.16: Vertical Deformation of Asphalt Overlay Pavement under Non-bonded Condition

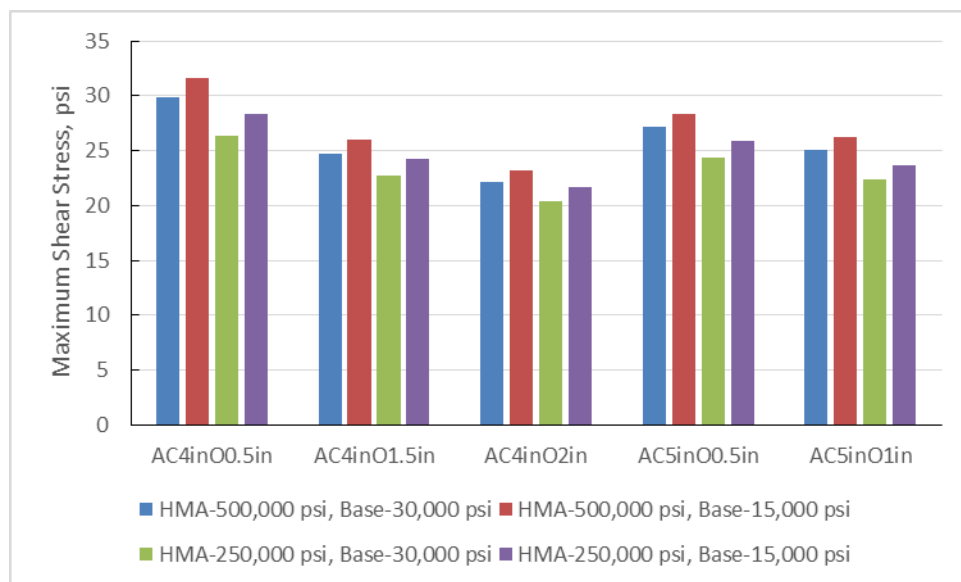


Figure 5.17: Maximum Shear Stress of AC Layer under Fully-bonded Condition

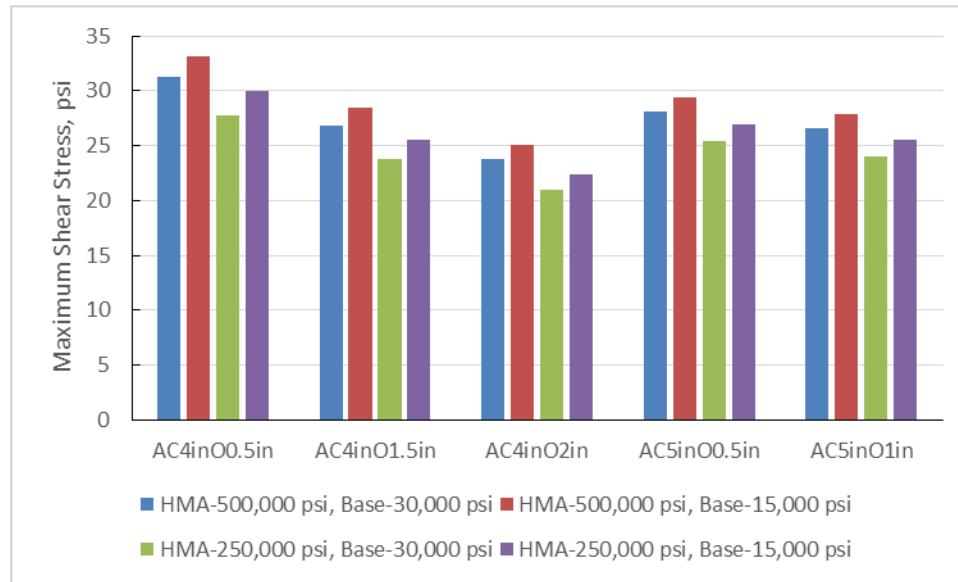


Figure 5.18: Maximum Shear Stress of AC Layer under Partially-bonded Condition

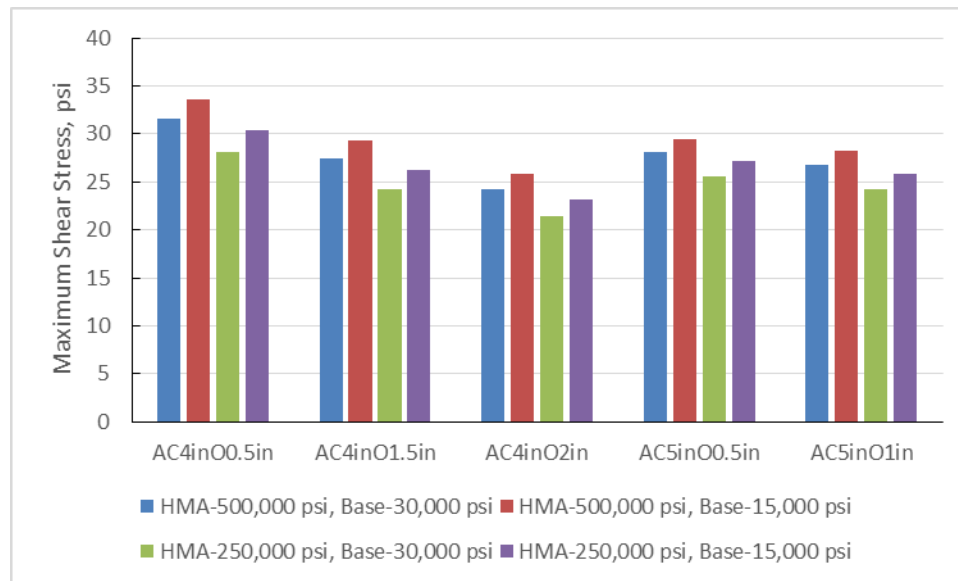


Figure 5.19: Maximum Shear Stress of AC Layer under Non-bonded Condition

Figure 5.17 to Figure 5.19 (above) show the maximum shear stress in the pavement's asphalt layer under different bonding conditions. A good bonding condition can somewhat reduce the stress level, while pavement thickness plays a more important role in governing the maximum value of shear stress.

5.2.2 Pavement Layer Elastic Modulus

The following subsection shows the results from an analysis of the effect of pavement layer property-elastic modulus on several critical responses.

Figure 5.20 (below) displays the results of tensile stress of A4O5 with different elastic modulus under different bonding conditions. It shows that the material property of elastic modulus has significant effect on the tensile stress level even when the bonding condition is the same. The larger the HMA modulus, the higher the tensile stress at the bottom of the AC layer. The case ID is referred to Table 3.4 in Chapter 3.

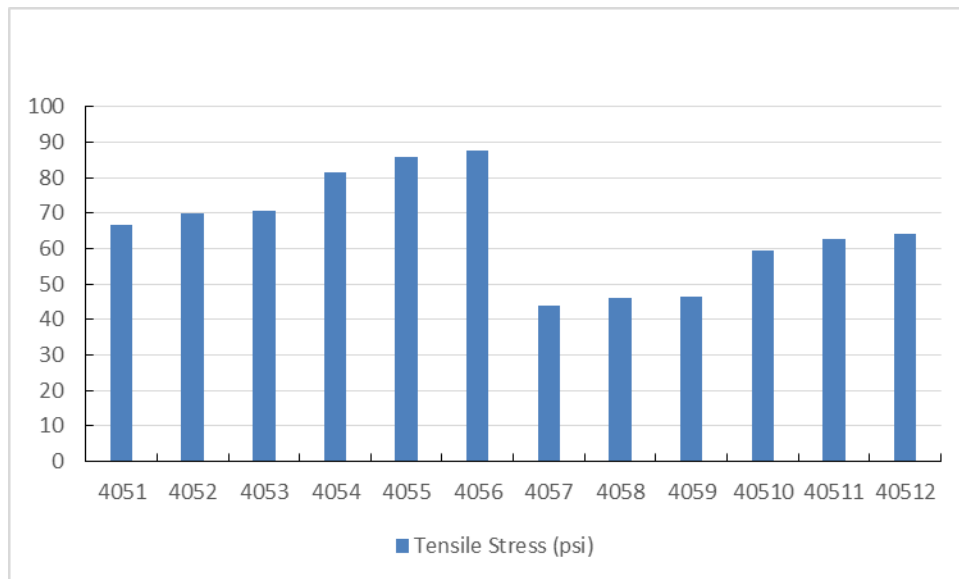


Figure 5.20: Tensile Stress at bottom of AC Layer

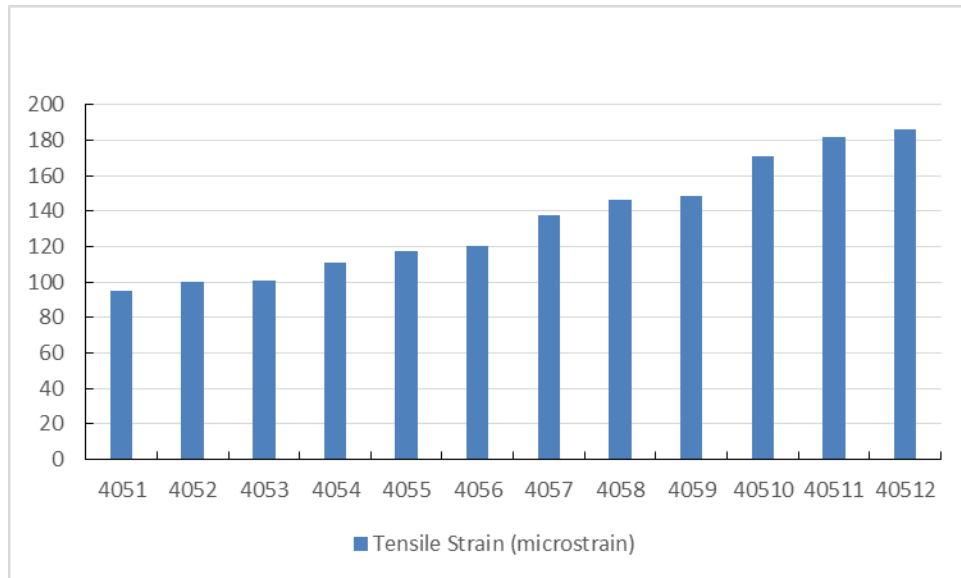


Figure 5.21: Tensile Strain at bottom of AC Layer

Figure 5.21 (above) shows how different layer properties and bonding conditions affect tensile strain at the bottom of the AC layer of A4O5. Here we see the strain level increase when the elastic modulus of asphalt layer, or base layer, is lower.

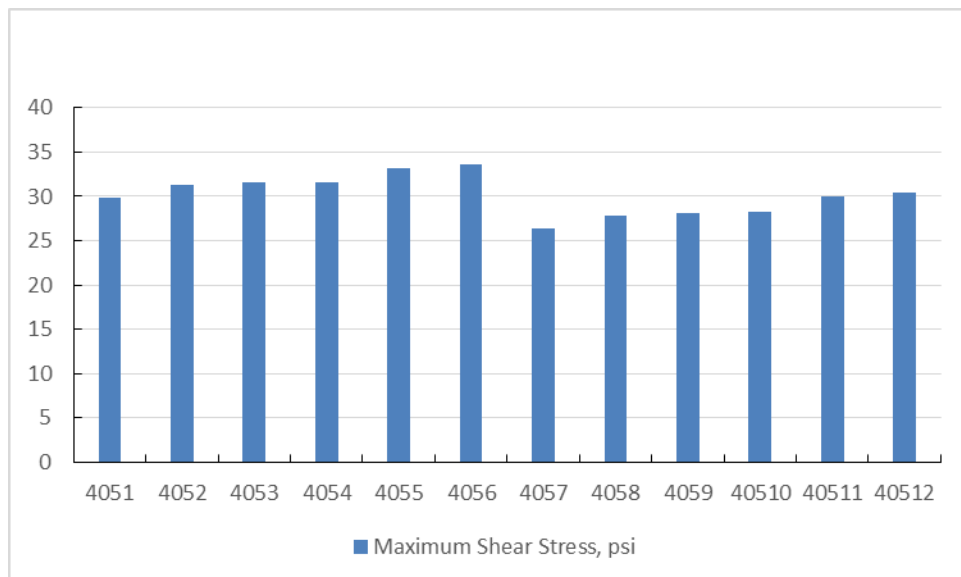


Figure 5.22: Maximum Shear Stress at AC layer

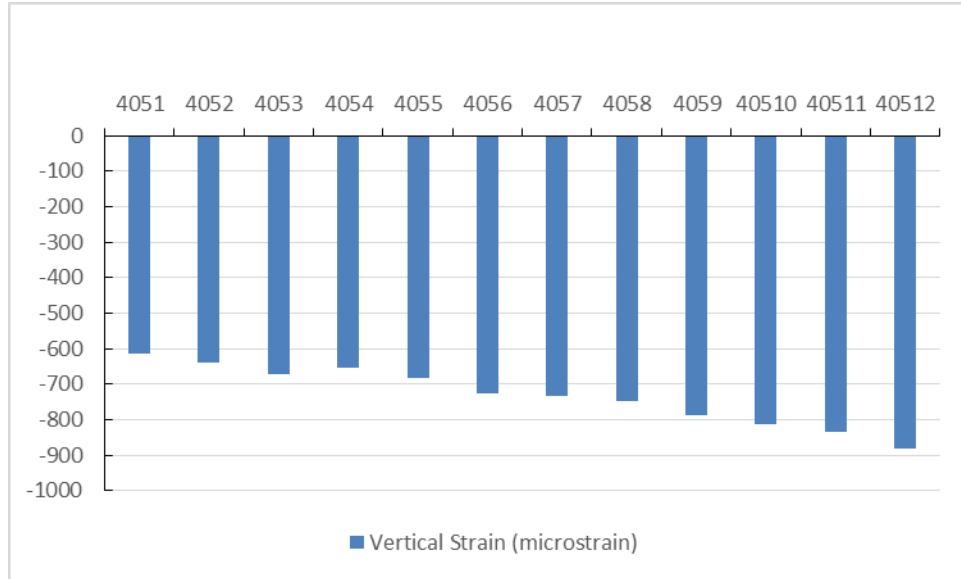


Figure 5.23: Vertical Strain at top of Subgrade

Figure 5.22 (above) shows the maximum shear stress of A4O5 with different properties of elastic modulus. Both the AC layer and the base layer modulus have an influence on the shear stress level of pavement structure. On the overlay surface the deformations ordered by decreasing are 2515, 2530, 5015, and 5030. On the top of the subgrade the deformations ordered by decreasing are 2530, 2515, 5030, and 5015. This shows that the higher the base layer modulus, the lower the rate of deformation increase.

Figure 5.23 and Figure 5.24 (see below) show the results of vertical deformation of pavement, and vertical strain at the top of the subgrade layer, respectively. This trend is similar to that of the tensile strain.

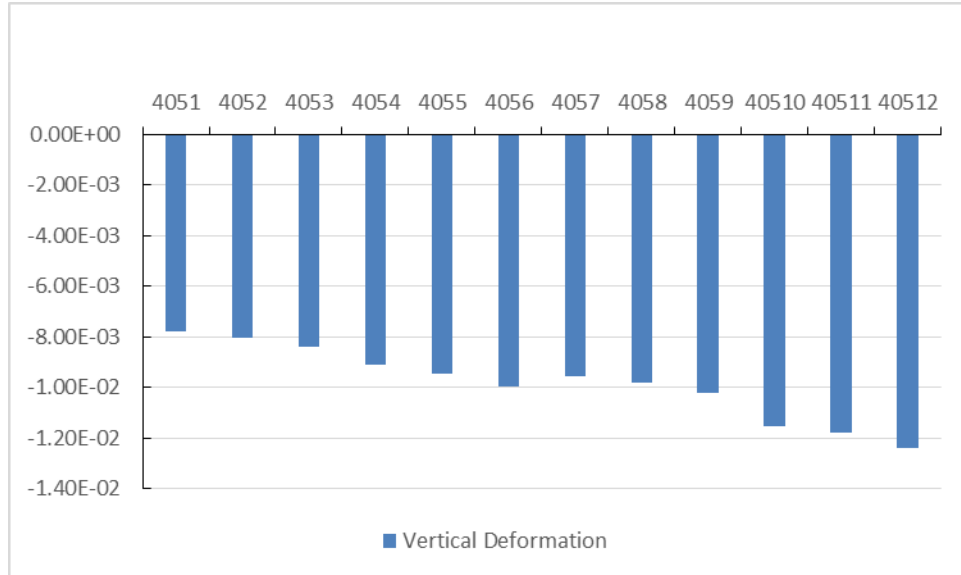


Figure 5.24: Vertical Deformation

The results with other overlay pavement structures are tabulated in Appendix A. Part of comparison study was conducted in following section.

5.2.3 Bonding Condition on Interface Response

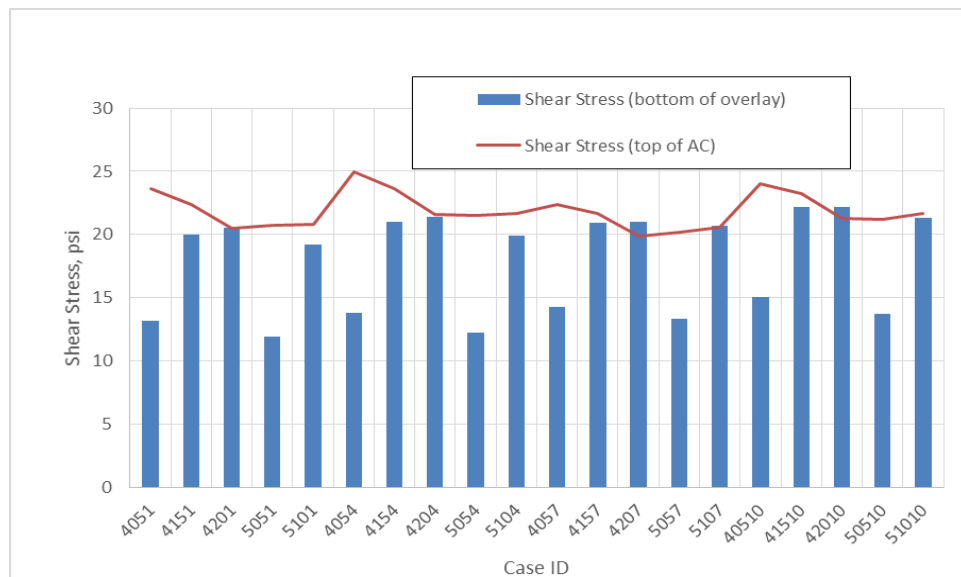


Figure 5.25: Shear Stress at the Interface under Full-bonding Condition

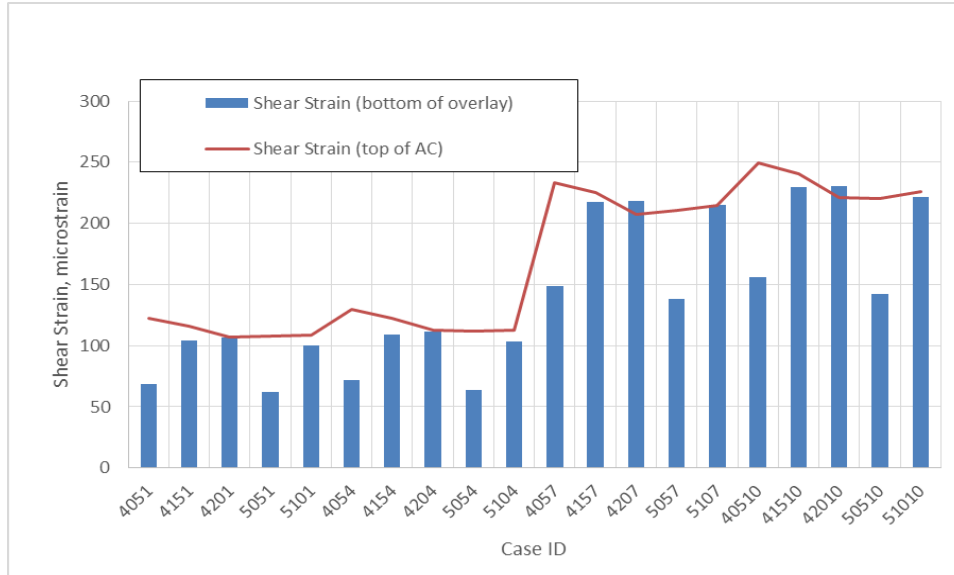


Figure 5.26: Shear Strain at the Interface under Full-bonding Condition

Figure 5.25 and 5.26 (above) show tensile stress and strain at the bottom of the AC layer. Generally, a good bonding condition helps reduce the tensile stress and strain level at the bottom of the AC layer. The shear strain indicates that the strain levels at the bottom of the overlay layer and top of the AC layer are close under full-bonding conditions. These plots also indicate the effect of layer thickness and layer modulus on the stress and strain. This has been discussed in the preceding subsections.

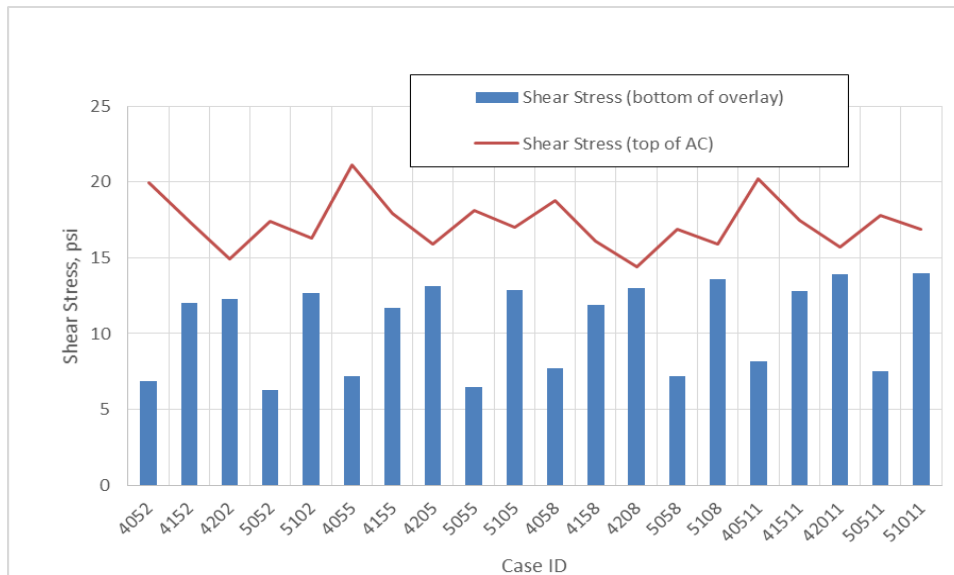


Figure 5.27: Shear Stress at the Interface under Partial-bonding Condition

Figure 5.27 and Figure 5.28 illustrate shear stress and strain at the interface under partial-bonding conditions. The difference between these two shear stresses increased at the interface under partial-bonding conditions. The shear stress at the bottom of overlay layer decreased in comparison with the full-bonding condition. We also see that the modulus of the AC layer plays an important role in determining the shear stress and strain.

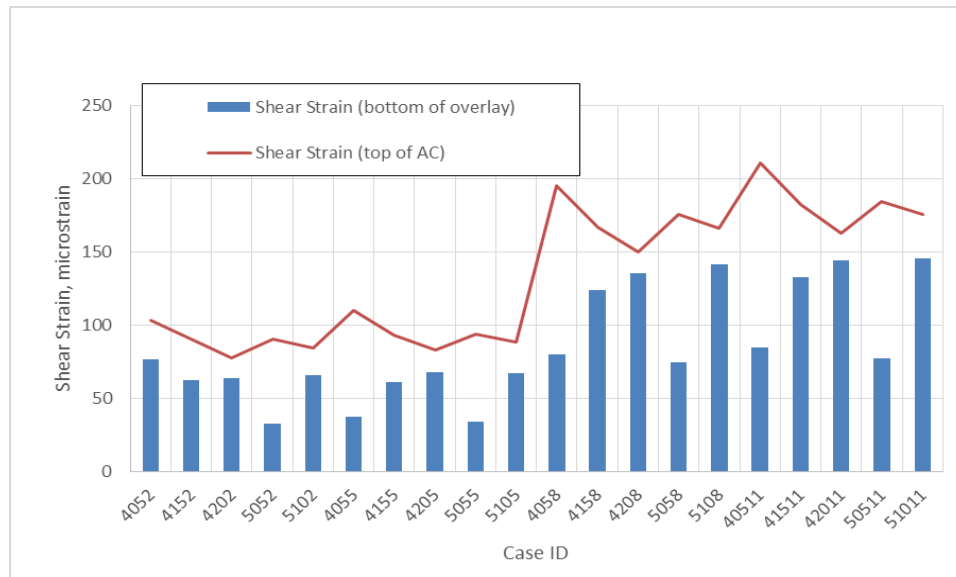


Figure 5.28: Shear Strain at the Interface under Partial-bonding Condition

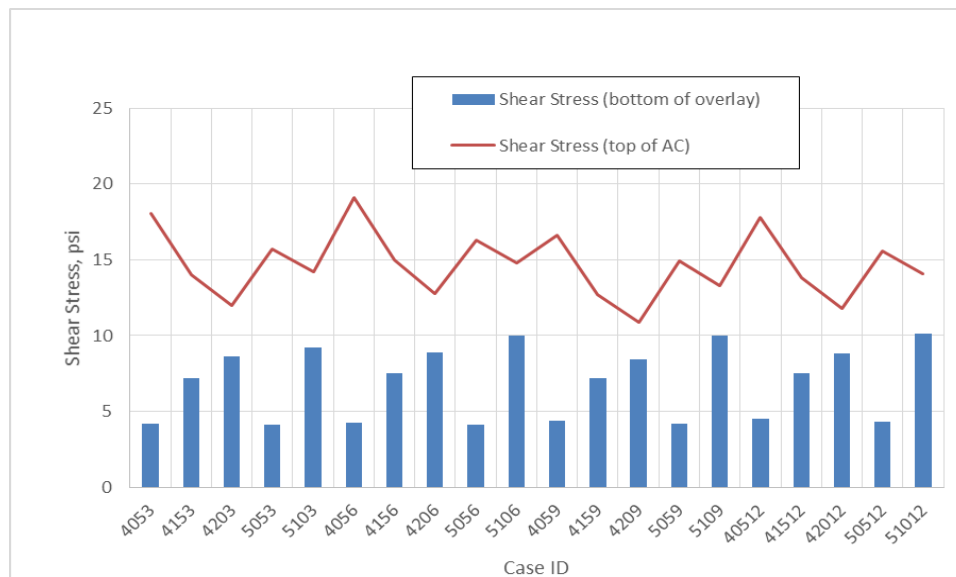


Figure 5.29: Shear Stress at the Interface under Non-bonding Condition

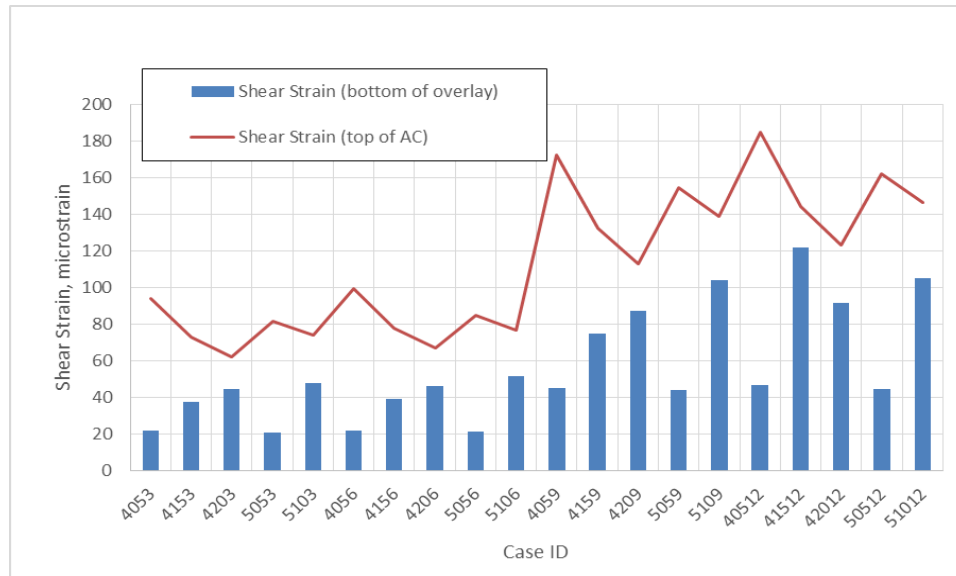


Figure 5.30: Shear Strain at the Interface under Non-bonding Condition

In Figure 5.29 (above) we see that when the bonding condition is weak, the shear stress at the bottom of overlay layer correlates closely with the thickness of overlay layer. The shear stress increased with thicker overlay. In addition, the effect of the pavement layer property-elastic modulus is minimized, while the shear strain level depends on the thickness of the overlay layer and the elastic modulus of overlay layer. (See Figure 5.30 above).

Chapter 6: Case Study: Taxes Thin Asphalt Overlay from LTPP

This chapter presents the structural information of the Texas asphalt overlay pavement experimental sections from the LTPP database.

6.1 LTPP OVERLAY CASE STUDY

In recent years, asphalt overlay has been applied as a cost-effective treatment to maintain pavement's functional performance at a satisfactory level. The aging infrastructure and budget constraints make the need for the development of an advanced pavement management system more urgent. Most state departments of transportation (DOTs) and their stakeholders recognize the need to establish a prevention model that encourages the right routine treatment on the right pavement at the right time. Costs are lower when the pavement is still in good condition, as shown in Figure 6.1 [79].

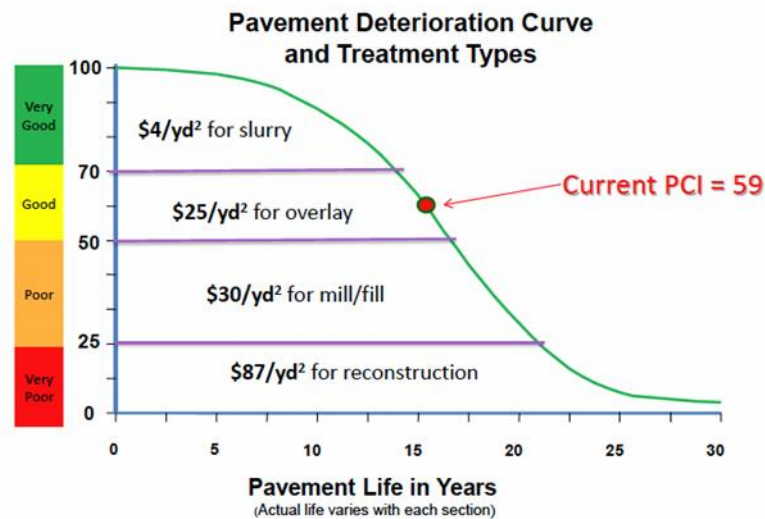


Figure 6.1: The Relation between Cost Rate of Treatment and Pavement Condition [79]

The purpose of this LTPP case study was to investigate the performance of asphalt overlays applied in LTPP experimental sections in Texas. Thirty LTPP sections consisted of asphalt overlay

on the existing asphalt pavements. The initial construction, main maintenance, location, and annual traffic volume information of these sections are tabulated in Table 6.1.

Table 6.1: LTPP Asphalt Overlay Construction, Location, and Traffic Volume Information of Texas Experimental Sections

SHRP_ID	Initial CT ¹	Overlay CT	Seal (Fog) Coat	Latitude	Longitude	Elevation	KEASL ²	Overlay Thickness (in.)
1039	6/1/1982	10/13/1996	11/4/2002	32.39	-96.82	564.2	324.6	1.7
1068	3/1/1987	11/1/2000	8/16/2004	33.50	-95.59	442.8	128.3	2
1087	12/1/1973	7/15/2011	6/15/2004	32.37	-95.33	544.5	102.0	0.8
1092	9/1/1983	9/15/1988;5/15/2010	7/15/1995	29.35	-99.07	827.5	150.3	1.7
1093	4/1/1980	9/15/1988	-	28.78	-98.31	242.7	519.8	1.9
1096	4/1/1981	6/15/2001	7/2/1996	29.36	-98.84	770.8	148.3	2
1111	9/1/1972	8/16/1999	6/15/2011	33.53	-101.80	3155.4	65.0	2.6
1113	1/1/1986	8/2/1992	6/8/1992	31.96	-94.70	438.2	-	1.2
1116	7/1/1987	10/18/1990;2/12/1992	-	31.89	-94.68	410	-	1.7
1119	5/1/1975	8/3/1989	-	32.00	-95.00	334.6	172.0	1.3
1130	10/1/1971	10/22/1992	7/22/1994	29.56	-97.94	518.2	37.3	1.6
2108	8/1/1985	9/21/2012	9/14/2012	29.35	-94.93	3.3	36.0	1
2176	7/1/1970	2/22/2001	6/15/2010	34.17	-101.71	3368.6	19.3	1.6
3669	5/1/1983	9/15/2000	6/11/2003;8/3/2011	31.33	-94.79	310	-	1.6
3729	6/1/1983	9/15/1999	4/10/1999	26.09	-97.58	36.4	-	1.5
3769	6/1/1976	5/9/2003	-	31.81	-106.26	3995	1422.0	1.8
3835	10/1/1991	6/24/2000	4/25/2000	30.73	-96.43	338.5	459.0	1.7
3855	10/1/1979	12/15/1998	9/15/2006	29.90	-96.81	318.2	180.2	1.9
3865	7/1/1969	5/18/2001	7/8/2003	31.57	-98.67	1467.1	135.7	0.5
3875	11/1/1985	6/27/1991	-	36.16	-102.03	3598.2	-	1
6079	8/1/1972	9/15/1999	-	35.18	-103.03	3823.2	1021.0	2.6
9005	7/1/1986	9/22/1998	9/15/1998	29.52	-98.72	907.2	59.0	1.9
A502	6/1/1977	9/26/1991	8/15/2015	32.61	-96.41	433	217.1	2.1
A503	6/1/1977	9/25/1991	8/15/2015	32.61	-96.41	446.1	217.1	2
A504	6/1/1977	10/21/1991	8/15/2015	32.61	-96.40	449.4	217.1	2.1
A505	6/1/1977	10/21/1991	8/15/2015	32.61	-96.40	463.1	217.3	2.1
A506	6/1/1977	10/21/1991	8/15/2015	32.61	-96.40	456.2	217.1	2.2
A507	6/1/1977	10/16/1991	8/15/2015	32.61	-96.40	452.6	217.1	1.9
A508	6/1/1977	9/25/1991	8/15/2015	32.61	-96.41	439.5	217.3	2
A509	6/1/1977	9/26/1991	8/15/2015	32.61	-96.41	438.2	217.1	2.1

Note: 1 – Construction Time;
2 – Annual Traffic Volume.

Figure 6.2 shows the pavement PCR index with time at LTPP Experimental Section 1068. After application of a two-in. asphalt overlay in 1993, the PCR index jumped to 100. From 1993 to 1998, the PCR index decreased from 100 to 40. Some unrecorded treatment was conducted on the pavement to improve its condition in 1993. As described in Chapter 3, the time gained by the preceding overlay maintenance can be calculated based on the pavement deterioration rate. The pavement condition deterioration rate of section 1068 can be determined by using the correlation method shown in Figures 6.2 and 6.3. The performance curve in Figure 6.3 was extracted from the PCR curve in Figure 6.2 in corresponding to the time duration of the specific overlay application. A linear function can be applied to characterize the deterioration rate of pavement performance from the time of overlay treatment to next pavement treatment in around 1999.

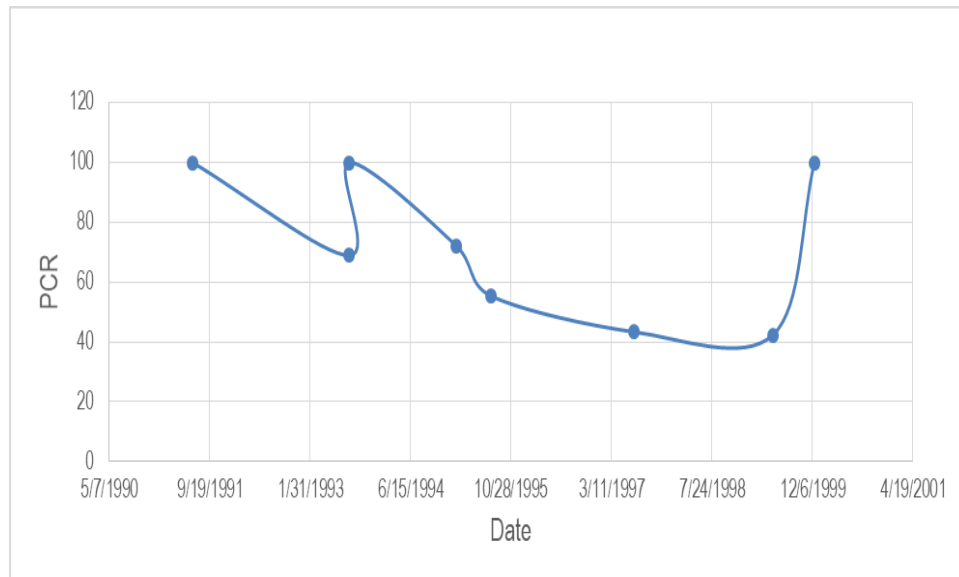


Figure 6.2: PCR Curve of Section 1068 over Time

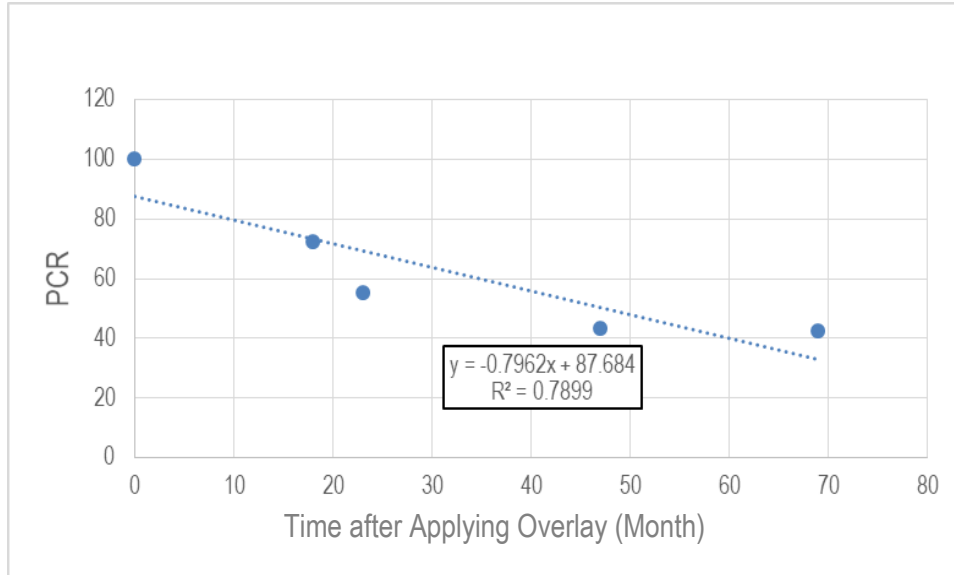


Figure 6.3: Pavement Condition Deterioration Rate of Section 1068 after Overlay

As indicated by the correlation equation, the decreasing rate is 0.796 of PCR index per month. In this study, the time gain of overlay treatment can be defined as the time interval between the beginning of asphalt overlay construction and the PCR index decreasing to 60. For Section 1068, the time gain is $40/0.796=50.6$ months (4.2 years). This method of analysis was applied to evaluate all other LTPP experimental sections. Appendix B contains all the results of the PCR curve and time increment for these LTPP sections.

Table 6.2 shows the structural information of the investigated sections, and the calculated results of life gain based on the PCR curve. Figure 6.4 is the calculated life gain for each pavement section, with the horizontal axle representing the overlay thickness. There is no strong correlation between the life gain after overlay treatment and the overlay layer thickness. Many factors could account for this, including the variations in traffic volume, inconsistent construction quality, and fluctuations in the survey's accuracy. The variation in life gain and traffic volume is shown in Figure 6.5. The life gain shows a weak trend toward the possibility that higher traffic volume has a shorter life gain after the overlay treatment.

Table 6.2 Structural Information and Pavement Performance of LTPP Sections

SHRP_ID	Subbase Layer	Base Layer	Seal Coat	AC	Seal Coat	Overlay	Seal Coat	Deterioration Rate (PCR/month)	Life Gain (years)
1039	7.8	14	-	7.4	0.4	1.7	0.2	0.087	38.3
1068	8	6	-	11.8	0.1	2	0.1	0.796	4.2
1087	-	7.2	-	6.9	0.3	0.8	-	0.779	4.3
1092	7	5.5	0.4	2.7	0.2	1.7	-	0.281	11.9
1093	-	17.2	-	2.4	0.5	1.9	-	0.604	5.5
1096	6	8.1	-	7.1	0.3	2	-	0.355	9.4
1111	-	8.4	-	7.1	0.1	2.6	0.5	0.352	9.5
1113	-	11.5	0.7	4	-	1.2	-	0.968	3.4
1116	-	10.9	-	1.5	-	1.7	-	0.559	6.0
1119	-	7.2	-	5.3	0.3	1.3	-	2.201	1.5
1130	8	17.9	-	2.3	0.4	1.6	0.4	0.302	11.0
2108	6.5	14.2	-	3	-	1	0.3	0.365	9.1
2176	-	9.4	-	2.7	-	1.6	0.5	0.347	9.6
3669	7.9	8	-	4.2	-	1.6	0.3	0.513	6.5
3729	5.4	10.5	-	10.1	0.3	1.5	0	-	-
3769	-	8.4	-	2	0.4	1.8	-	0.667	5.0
3835	6	13	-	12.8	-	1.7	-	0.851	3.9
3855	6	16.8	0.3	0.9	0.2	1.9	0.5	1.509	2.2
3865	10	7.5	-	1.9	0.3	0.5	-	0.723	4.6
3875	-	16.7	-	1	-	1	-	1.331	2.5
6079	-	5	-	6.8	0.5	2.6	-	0.747	4.5
9005	-	9.4	0.4	1.2	0.3	1.9	-	0.255	13.1
A502	8	14.6	-	9.3	-	2.1	0.5	-	-
A503	9	10.8	-	12.6	-	2	0.5	-	-
A504	8	10	-	11.8	-	2.1	0.5	-	-
A505	10.4	15	-	9.4	-	2.1	0.5	-	-
A506	10.4	15	-	9.2	-	2.2	0.5	-	-
A507	8.3	15	-	12.1	-	1.9	0.5	-	-
A508	8	14	-	13.4	-	2	0.5	-	-
A509	8	14.6	-	10	-	2.1	0.5	-	-

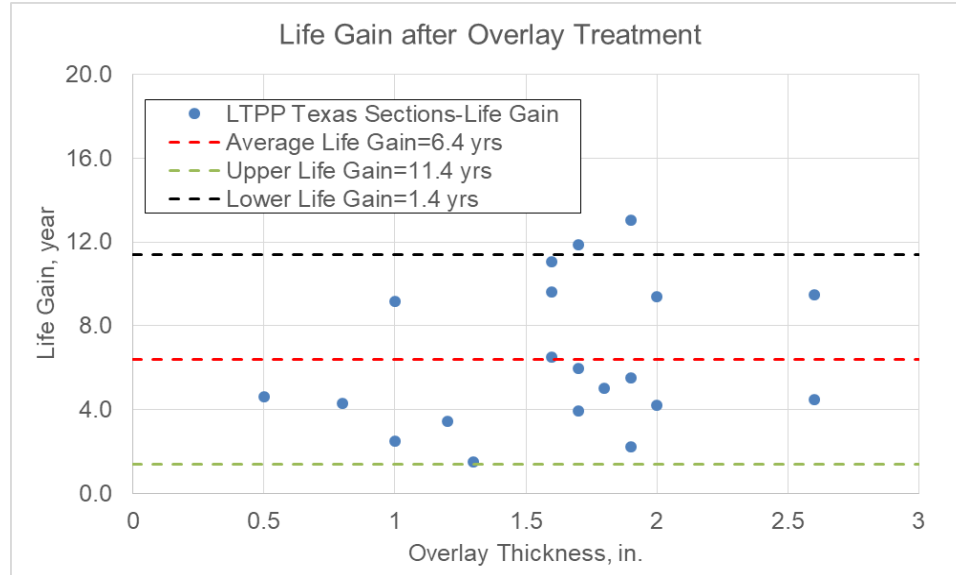


Figure 6.4: Life Gain after Overlay Treatment

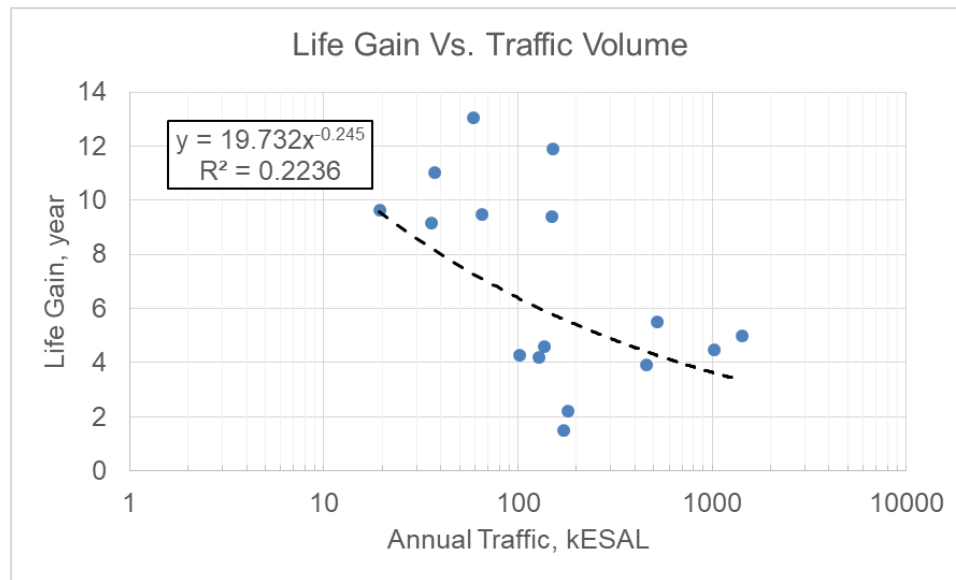


Figure 6.5: Correlation between Life Gain and Traffic Volume

6.2 ABAQUS MODELING OF SECTIONS 1087 AND 6079

As LTPP sections 1087 and 6079 had similar pavement structures with the cases in our ABAQUS study, sections 1087 and 6079 were selected to be simulated by using ABAQUS modeling. The tensile strain of Section 1087 at the bottom of the AC layer is $93 \mu\epsilon$, and the tensile

strain of Section 6079 is 59 $\mu\epsilon$. Once these tensile strains have been obtained, the fatigue life can be calculated by using the Asphalt Institute fatigue model (see Section 3.2).

Table 6.3 shows the pavement structural information and the ABAQUS simulation of Sections 1087 and 6079. The calculated fatigue lives for Sections 1087 and 6079 are 6.1 and 3.4 years, respectively. The calculated life gains based on the PCR curves for these two sections are 4.3 and 3.4 years. Section 1087 has thinner and lower annual traffic volume (see Table 6.1). This explains why Section 1087 has a slightly longer life gain after the overlay. The ABAQUS modeling indicates that the pavement structure of Section 1087 has longer service life-6.1 years before fatigue failure. The fatigue life obtained by the numerical modeling for section 6079 is around 4.5 years which is also lower than section 1087's fatigue life.

Table 6.3: ABAQUS Modeling of LTPP Sections 1087 and 6079 and PCR Results

Layers	PCR- 1087	ABAQUS 1087	PCR- 6079	ABAQUS 6079
Overlay	0.8	1	2.6	2
AC	6.9	7	6.8	7
Base	7.2	7	5	5
Subgrade	-	12	-	12
Life Gain (yrs)	4.3	6.1	3.4	4.5

Chapter 7: Conclusion and Recommendation

This Chapter summarizes the main findings in this study and describes the recommendations for future work.

7.1 CONCLUSION

This study investigated factors affecting the performance of thin overlays by the use of three methods: laboratory tests with seven tack coat materials, finite element modeling with overlay pavement structure using the ABAQUS program, and an LTPP case study. Based on the results and analyses the following conclusions can be drawn:

- 1) Modified direct shear test is a reliable approach for qualifying and quantifying the bonding strength of tack coat materials.
- 2) The CAM model is capable of characterizing the dynamic modulus of different tack coat materials;
- 3) The results of ABAQUS modeling indicate that the bonding condition between the overlay and the existing AC layer can affect the response, being horizontal stress, shear stress, vertical strain and vertical deformation, level under traffic load;
- 4) In full-bonded condition, the asphalt overlays with the same total HMA thickness experience similar responses under the same loading conditions. When the bonding condition is compromised, the responses of these pavements vary;
- 5) Both the overlay thickness and layer property affect the stress level of the overlay pavement structure;
- 6) The PCR curve successfully characterizes the overlay pavement condition of Texas LTPP experimental sections;
- 7) The LTPP case study showed that there is no apparent correlation between the asphalt overlay thickness and the life gain by overlay treatment. Calculation of life gain varied section by section;

- 8) Due to the complexity in the field of overlay pavement, evaluation of long-term performance should be approached with more caution.

7.2 RECOMMENDATION

There are a lot of limitations in this study. Some of them are: 1) laboratory testing on tack coat is limited to shear strength test and rheological performance, without consideration on the field mixture texture; 2) ABAQUS modeling did not investigate other parameters, such as viscoelastic property of HMA and dynamic loading, etc.; and 3) the LTPP case study only considered the experimental sections in the state of Texas.

The recommendation would be given that more effort should be taken to investigate other factors to obtain an inherent understanding on the importance of bonding condition to thin overlay pavement.

References

1. Christopher, B. R., Schwartz, C. W., Boudreau, R. L. (2010). Geotechnical aspects of pavements: Reference manual. US Department of Transportation, Federal Highway Administration.
2. Mohammad, L. N., Elsifi, M.A., Bae, A., Patel, N., Button, J., Scherocman, J. A. (2012). Optimization of tack coat for HMA placement. NCHRP Research Report 712. Transportation Research Board. <https://doi.org/10.17226/13652>.
3. FHWA TechBrief (2016). Tack Coat Best Practices. FHWA-HIF-16-017. US Department of Transportation, Federal Highway Administration.
4. Wu, T. F., Cai, Y. Q., Guo, L., Ling D. S., Wang J. (2017). "Influence of shear stress level on cyclic deformation behaviour of intact Wenzhou soft clay under traffic loading." *Engineering Geology* 228: 61-70.
5. Walubita, L. F., Faruk A. N., Das G., Tanvir, H., Zhang J., Scullion, T. (2012). The overlay tester: a sensitivity study to improve repeatability and minimize variability in the test results. No. FHWA/TX-12/0-6607-1. Texas Transportation Institute.
6. Zhou, F. J., Hu, S., Hu, X.D., Scullion, T. (2009) Mechanistic-empirical asphalt overlay thickness design and analysis system. No. FHWA/TX-09/0-5123-3. Texas Transportation Institute.
7. National Asphalt Pavement Association (NAPA) website: Thin Overlays. <http://www.asphaltpavement.org/thinlay>.
8. Wilson, B. T., Scullion, T., Faruk, A. N., Zimmer, R., Fernando, E., Tuan, C. Y., Gerbino-Bevins, B., (2015). Evaluation of Design and Construction Issues of Thin HMA Overlays. No. FHWA/TX-15/0-6742-1. Texas A & M Transportation Institute.
9. Cantrell, L. Design and evaluation of 4.75 mm mixture for thin asphalt overlay in Washington State. MS thesis, Washington State University, 2013.
10. You, Taesun, Sookyok Im, Yong-Rak Kim, Hamzeh Haghshenas, and Gabriel Nsengiyumva. (2015). Evaluation of Thin Asphalt Overlay Practice Preserving Nebraska's Asphalt Pavements. No. SPR-P1 (15) M017. Nebraska Transportation Center.
11. Hajj, E. Y., Sebaaly, P. E., Habbouche, J. (2016). Laboratory evaluation of thin asphalt concrete overlays for pavement preservation. Report No. SOLARIS-201601, Department of Civil and Environmental Engineering, University of Nevada, Reno, USA.
12. Su, K., Sun, L. J., Hachiya, Y., Maekawa, R. (2008). "Analysis of shear stress in asphalt pavements under actual measured tire-pavement contact pressure." *Proceedings of the 6th ICPT*, Sapporo, Japan: 11-18.
13. ASTM Standard D8-18c. (2018). Standard Terminology Relating to Materials for Roads and Pavements.
14. Thomas. (May 2011). Tack Coat Materials and Methods for Optimizing for Thin HMA Applications, Pavement Preservation Workshop. https://www.pavementpreservation.org/wp-content/uploads/presentations/41_Thomas.pdf
15. Bowman, B. (1919). "Europe Moves to Modified Binders." *Journal of Plant and Civil Engineer* 3, no. 5.
16. Salomon, D. (2006). Transportation research circular E-C102: Asphalt emulsion technology. Transportation Research Board, Washington, DC. <http://www.trb.org/Main/Blurbs/157696.aspx>

17. Hazlett, D. (2007). Transportation Research Circular E-C122: Emulsion Residue Recovery Techniques: How Do We Get Emulsion Residue Representative of In-Service Binder. Transportation Research Board of the National Academies, Washington, DC. <http://www.trb.org/main/blurbs/159352.aspx>
18. Kadrmas, A. (2013). Transportation Research Circular E-C182: Progress toward Performance-Graded Emulsified Asphalt Specifications. Transportation Research Board of the National Academies, Washington, DC. <http://www.trb.org/Main/Blurbs/170143.aspx>
19. Kim, Y. R., Adams, J., Castorena, C., Ilias, M., Im, J. H., Bahia, H., Chaturabong, P., Hanz, A., Johannes, P.T. (2017). Performance-Related Specifications for Emulsified Asphaltic Binders Used in Preservation Surface Treatments. NCHRP Research Report 837. Transportation Research Board. <https://doi.org/10.17226/24694>
20. Hakimzadeh, S., Kebede, N. A., Buttlar, W.G. (2012). "Comparison between Optimum Tack Coat Application Rates as Obtained from Tension-And Torsional Shear-Type Tests." In 7th RILEM International Conference on Cracking in Pavements, (2012):287-297. DOI: 10.1007/978-94-007-4566-7_28, https://link.springer.com/chapter/10.1007/978-94-007-4566-7_28
21. Johnston, J. B., and King, G. (2008). Using Polymer Modified Asphalt Emulsions in Surface Treatments - A Federal Lands Highway Interim Report. https://www.pavementpreservation.org/wpcontent/uploads/2012/04/Polymer_Modified_Asphalt_Emulsions.pdf
22. Al-Qadi, I.L., Carpenter, S. H., Leng, Z., Ozer, H., Trepanier J. (2008). Tack coat optimization for HMA overlays: Laboratory testing. Illinois Center for Transportation. <http://hdl.handle.net/2142/12117>
23. Coleri, E., Covey, D., Mahmoud, Batti, A. J., Anisimova, N. (2017). HMAC Layer Adhesion through Tack Coat. Report No. FHWA-OR-RD-17-05. Oregon Department of Transportation. http://www.oregon.gov/ODOT/Programs/ResearchDocuments/SPR782_HMAC_Layer_Adhesion_Tack_Coat_Final.pdf
24. Wilson, B.T., Seo, A. Y., Sakhaeifar, M. (2016). Performance Evaluation and Specification of Trackless Tack. No. FHWA/TX-16/0-6814-1. Texas A & M Transportation Institute. <https://static.tti.tamu.edu/tti.tamu.edu/documents/0-6814-1.pdf>
25. Chen, Y., Tebaldi, G., Roque, R., Lopp, G. (2012). "Effects of Trackless Tack Interface on Pavement Top-down Cracking Performance." Procedia-Social and Behavioral Sciences Journal, Vol. 53, No. 3, 2012:432-439. <https://doi.org/10.1016/j.sbspro.2012.09.894>
26. ABAQUS tutorials: <http://www.simulia.com/academics/tutorials.html>
27. Uddin, W., Zhang, D. M., Fernandez, F. (1994). "Finite element simulation of pavement discontinuities and dynamic load response." Paper No. 1448. Transportation Research Record.
28. Masad, E., Somadevan, N., Bahia H. U., Kose, S. (2001). "Modeling and experimental measurements of strain distribution in asphalt mixes." Journal of Transportation Engineering 127(6): 477-485.
29. Elseifi, M. A., Al-Qadi, I. L., Yoo, P. J. (2006). "Viscoelastic modeling and field validation of flexible pavements." Journal of engineering mechanics 132, no. 2: 172-178.
30. Dai, Q. L., and You, Z. P. (2007). "Prediction of creep stiffness of asphalt mixture with micromechanical finite-element and discrete-element models." Journal of Engineering Mechanics 133(2), 163-173.

31. Sadd, M. H., Dai, Q. L., Parameswaran, V., Shukla, A. (2004). "Microstructural simulation of asphalt materials: Modeling and experimental studies." *Journal of materials in civil engineering*, 16(2), 107-115.
32. Abbas, A. R., Papagiannakis, A. T., Masad, E. A. (2004). "Linear and nonlinear viscoelastic analysis of the microstructure of asphalt concretes." *Journal of Materials in Civil Engineering*, 16(2), 133-139.
33. Papagiannakis, A. T., Abbas, A., Masad, E. (2002). "Micromechanical analysis of viscoelastic properties of asphalt concretes." *Transportation Research Record*, 1789(1), 113-120.
34. Huang, C. W., Abu Al-Rub, R. K., Masad, E. A., Little, D. N. (2011). "Three-dimensional simulations of asphalt pavement permanent deformation using a nonlinear viscoelastic and viscoplastic model." *Journal of Materials in Civil Engineering*, 23(1), 56-68.
35. Kim, Y. R., and Aragão, F. T. S. (2013). "Microstructure modeling of rate-dependent fracture behavior in bituminous paving mixtures." *Journal of Finite Elements in Analysis and Design*, 63, 23-32.
36. Ameri, M., Mansourian, A., Khavas, M. H., Aliha, M. R. M., Ayatollahi, M. R. (2011). "Cracked asphalt pavement under traffic loading—A 3D finite element analysis." *Journal of Engineering Fracture Mechanics*, 78(8), 1817-1826.
37. Caro, S., Masad, E., Bhasin, A., Little, D. (2010). "Micromechanical modeling of the influence of material properties on moisture-induced damage in asphalt mixtures." *Journal of Construction and Building Materials*, 24(7), 1184-1192.
38. Hadi, M. N., and Bodhinayake, B. C. (2003). "Non-linear finite element analysis of flexible pavements." *Journal of Advances in Engineering Software*, 34(11-12), 657-662.
39. Huang, B., Mohammad, L. N., Rasoulia, M. (2001). "Three-dimensional numerical simulation of asphalt pavement at Louisiana accelerated loading facility." *Transportation research record*, 1764(1), 44-58.
40. Huang, X., and Zhang, Y. (2010). "A new creep test method for asphalt mixtures." *Journal of Road Materials and Pavement Design*, 11(4), 969-991.
41. Hua, J. F. (2000). "Finite element modeling and analysis of accelerated pavement testing devices and rutting phenomenon." PhD diss., West Lafayette: Purdue University.
42. Elseifi, M. A., Mohammad, L. N., Ying, H., Cooper III, S. (2012). "Modeling and evaluation of the cracking resistance of asphalt mixtures using the semi-circular bending test at intermediate temperatures." *Journal of Road Materials and Pavement Design*, 13(sup1), 124-139.
43. Dave, E. V., Song, S. H., Buttlar, W. G., Paulino, G. H. (2007). "Reflective and thermal cracking modeling of asphalt concrete overlays." *Journal of Advanced Testing and Characterization of Bituminous Materials*, 2, 1241-1252.
44. Dormohammadi, A. (2017). "Influence of overlay thickness on interface bonding." MS thesis, University of Texas at El Paso.
45. Wang, H., Al-Qadi, I. L., Stanculescu, I. (2010). Effect of friction on rolling tire-pavement interaction. USDOT Region V Regional University Transportation Center Final Report. NEXTRANS Center, Purdue University.
46. Ozer, H., Al-Qadi, I. L., Duarte, C. A. (2011). "A three-dimensional generalised finite element analysis for the near-surface cracking problem in flexible pavements." *International Journal of Pavement Engineering*, 12(4), 407-419.

47. Gungor, O. E., Al-Qadi, I. L., Gamez, A., Hernandez, J. A. (2017). "Development of adjustment factors for MEPDG pavement responses utilizing finite-element analysis." *Journal of Transportation Engineering, Part A: Systems*, 143(7), 04017022.
48. Tozzo, C., D'Andrea, A., Al-Qadi, I. L. (2016). "Dilatancy in the analysis of interlayer cyclic shear test results." *Journal of Materials in Civil Engineering*, 28(12), 04016171.
49. Ziyadi, M., and Al-Qadi, I. L. (2017). "Efficient surrogate method for predicting pavement response to various tire configurations." *Journal of Neural Computing and Applications*, 28(6), 1355-1367.
50. Dessouky, S. H., Al-Qadi, I. L., Yoo, P. J. (2014). "Full-depth flexible pavement responses to different truck tyre geometry configurations." *International Journal of Pavement Engineering*, 15(6), 512-520.
51. Hernandez, J. A., and Al-Qadi, I. L. (2016). "Hyperelastic modeling of wide-base tire and prediction of its contact stresses." *Journal of Engineering Mechanics*, 142(2), 04015084.
52. Al-Qadi, I. L., Elseifi, M. A., Yoo, P. J., Dessouky, S. H., Gibson, N., Harman, T., D'Angelo, J., Petros, K. (2008). Accuracy of current complex modulus selection procedure from vehicular load pulse: NCHRP Project 1-37A mechanistic-empirical pavement design guide. *Transportation research record*, 2087(1), 81-90.
53. Hernandez, J. A., and Al-Qadi, I. L. (2015). *Airfield Pavement Response Caused by Heavy Aircraft Takeoff: Advanced Modeling for Consideration of Wheel Interaction*. *Transportation Research Record*, 2471(1), 40-47.
54. Wang, H., Ozer, H., Al-Qadi, I. L., Duarte, C. A. (2013). Analysis of near-surface cracking under critical loading conditions using uncracked and cracked pavement models. *Journal of transportation engineering*, 139(10), 992-1000.
55. Wang, H., and Al-Qadi, I. L. (2009). Combined effect of moving wheel loading and three-dimensional contact stresses on perpetual pavement responses. *Transportation research record*, 2095(1), 53-61.
56. Wikipedia Website on Long-Term Pavement Performance. https://en.wikipedia.org/wiki/Long-Term_Pavement_Performance
57. Elkins, G. E., Schmalzer, P. N., Thompson, T., Simpson, A. (2003). Long-term pavement performance information management system: Pavement performance database user reference guide (No. FHWA-RD-03-088). Turner-Fairbank Highway Research Center.
58. Malla, R. B., and Joshi, S. (2007). "Resilient modulus prediction models based on analysis of LTPP data for subgrade soils and experimental verification." *Journal of Transportation Engineering*, 133(9), 491-504.
59. Dong, Q., and Huang, B. (2012). "Evaluation of effectiveness and cost-effectiveness of asphalt pavement rehabilitations utilizing LTPP data." *Journal of Transportation Engineering*, 138(6), 681-689.
60. Dong, Q., and Huang, B. (2014). "Evaluation of influence factors on crack initiation of LTPP resurfaced-asphalt pavements using parametric survival analysis." *Journal of Performance of Constructed Facilities*, 28(2), 412-421.
61. Von Quintus, H. L., and Simpson, A. L. (2002). Back-calculation of layer parameters for LTPP test sections, Volume II: Layered elastic analysis for flexible and rigid pavements (No. FHWA-RD-01-113). United States. Federal Highway Administration. Office of Engineering Research and Development.

62. Khazanovich, L., and Gotlif, A. (2003). Evaluation of joint and crack load transfer final report (No. FHWA-RD-02-088). United States. Federal Highway Administration. Office of Infrastructure Research and Development.
63. Kim, Y. R., Underwood, B., Far, M. S., Jackson, N., Puccinelli, J., Engineers, N. C. (2011). LTPP computed parameter: dynamic modulus (No. FHWA-HRT-10-035). United States. Federal Highway Administration.
64. Hall, K. T., Simpson, A. L., Correa, C. E. (2002). LTPP data analysis: effectiveness of maintenance and rehabilitation options. Washington, DC: National Cooperative Highway Research Program.
65. Elwardany, M. D., Lee, K., Lee, J. H., Brown, C., Castorena, C., Kim, Y. R. (2018). Proposed Performance-Prediction Equations and Threshold Triggers for Thin-Overlay Treatments Using the Long-Term Pavement Performance Database (No. FHWA-HRT-17-111). United States. Federal Highway Administration. Office of Infrastructure Research and Development.
66. Hajj, R., Filonzi, A., Bhasin, A., Dormohammadi, A., Zhu, C., Tandon, V. (2018). Design and Construction of Ultra Thin Overlays as an Alternative to Seal Coats (No. FHWA/TX-18/0-6857-1, Technical Reprot 0-6857-1). University of Texas at Austin. Center for Transportation Research.
67. Witczak, M. W., and El-Basyouny, M. M. (2004). Appendix II-1: Calibration of Fatigue Cracking Models for Flexible Pavements. Guide for Mechanistic–Empirical Design of New and Rehabilitated Pavement Structures.
68. Federal Highway Administration. (2006). Pavement Distress Identification Manual for the NPS Road Inventory Program, Cycle 4, 2006-2009.
69. Miller, J. S., and Bellinger, W. Y. (2003). Distress identification manual for the long-term pavement performance program (No. FHWA-RD-03-031). United States. Federal Highway Administration. Office of Infrastructure Research and Development.
70. Marasteanu, M. O., and Anderson, D. A. (1999, May). Improved model for bitumen rheological characterization. In Eurobitume workshop on performance related properties for bituminous binders (Vol. 133). Brussels, Belgium: European Bitumen Association.
71. Zhu, C. (2015). Evaluation of Thermal Oxidative Aging Effect on the Rheological Performance of Modified Asphalt Binders. MS Thesis, University of Nevada, Reno. <https://search.proquest.com/docview/1760591335?pq-origsite=gscholar>
72. Zhu, C., Sebaaly, P., Hajj, E., Morian, N., Tandon, V. (2017). Effect of Isothermal Oxidative Aging on Asphalt Binders: Kinetic Factors and Block Cracking Index of Glover-Rowe Parameter (No. 17-00166). <https://trid.trb.org/view.aspx?id=1437150>
73. Rowe, G. M., and Sharrock, M. J. (2011). Alternate shift factor relationship for describing temperature dependency of viscoelastic behavior of asphalt materials. Transportation Research Record, 2207(1), 125-135. <https://doi.org/10.3141/2207-16>
74. Morian, N., Zhu, C., Hajj, E. Y. (2015). Rheological indexes: Phenomenological aspects of asphalt binder aging evaluations. Transportation Research Record, 2505(1), 32-40. <https://doi.org/10.3141/2505-05>
75. AASHTO TP70. (2013). Standard Specifications for Transportation Materials and Methods of Sampling and Testing, 33rd Edition, American Association of State Highway and Transportation Officials, Washington D.C.
76. Anderson, M., (Nov. 2012). Presentation-SEAUPG Evaluation of MSCR Recovery as a Replacement for PG Plus Tests, Asphalt Institute. <http://www.asphaltinstitute.org/wp->

[content/uploads/SEAUPG%20Evaluation%20of%20MSCR%20Recovery%20as%20a%20Replacement%20for%20PG%20Plus%20Tests.pdf](#)

- 77. Huang, Y.H. (2003). Pavement analysis and design, 2nd Edition.
- 78. Dassault, S. (2014). "Abaqus analysis user's guide." Solid (Continuum) Elements.
- 79. Modesto, California Pavement Condition Survey Website: <https://www.stanislaus-localroadsfirst.com/modesto.html>

Appendix

Appendix A- ABAQUS Modeling Results

Appendix B- Plots of LTTP Case Study Results

APPENDIX A-ABAQUS MODELING RESULTS

1) Results of 4-inch AC with 0.5-inch Overlay

Case ID	Vertical Strain (microstrain)	Vertical Deformation	Tensile Stress (psi)	Tensile Strain (microstrain)	Shear Stress (bottom of overlay)	Shear Stress (top of AC)	Shear Strain (bottom of overlay)	Shear Strain (top of AC)	Maximum Shear Stress, psi
4051	-614.4	-7.76E-03	66.68	94.81	13.15	23.59	68.4	122.7	29.9
4052	-637.7	-8.03E-03	70	100	6.88	19.93	76.8	103.6	31.3
4053	-671.9	-8.41E-03	70.57	101.1	4.2	18.04	21.8	93.8	31.6
4054	-654.7	-9.09E-03	81.34	111.2	13.76	24.94	71.5	129.7	31.6
4055	-682.7	-9.45E-03	85.91	117.8	7.2	21.15	37.5	110	33.2
4056	-725	-9.98E-03	87.48	120	4.27	19.1	22.2	99.2	33.6
4057	-732.2	-9.53E-03	43.88	137.4	14.3	22.4	148.6	233	26.4
4058	-749	-9.80E-03	46.18	146	7.7	18.78	80	195.3	27.8
4059	-785.7	-1.02E-02	46.5	148.3	4.4	16.6	45.4	172.1	28.1
40510	-811.2	-1.15E-02	59.4	170.9	15.03	23.99	156.3	249.4	28.3
40511	-833.2	-1.18E-02	62.8	182.1	8.2	20.2	84.8	210.5	30
40512	-881.3	-1.24E-02	64.1	186.4	4.5	17.8	46.6	184.9	30.4

2) Results of 4-inch AC with 1.5-inch Overlay

Case ID	Vertical Strain (Microstrain)	Vertical Deformation	Tensile Stress (psi)	Tensile Strain (microstrain)	Shear Stress (bottom of overlay)	Shear Stress (top of AC)	Shear Strain (bottom of overlay)	Shear Strain (top of AC)	Maximum Shear Stress, psi
4151	-515.4	-6.68E-03	58.78	82.8	20	22.36	103.9	116.3	24.7
4152	-572	-7.35E-03	64.6	91.6	12	17.4	62.6	90.7	26.8
4153	-657.8	-8.32E-03	66.02	94	7.2	14	37.7	73	27.5
4154	-537.6	-7.65E-03	70	95.4	21	23.61	108.9	122.8	26
4155	-618	-8.69E-03	79.1	108	11.7	17.96	60.9	93.4	28.5
4156	-706.7	-9.80E-03	81.9	111.6	7.5	15	39	78	29.3
4157	-627	-8.43E-03	38.8	118.4	20.9	21.7	217.2	225	22.7
4158	-684.3	-9.21E-03	43	134.1	11.9	16.1	124	167	23.8
4159	-770	-1.02E-02	43.2	137	7.2	12.73	74.7	132.4	24.3
41510	-678.4	-9.91E-03	50.9	144.7	22.2	23.2	230	240.8	24.2
41511	-749.1	-1.09E-02	57.6	165.5	12.8	17.5	133	182	25.5
41512	-859.5	-1.23E-02	59.7	172.5	7.5	13.8	122	144	26.3

3) Results of 4-inch AC with 2.0-inch Overlay

Case ID	Vertical Strain (Microstrain)	Vertical Deformation	Tensile Stress (psi)	Tensile Strain (microstrain)	Shear Stress (bottom of overlay)	Shear Stress (top of AC)	Shear Strain (bottom of overlay)	Shear Strain (top of AC)	Maximum Shear Stress, psi
4201	-474.8	-6.23E-03	54.1	75.8	20.5	20.52	106.5	106.7	22.1
4202	-557.7	-7.19E-03	60.5	85.5	12.3	14.9	64.2	77.4	23.8
4203	-643.5	-8.16E-03	61.3	86.8	8.6	12	44.5	62.4	24.2
4204	-491	-7.06E-03	63.8	86.8	21.4	21.6	111.4	112.4	23.2
4205	-585	-8.27E-03	73.1	99.5	13.1	15.9	67.8	82.8	25.1
4206	-688	-9.57E-03	76	103.2	8.9	12.8	46.3	66.8	25.8
4207	-582.7	-7.95E-03	35.9	108.3	21	19.9	218.4	207.4	20.4
4208	-653.5	-8.86E-03	39.9	123.5	13	14.4	135.2	149.6	21
4209	-756.5	-1.00E-02	39.9	125.8	8.4	10.9	87.1	112.8	21.4
42010	-624.3	-9.25E-03	46.6	131.6	22.2	21.3	230.7	221.4	21.7
42011	-709.2	-1.04E-02	53.2	152	13.9	15.7	144.5	163	22.4
42012	-840	-1.21E-02	55.2	158.7	8.8	11.8	91.4	123.2	23.2

4) Results of 5-inch AC with 0.5-inch Overlay

Case ID	Vertical Strain (Microstrain)	Vertical Deformation	Tensile Stress (psi)	Tensile Strain (microstrain)	Shear Stress (bottom of overlay)	Shear Stress (top of AC)	Shear Strain (bottom of overlay)	Shear Strain (top of AC)	Maximum Shear Stress
5051	-500.8	-6.48E-03	55	76.6	11.9	20.7	61.8	107.6	27.2
5052	-516.7	-6.68E-03	57.5	80.2	6.3	17.4	32.9	90.3	28.1
5053	-542.3	-6.97E-03	58.4	81.5	4.1	15.7	21.1	81.8	28.1
5054	-521.6	-7.41E-03	65.3	88.3	12.2	21.5	63.6	111.7	28.4
5055	-539.6	-7.65E-03	68.5	92.7	6.5	18.1	34	94.1	29.4
5056	-569.6	-8.04E-03	70.2	94.8	4.1	16.3	21.3	84.9	29.5
5057	-617.8	-8.27E-03	37.1	111.7	13.3	20.2	138	210.4	24.4
5058	-630	-8.48E-03	38.8	117.5	7.2	16.9	74.7	175.3	25.4
5059	-658.7	-8.81E-03	39.4	119.8	4.2	14.9	44.1	154.4	25.6
50510	-667.6	-9.72E-03	48.5	136.7	13.7	21.2	142.6	220.6	25.9
50511	-682.6	-9.97E-03	50.9	143.8	7.5	17.8	77.7	184.6	27
50512	-718.4	-1.04E-02	52.2	147.7	4.3	15.6	44.8	162.1	27.2

5) Results of 5-inch AC with 0.5-inch Overlay

Case ID	Vertical Strain (Microstrain)	Vertical Deformation	Tensile Stress (psi)	Tensile Strain (microstrain)	Shear Stress (bottom of overlay)	Shear Stress (top of AC)	Shear Strain (bottom of overlay)	Shear Strain (top of AC)	Maximum Shear Stress
5101	-461	-6.07E-03	51	72.2	19.2	20.8	100	108.4	25.1
5102	-495.9	-6.50E-03	56.15	78.4	12.7	16.3	65.8	84.7	26.6
5103	-538.5	-6.99E-03	57.45	80.3	9.2	14.2	47.9	73.9	26.8
5104	-476.2	-6.87E-03	61	82.7	19.9	21.7	103.3	112.8	26.2
5105	-515.3	-7.40E-03	66.7	90.3	12.9	17.03	67.2	88.6	27.9
5106	-565.1	-8.04E-03	69.1	93.4	10	14.8	51.5	76.9	28.2
5107	-573	-7.84E-03	34.9	104.6	20.7	20.6	214.9	214.8	22.4
5108	-602.3	-8.27E-03	37.9	114.7	13.6	15.9	141.4	165.8	24
5109	-653.2	-8.87E-03	38.73	117.9	10	13.3	103.8	138.8	24.3
51010	-613.5	-9.10E-03	45.1	126.9	21.3	21.7	221.5	225.8	23.7
51011	-648.6	-9.66E-03	49.4	139.6	14	16.9	145.7	175.7	25.5
51012	-711.7	-1.05E-02	51.3	145.3	10.1	14.1	105.2	146.3	25.9

APPENDIX B-PLOTS OF LTPP CASE STUDY RESULTS.

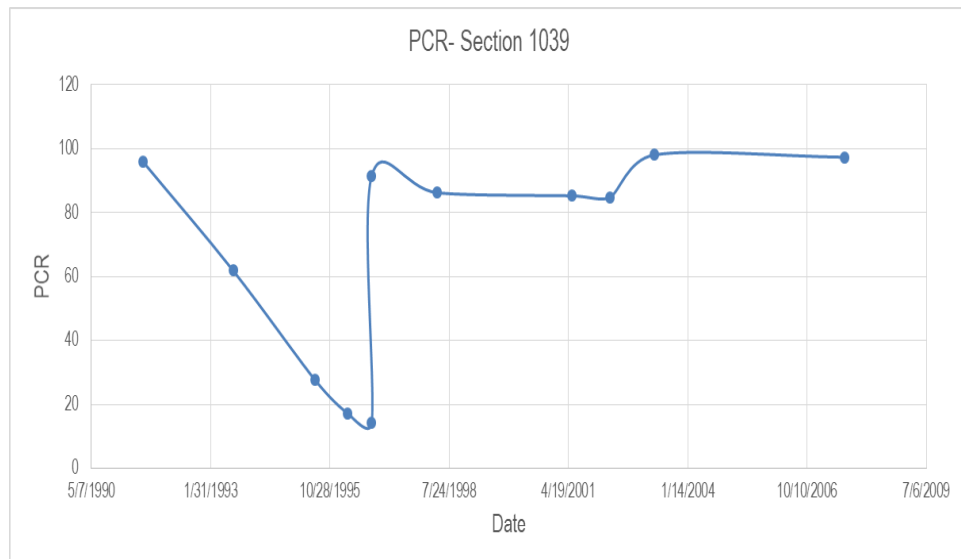


Figure B1 PCR Curve over Time of Section 1039.

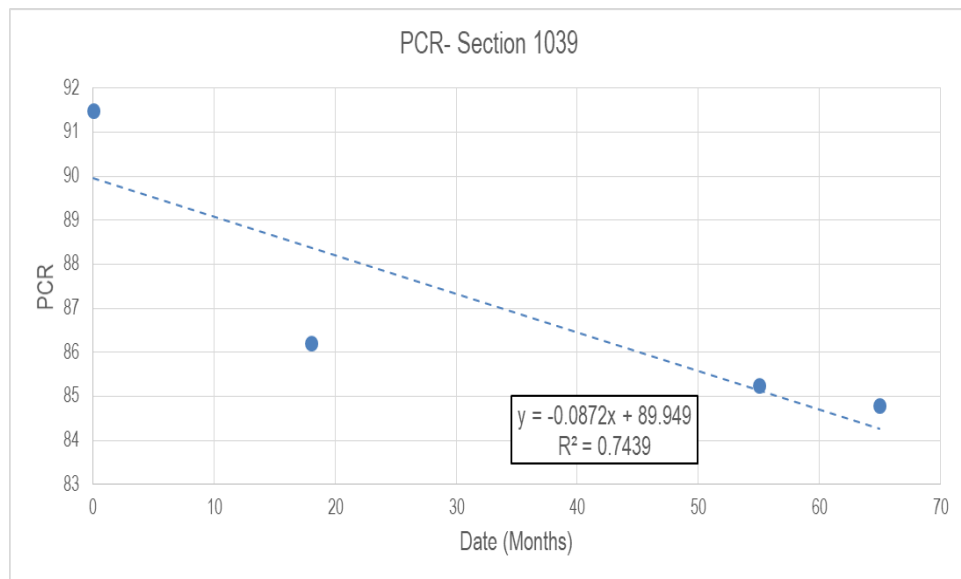


Figure B2 PCR Dropping Rate of Section 1039 after Overlay Construction.

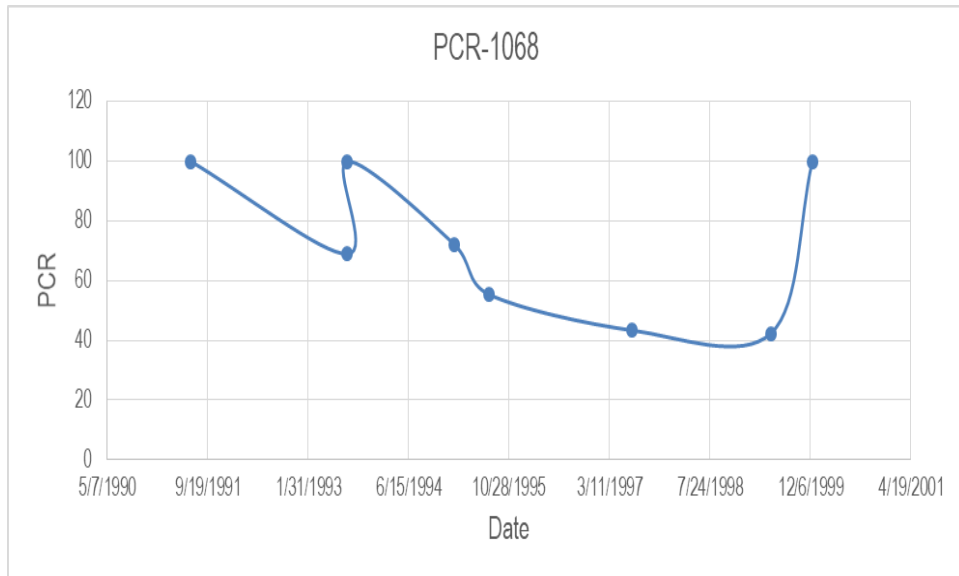


Figure B3 PCR Curve over Time of Section 1068.

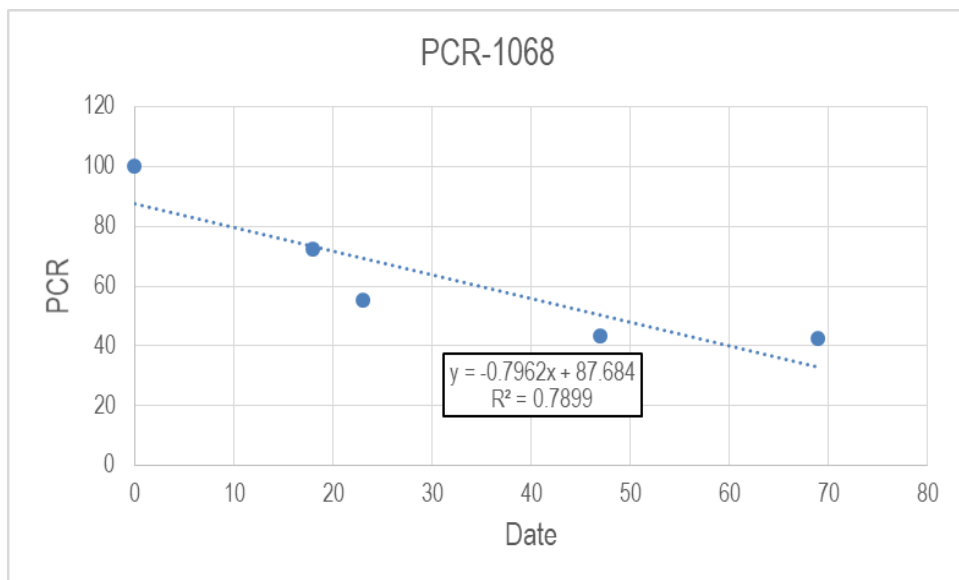


Figure B4 PCR Dropping Rate of Section 1068 after Overlay Construction.

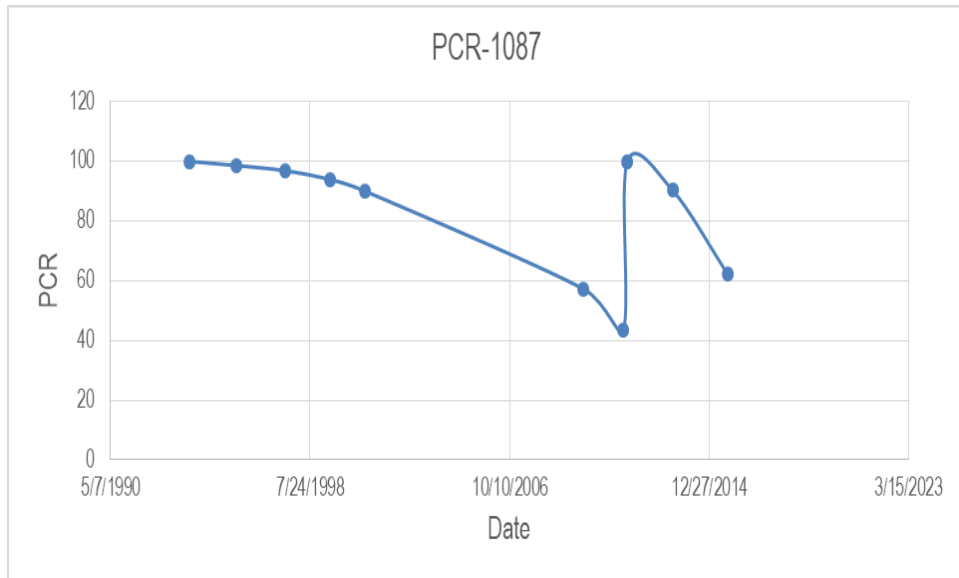


Figure B5 PCR Curve over Time of Section 1087.

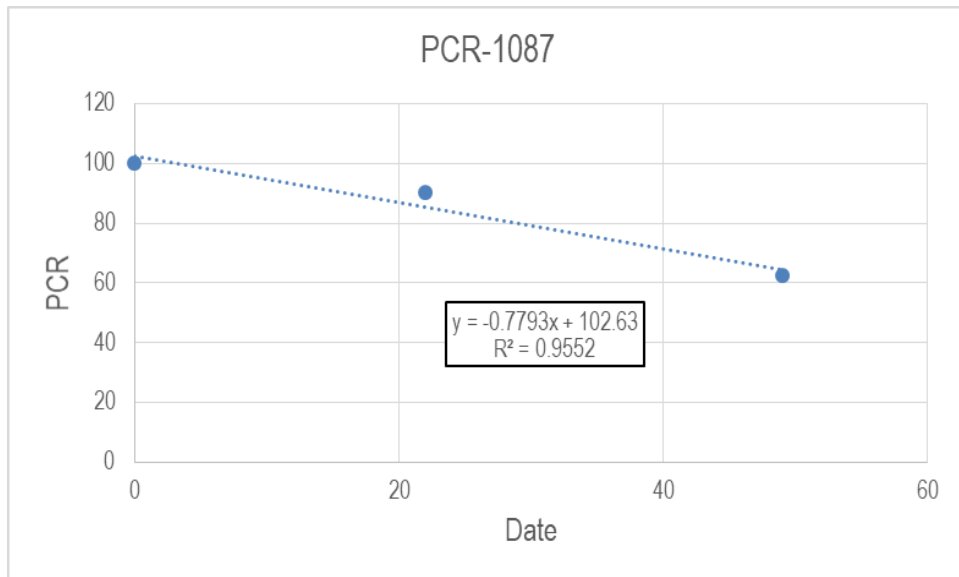


Figure B6 PCR Dropping Rate of Section 1087 after Overlay Construction.

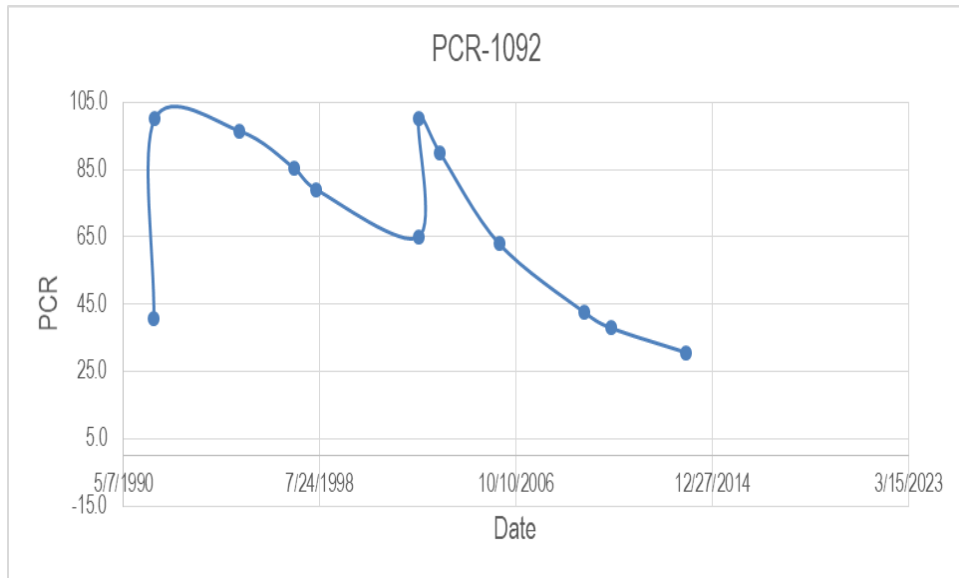


Figure B7 PCR Curve over Time of Section 1092.

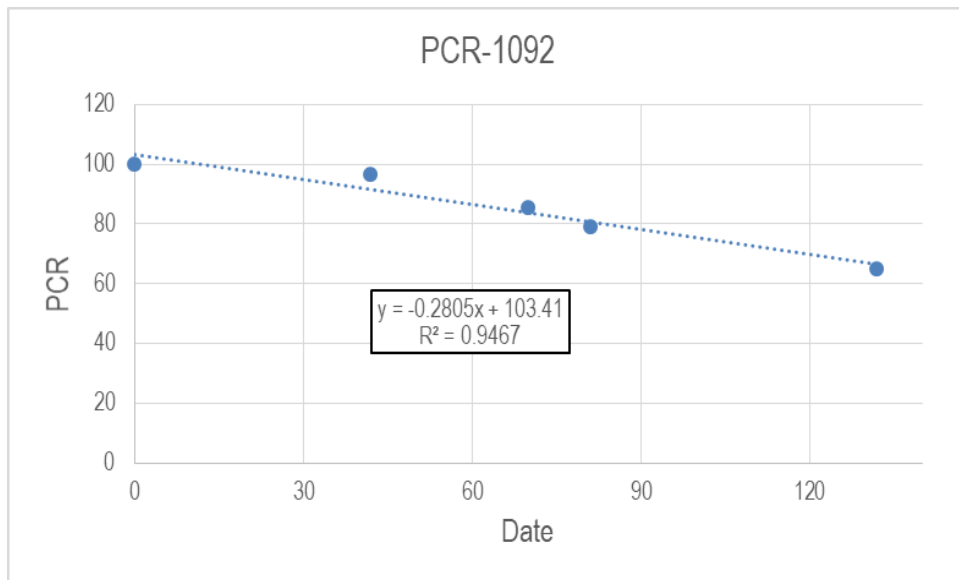


Figure B8 PCR Dropping Rate of Section 1092 after Overlay Construction.

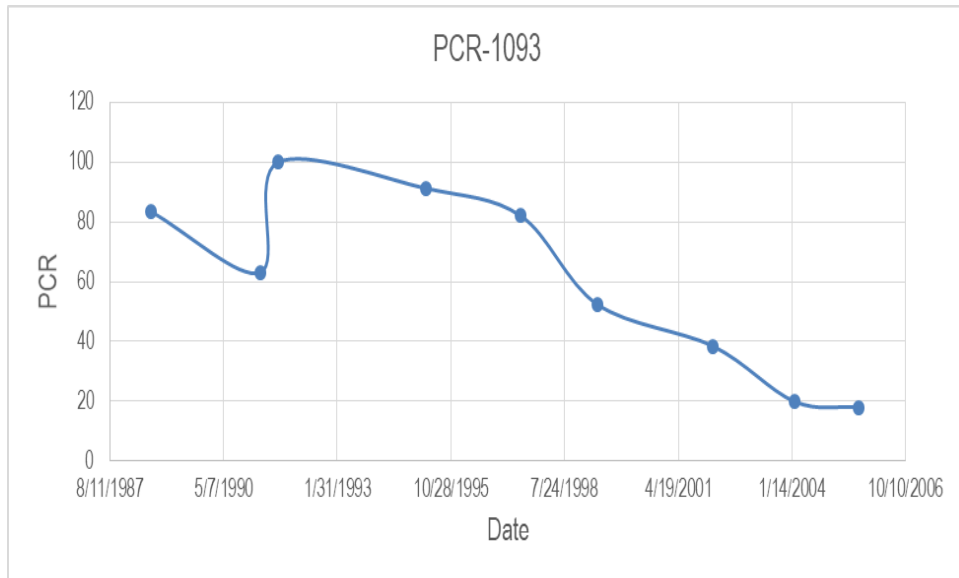


Figure B9 PCR Curve over Time of Section 1093.

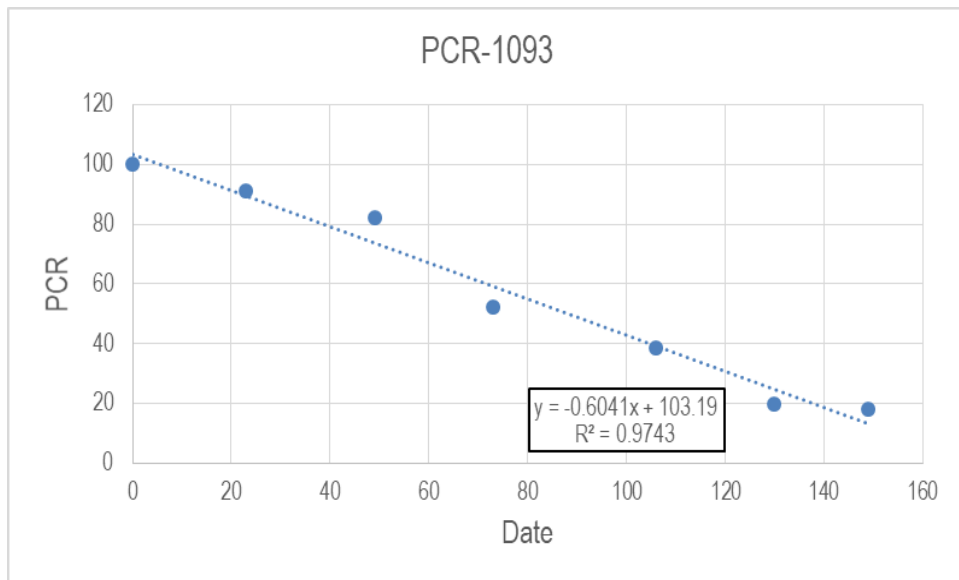


Figure B10 PCR Dropping Rate of Section 1093 after Overlay Construction.

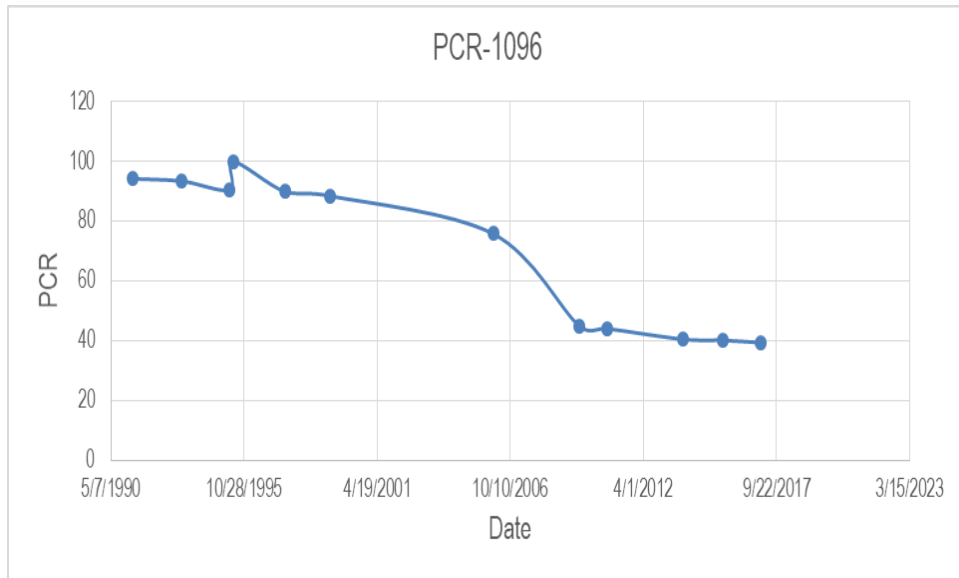


Figure B11 PCR Curve over Time of Section 1096.

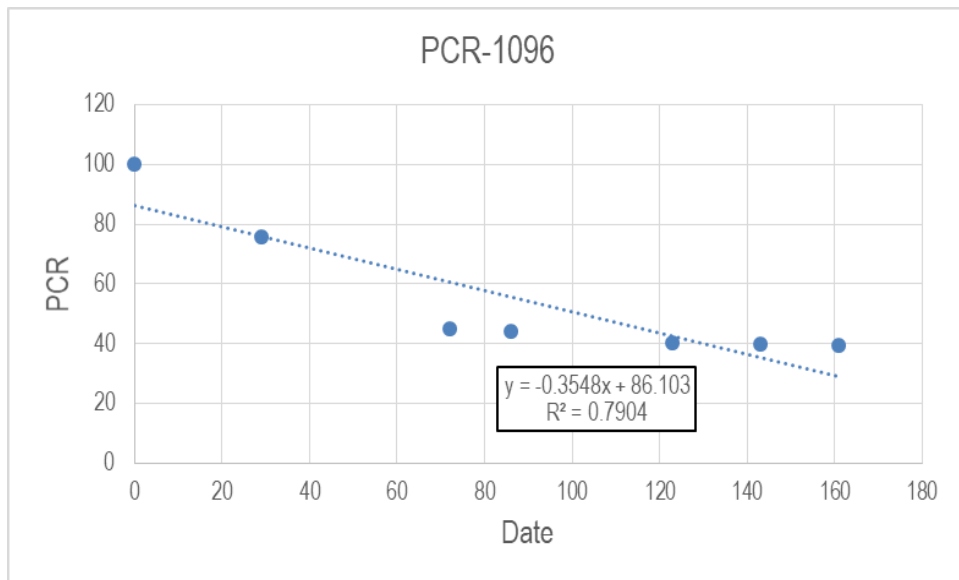


Figure B12 PCR Dropping Rate of Section 1096 after Overlay Construction.

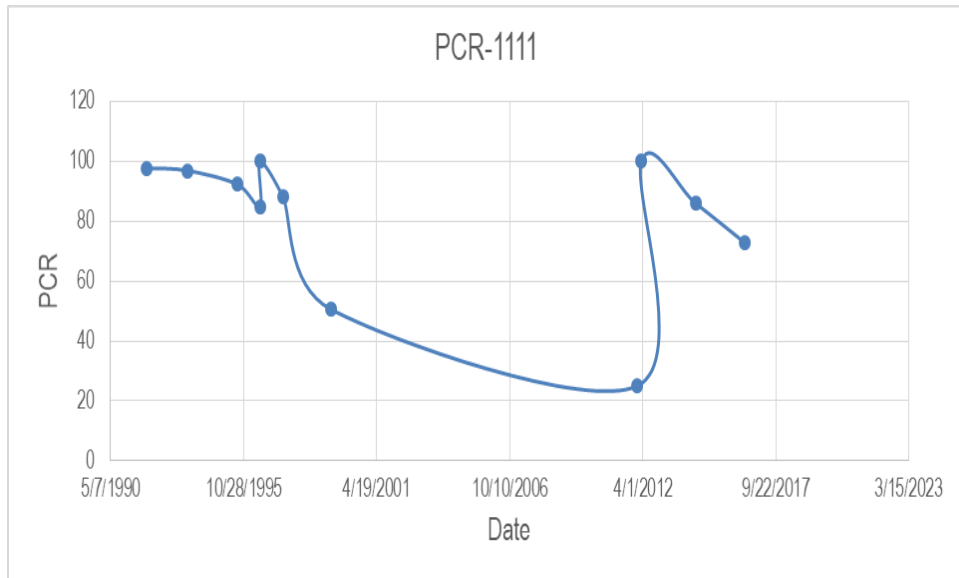


Figure B13 PCR Curve over Time of Section 1111.

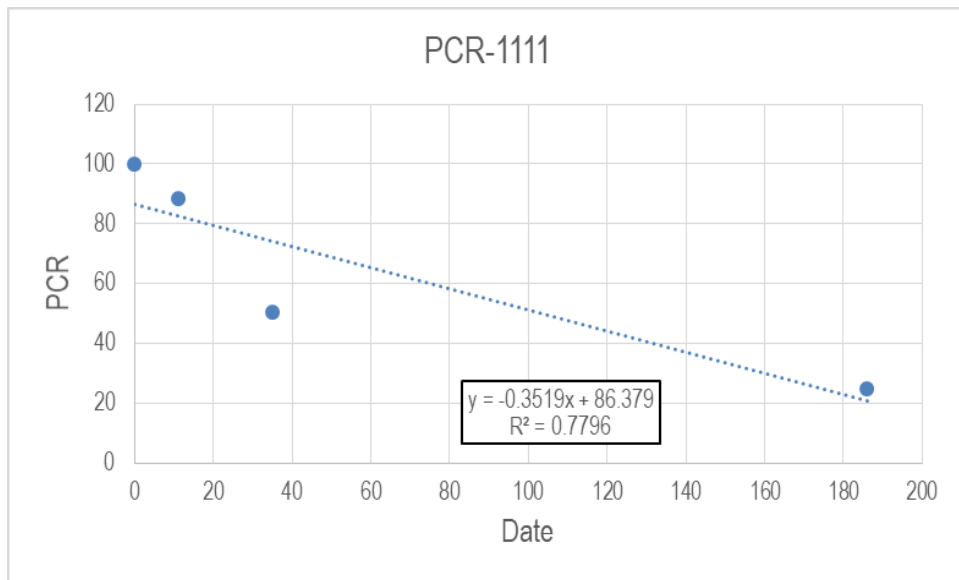


Figure B14 PCR Dropping Rate of Section 1111 after Overlay Construction.

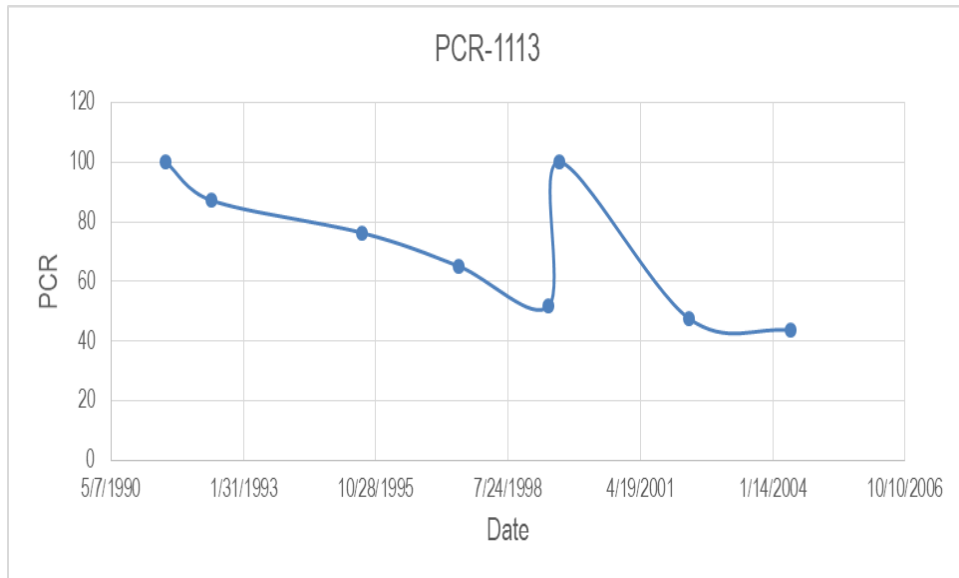


Figure B15 PCR Curve over Time of Section 1113.

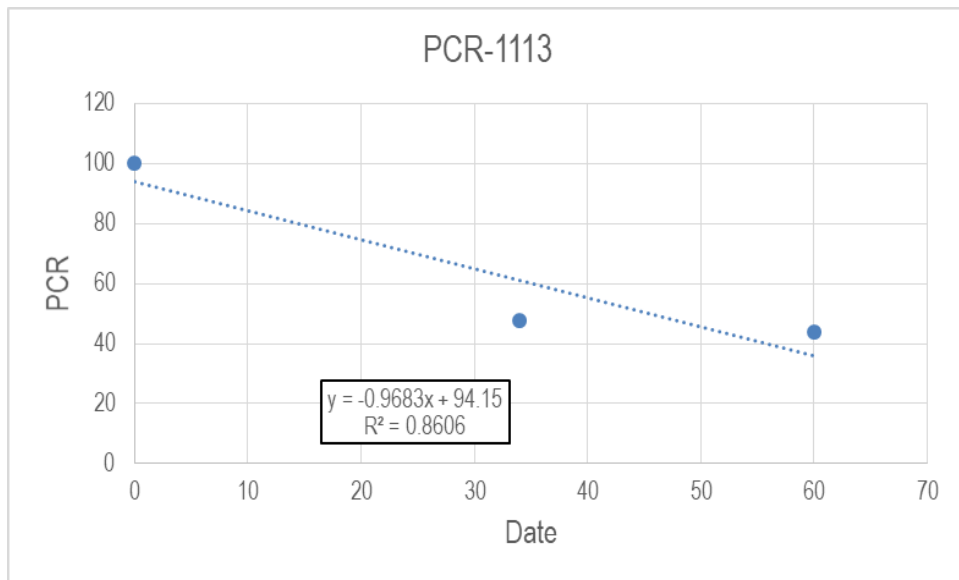


Figure B16 PCR Dropping Rate of Section 1113 after Overlay Construction.

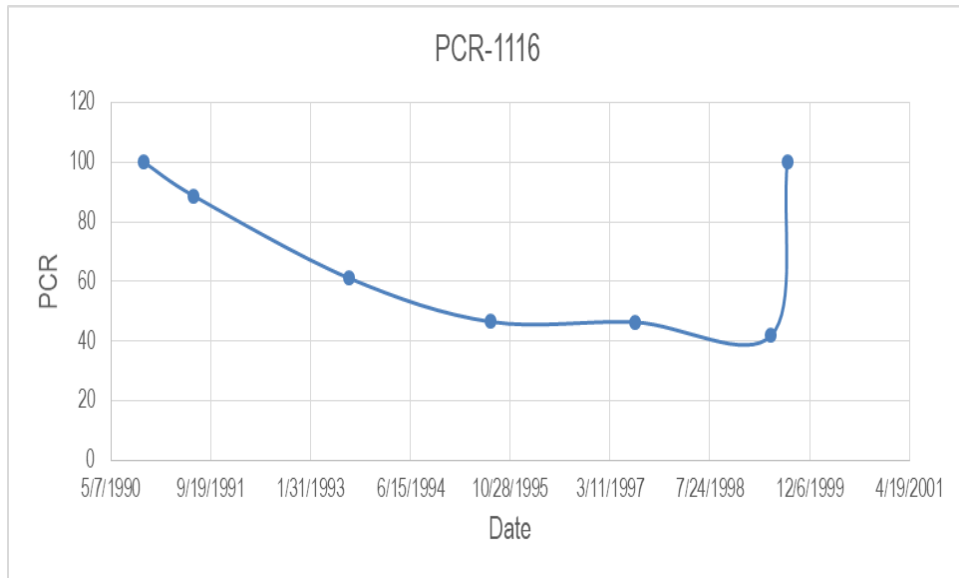


Figure B17 PCR Curve over Time of Section 1116.

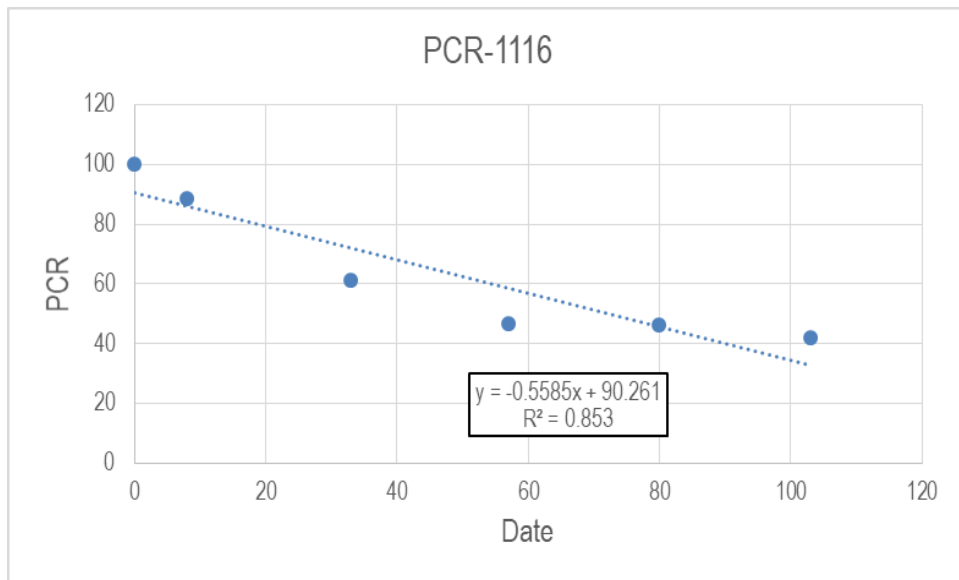


Figure B18 PCR Dropping Rate of Section 1116 after Overlay Construction.

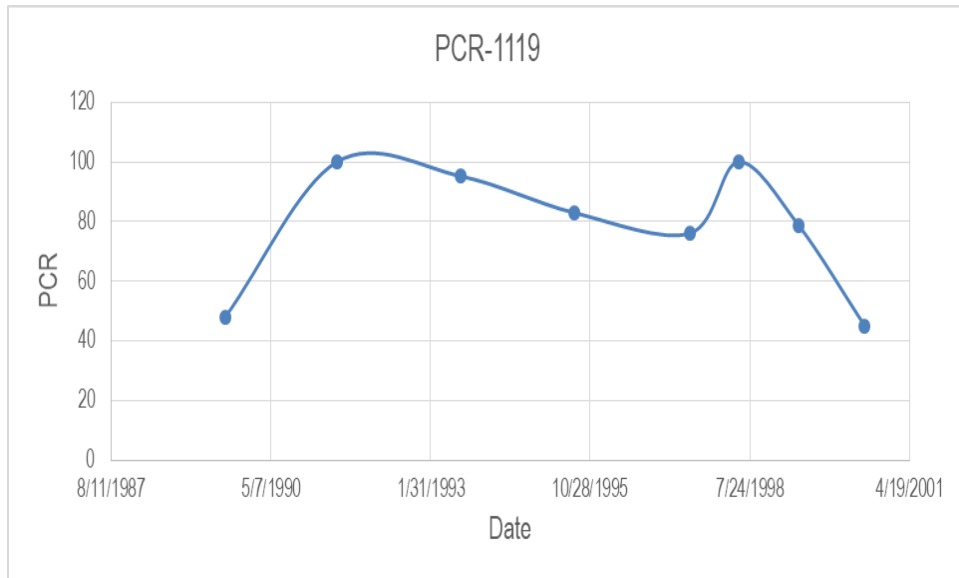


Figure B19 PCR Curve over Time of Section 1119.

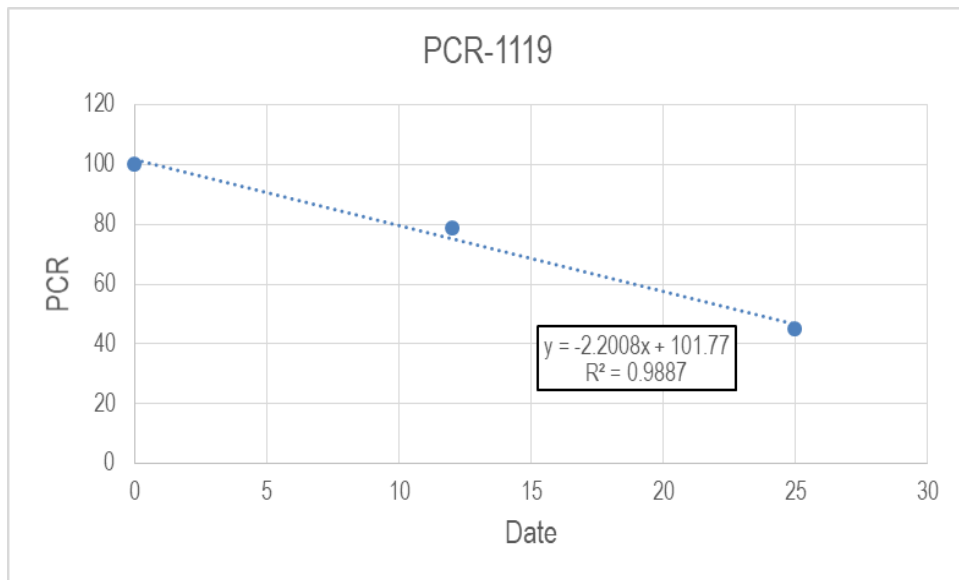


Figure B20 PCR Dropping Rate of Section 1119 after Overlay Construction.

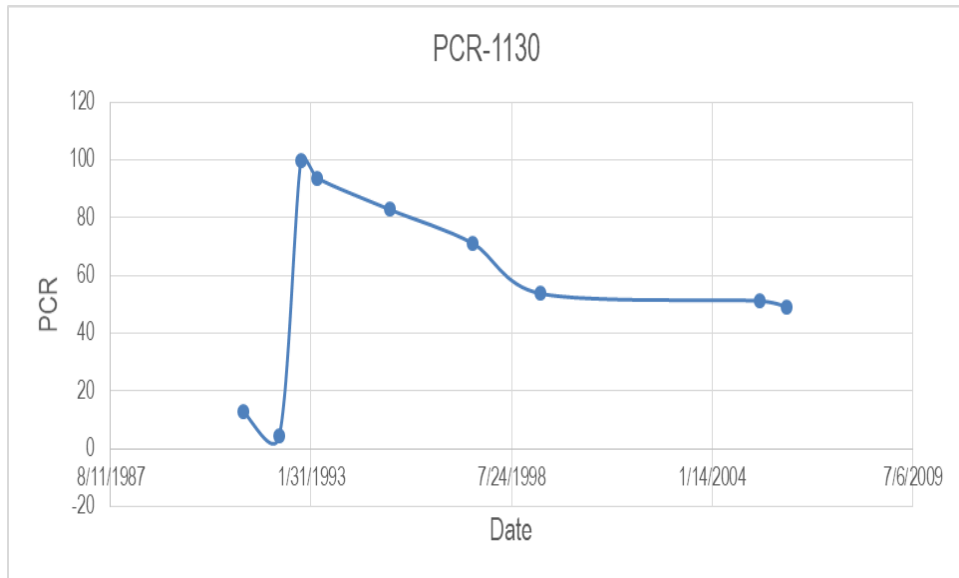


Figure B21 PCR Curve over Time of Section 1130.

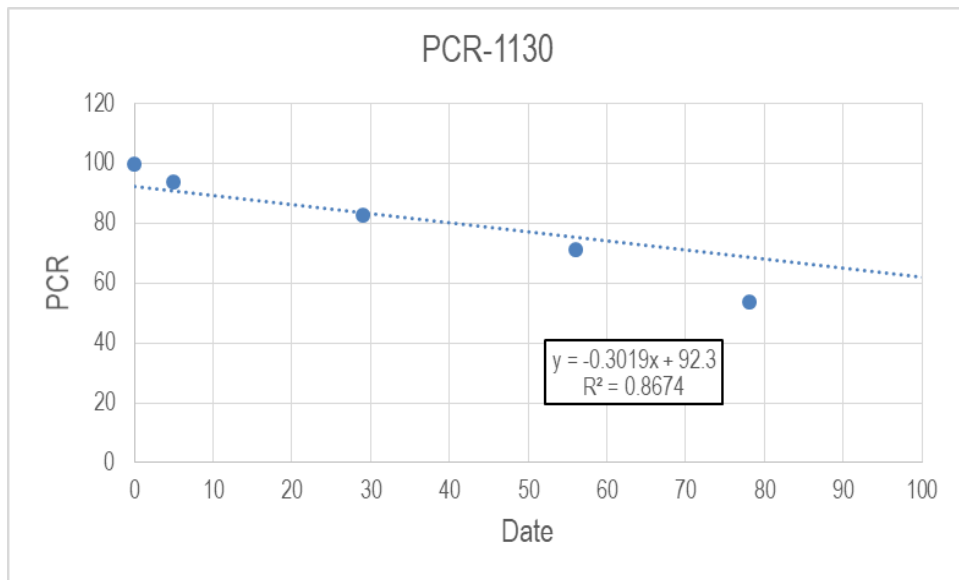


Figure B22 PCR Dropping Rate of Section 1130 after Overlay Construction.

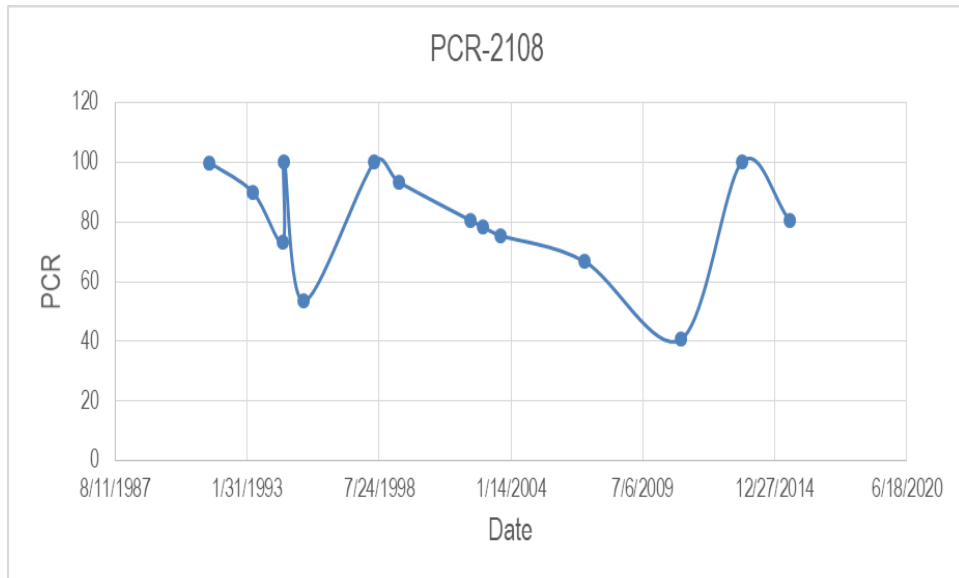


Figure B23 PCR Curve over Time of Section 2108.

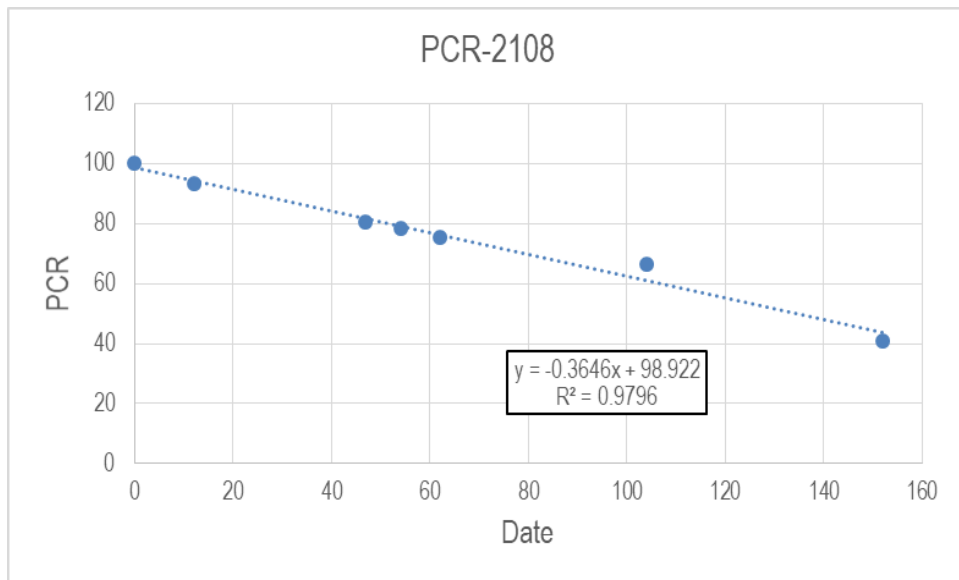


Figure B24 PCR Dropping Rate of Section 2108 after Overlay Construction.

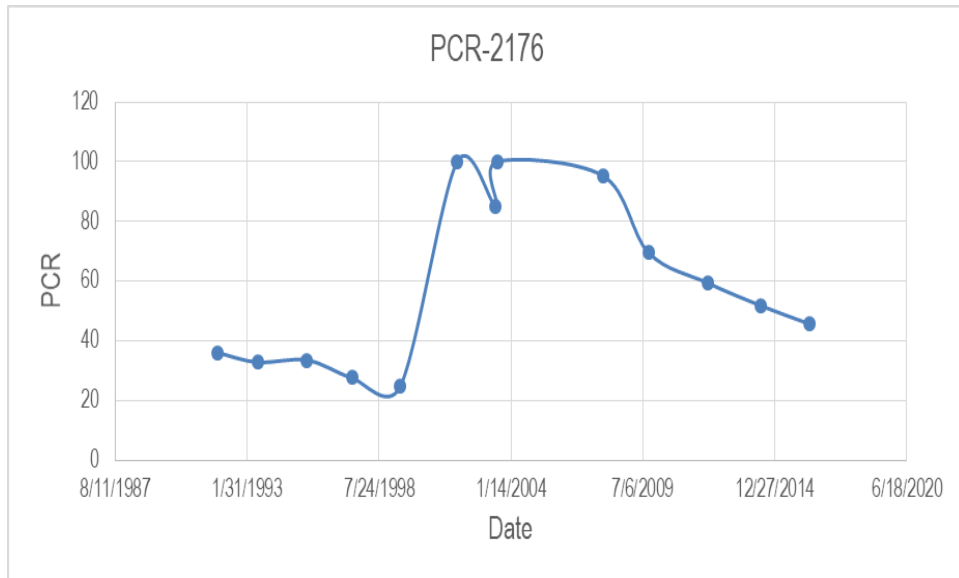


Figure B25 PCR Curve over Time of Section 2176.

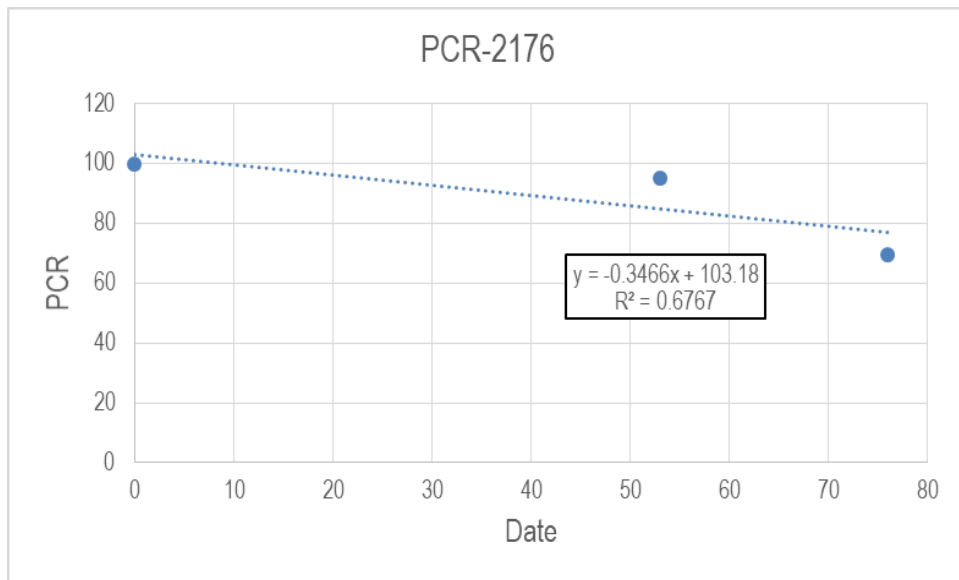


Figure B26 PCR Dropping Rate of Section 2176 after Overlay Construction.

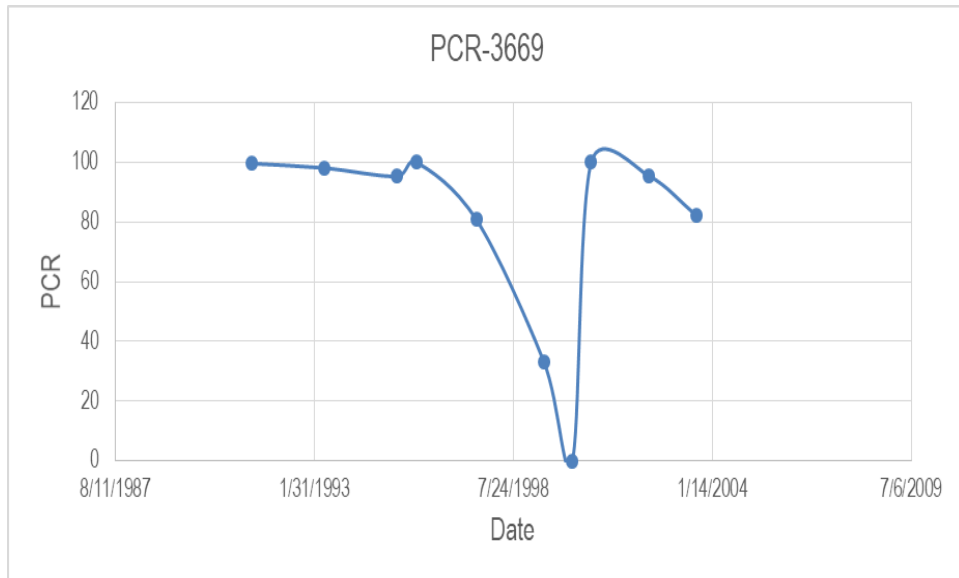


Figure B27 PCR Curve over Time of Section 3669.

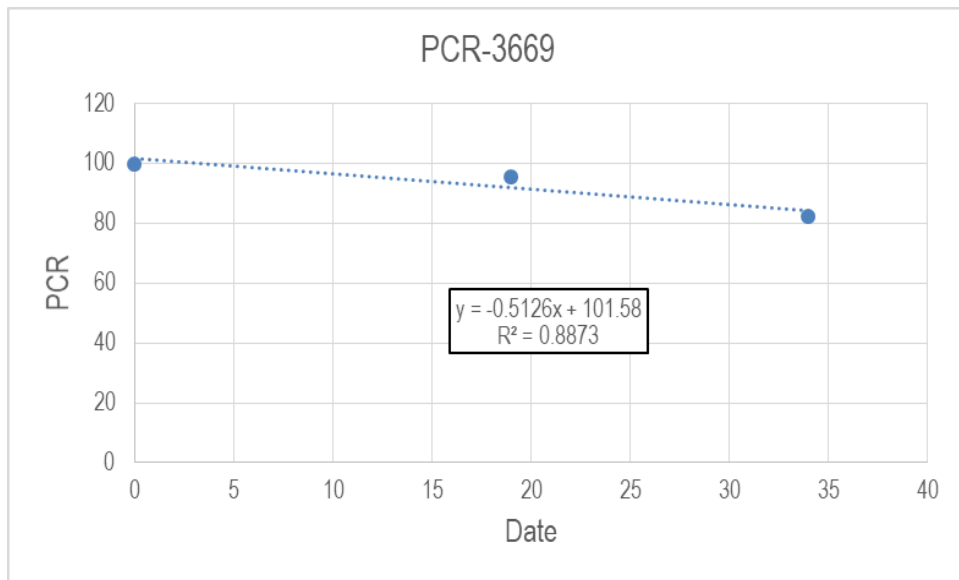


Figure B28 PCR Dropping Rate of Section 3669 after Overlay Construction.

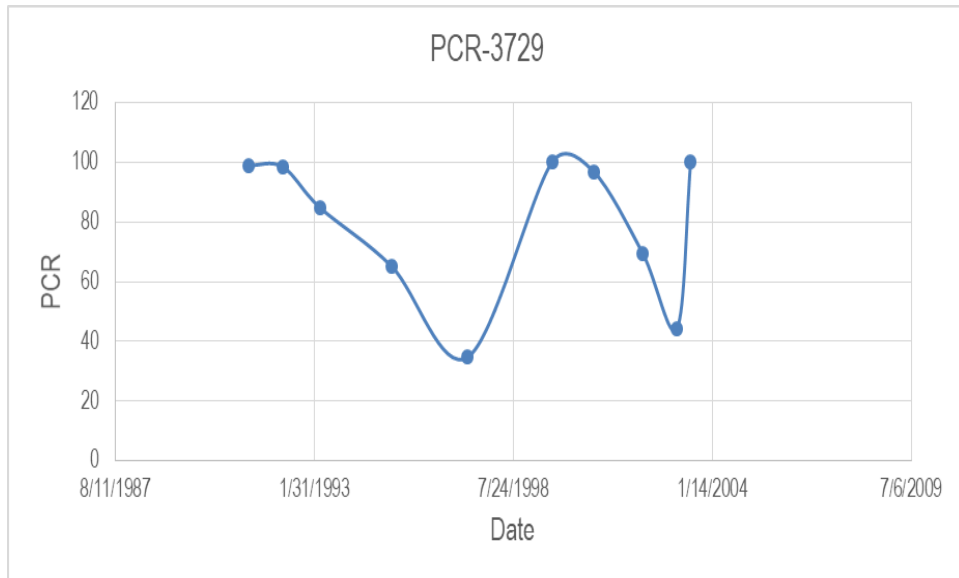


Figure B29 PCR Curve over Time of Section 3729.

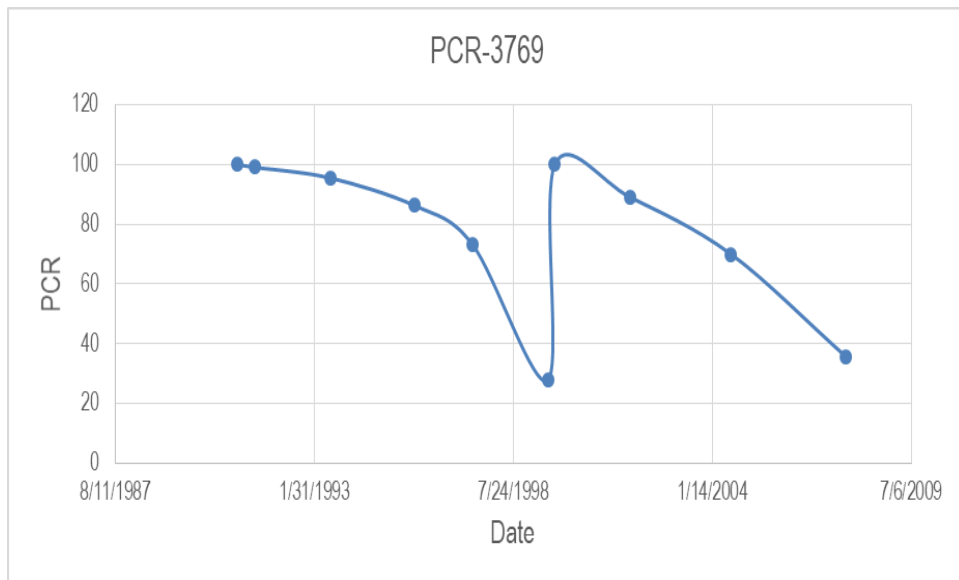


Figure B30 PCR Curve over Time of Section 3769.

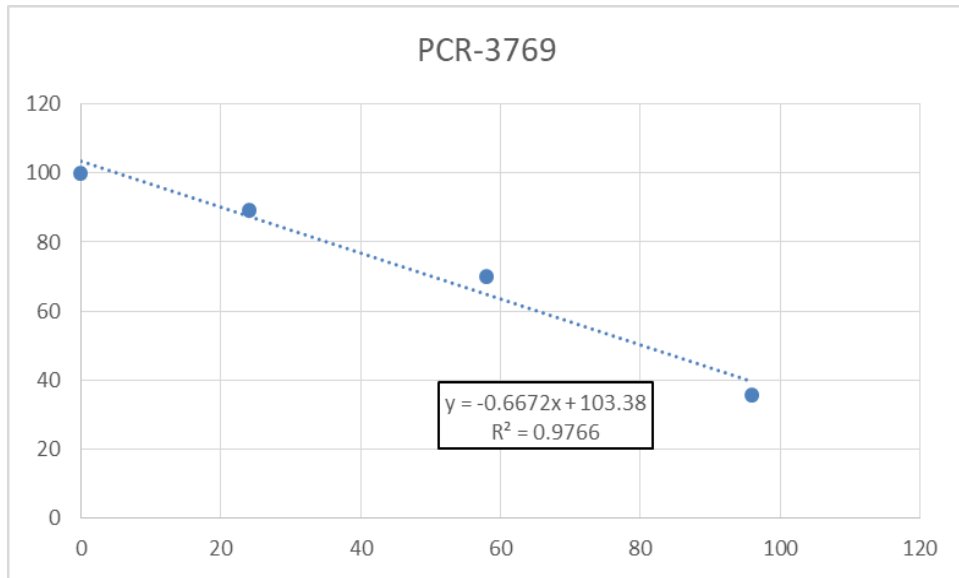


Figure B31 PCR Dropping Rate of Section 3769 after Overlay Construction.

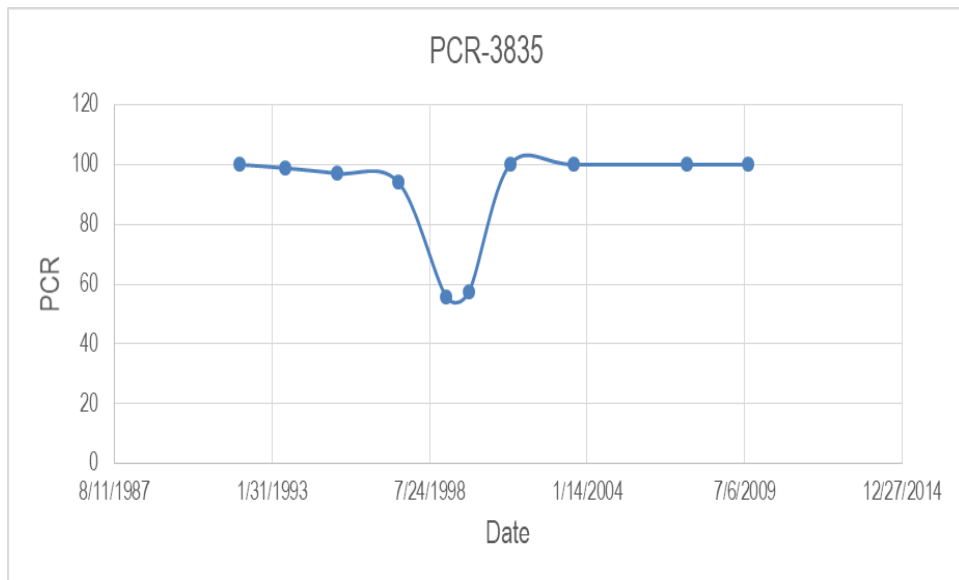


Figure B32 PCR Curve over Time of Section 3835.

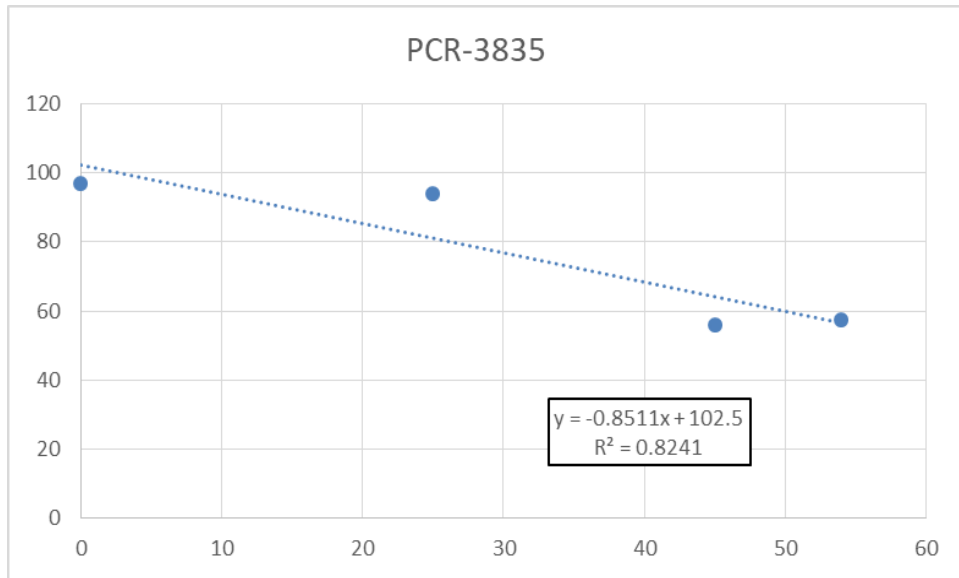


Figure B33 PCR Dropping Rate of Section 3835 after Overlay Construction.

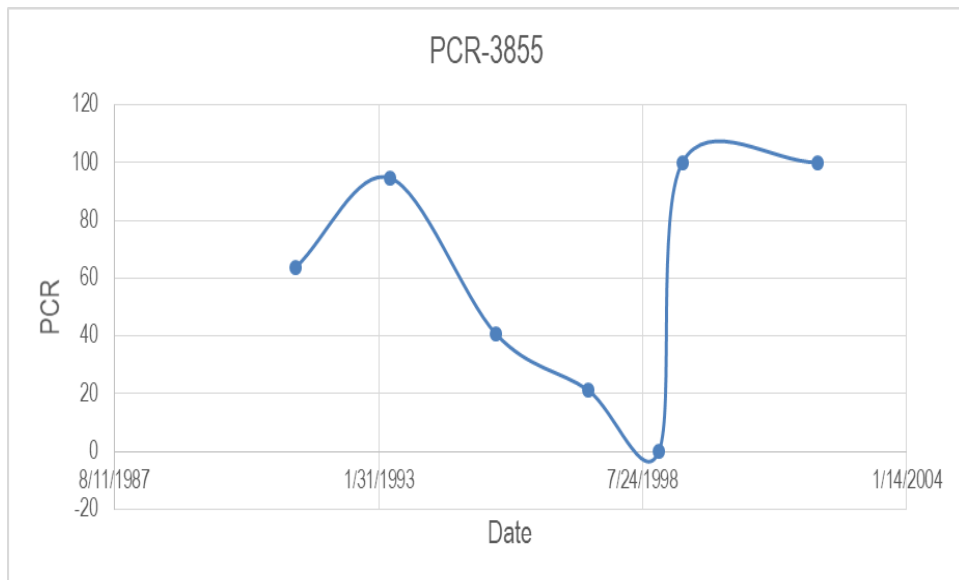


Figure B34 PCR Curve over Time of Section 3855.

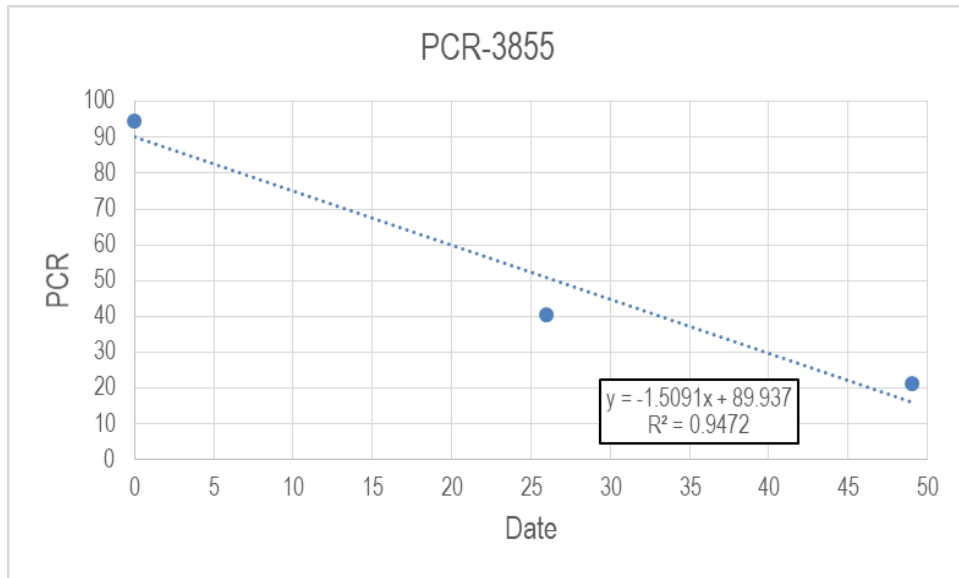


Figure B35 PCR Dropping Rate of Section 3855 after Overlay Treatment.

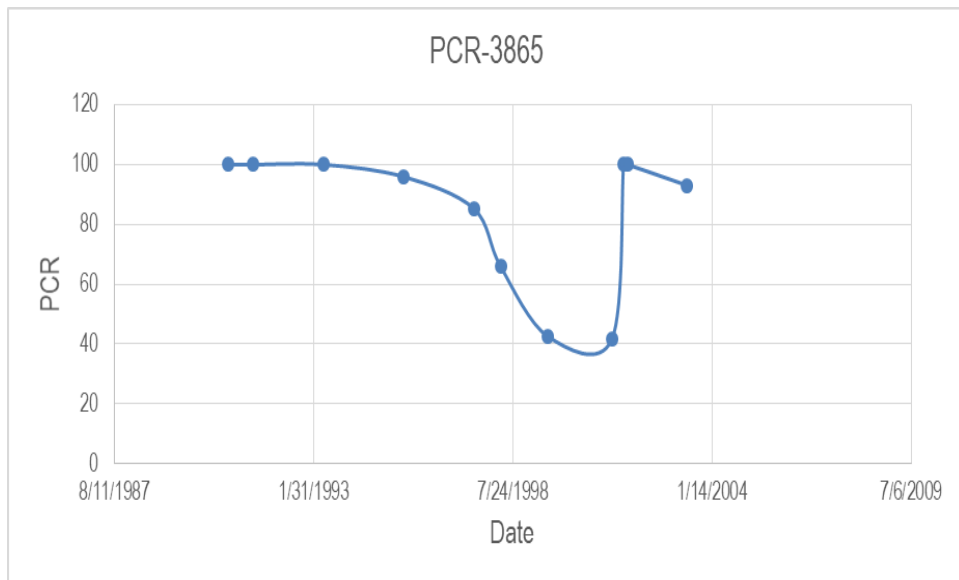


Figure B36 PCR Curve over Time of Section 3865.

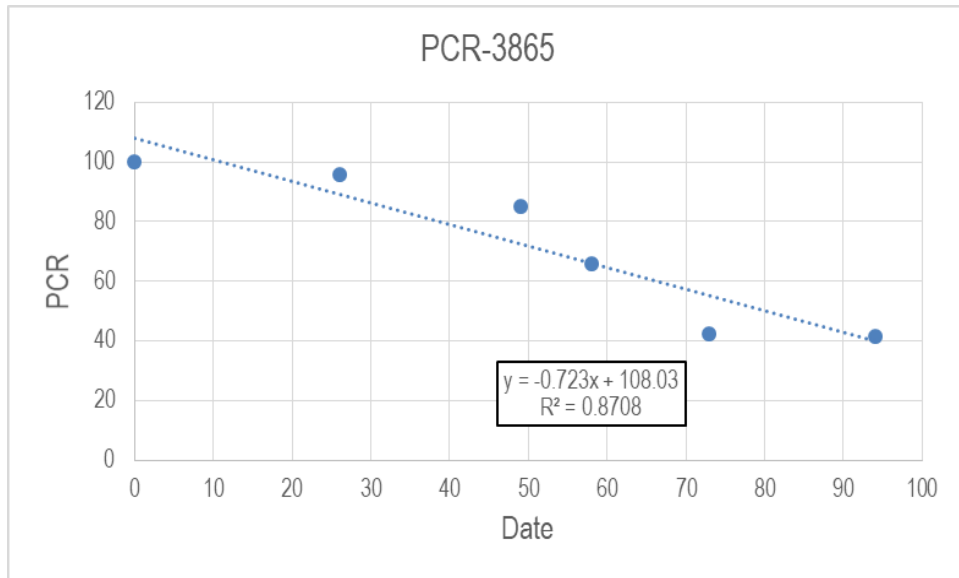


Figure B37 PCR Dropping Rate of Section 3865 after Overlay Construction.

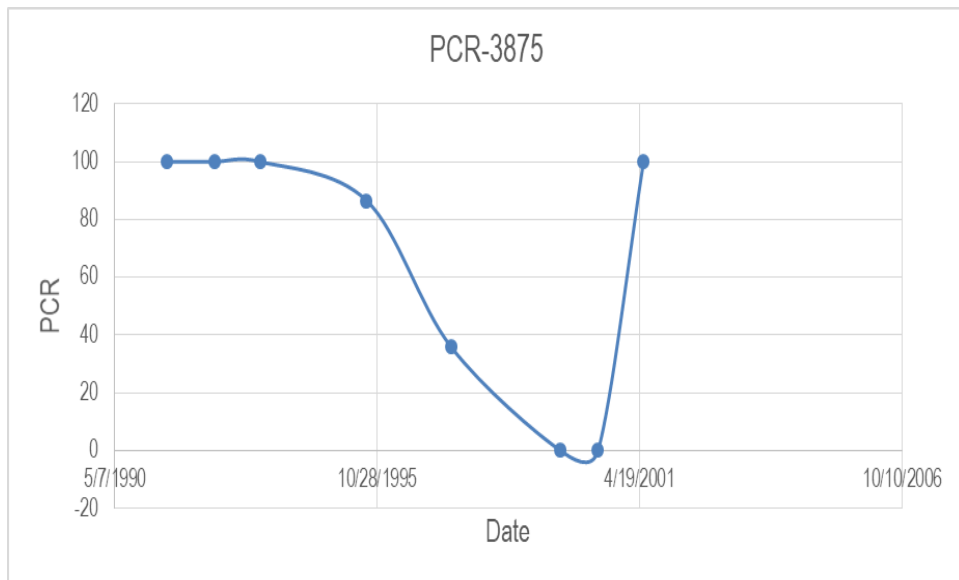


Figure B38 PCR Curve over Time of Section 3875.

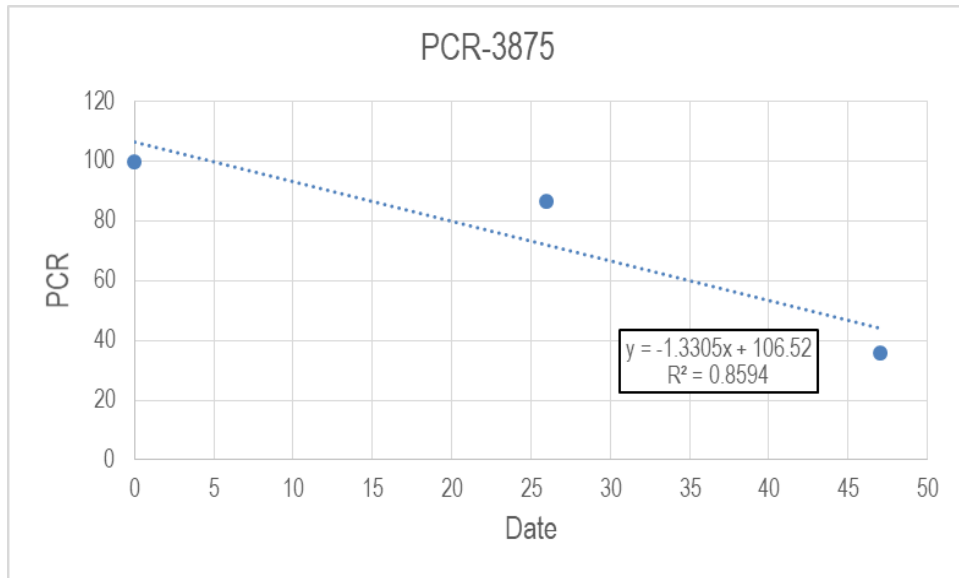


Figure B39 PCR Dropping Rate of Section 3875 after Overlay Construction.

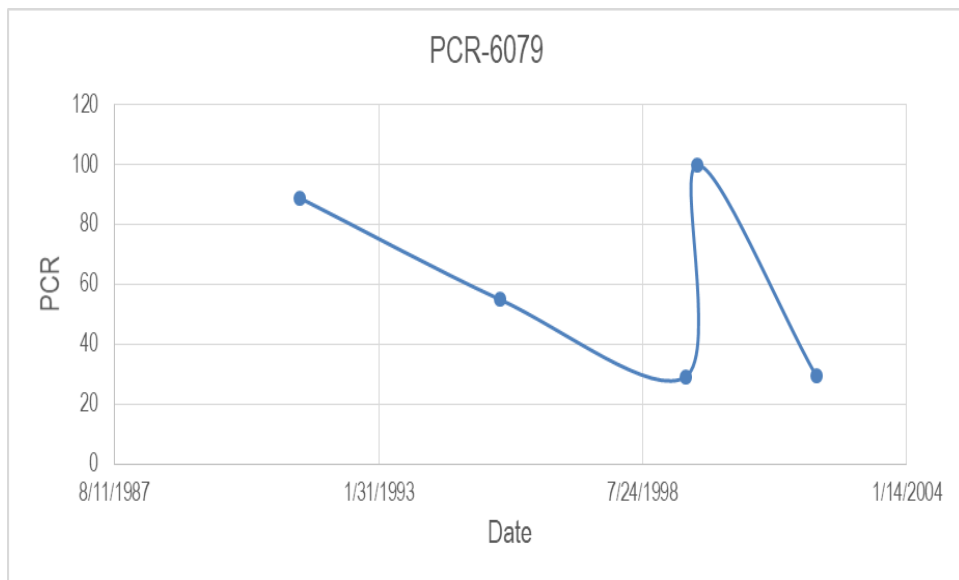


Figure B40 PCR Curve over Time of Section 6079.

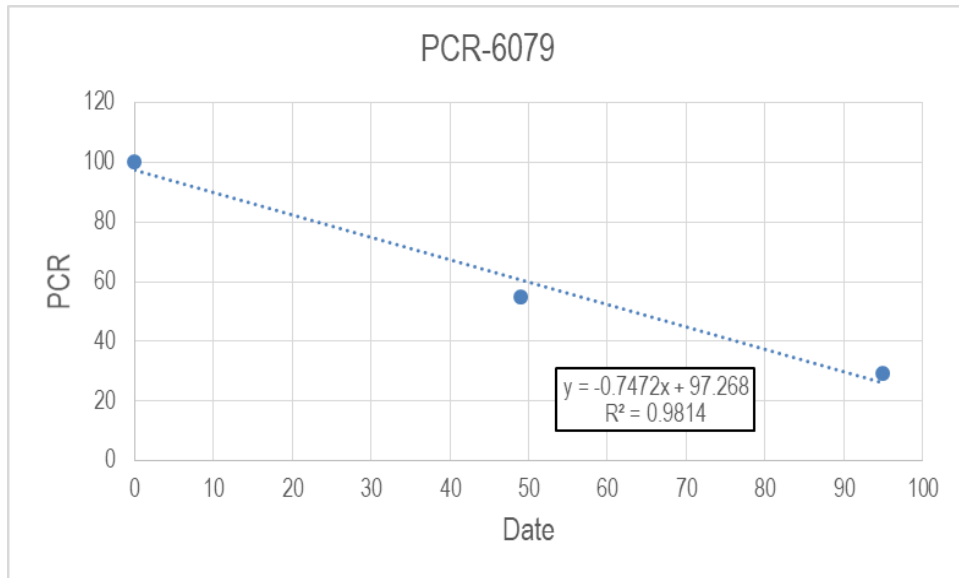


Figure B41 PCR Dropping Rate of Section 6079 after Overlay Construction.

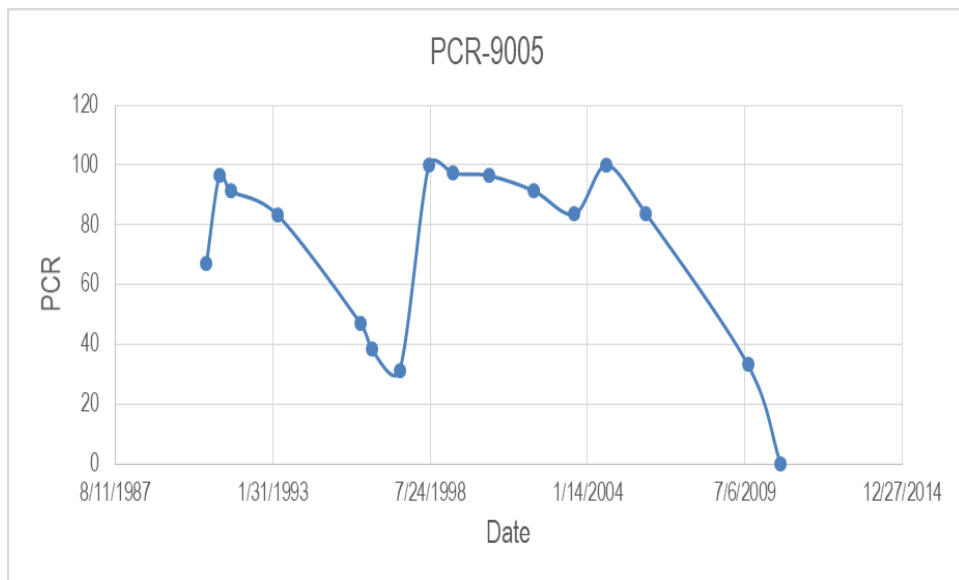


Figure B42 PCR Curve over Time of Section 9005.

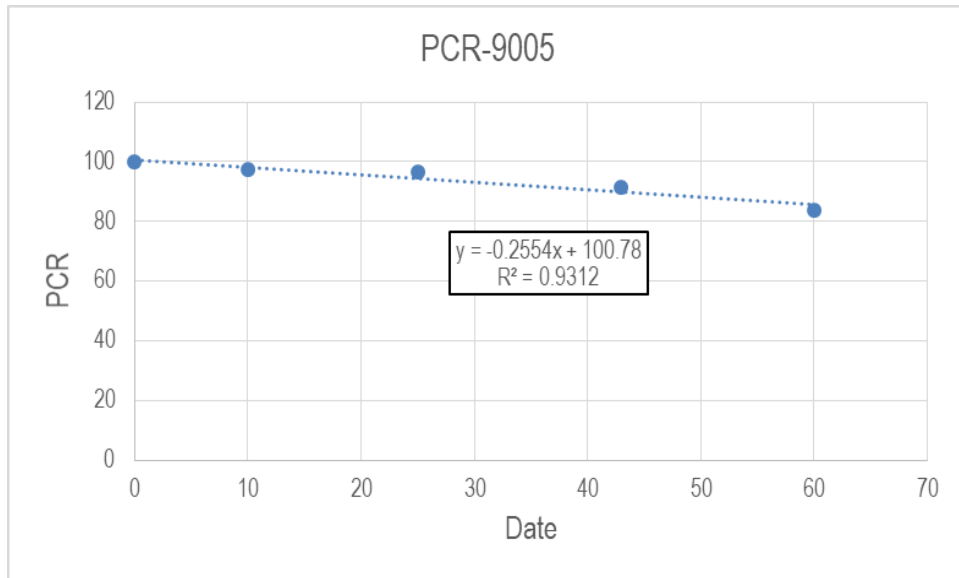


Figure B43 PCR Dropping Rate of Section 9005 after Overlay Construction.

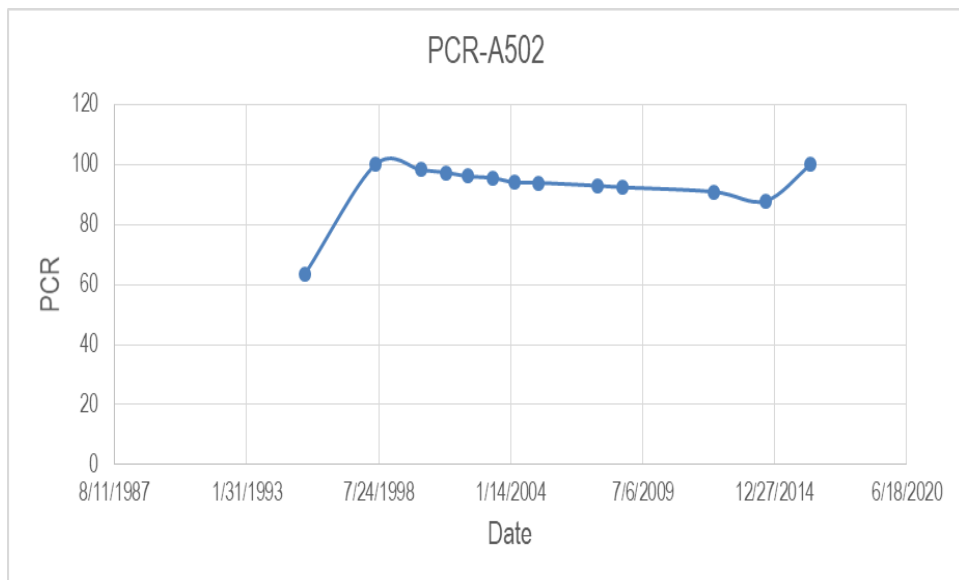


Figure B44 PCR Curve over Time of Section A502.

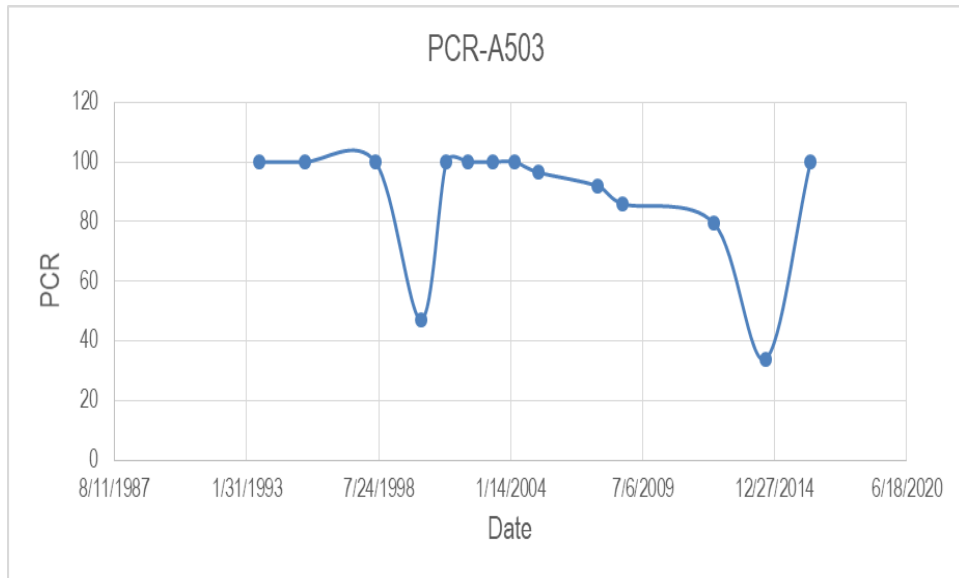


Figure B45 PCR Curve over Time of Section A503.

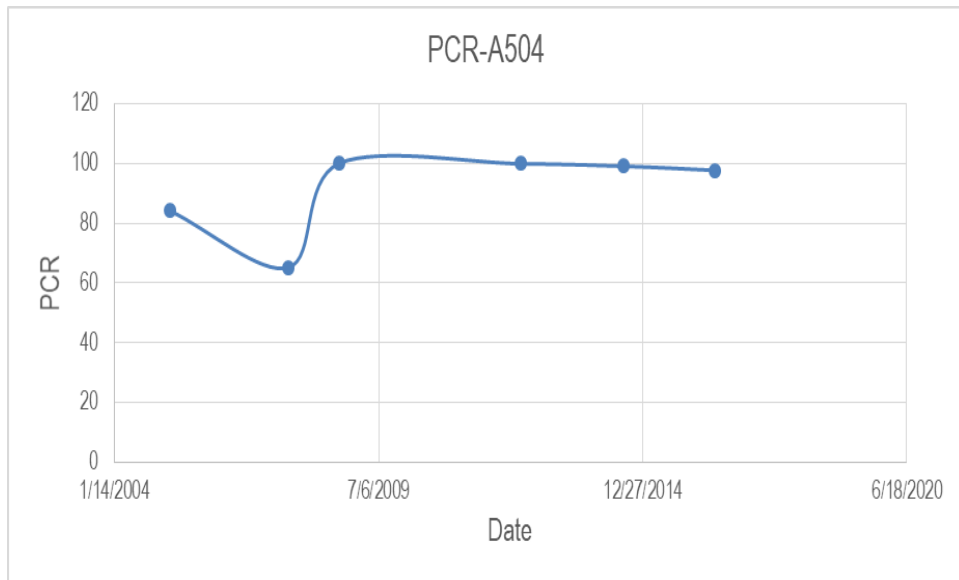


Figure B46 PCR Curve over Time of Section A504.

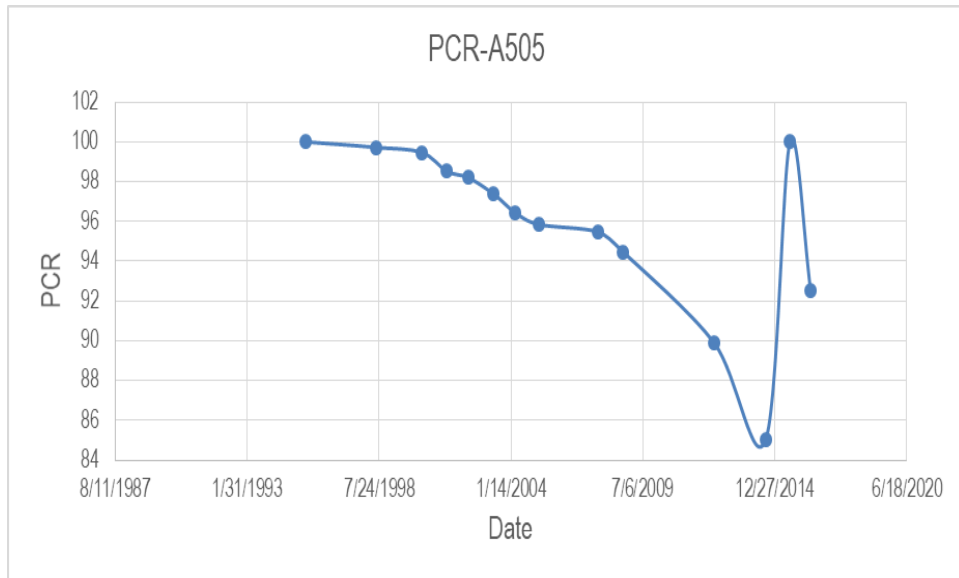


Figure B47 PCR Curve over Time of Section A505.

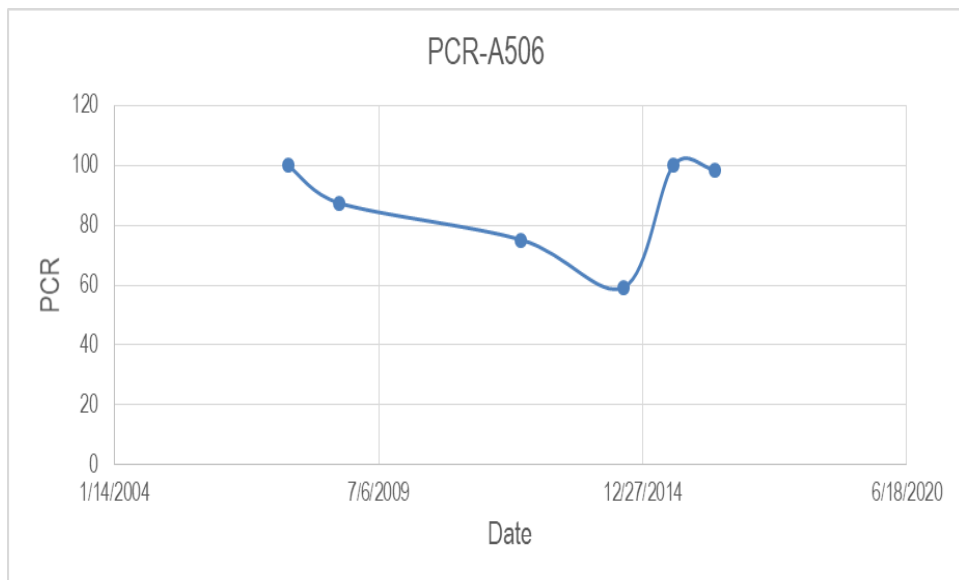


Figure B48 PCR Curve over Time of Section A506.

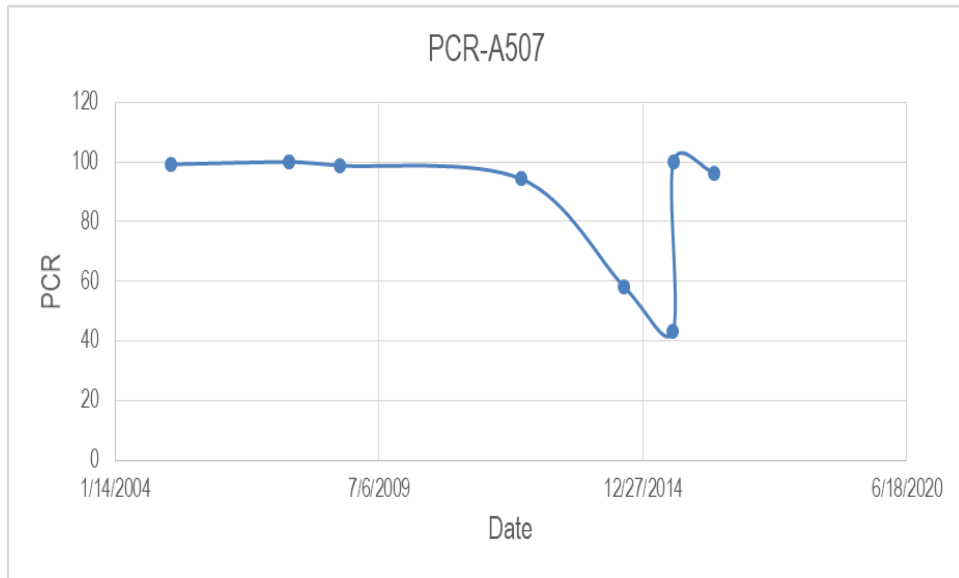


Figure B49 PCR Curve over Time of Section A507.

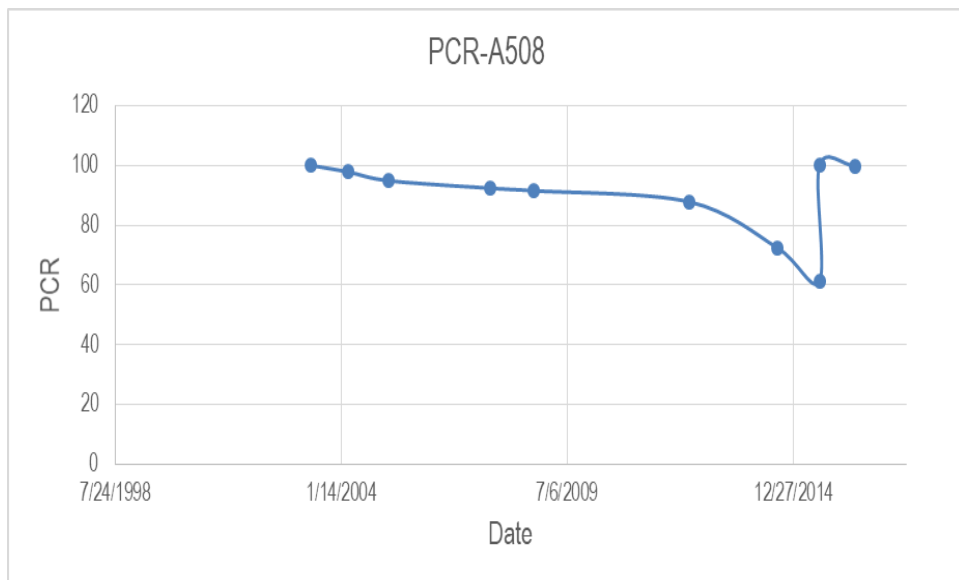


Figure B50 PCR Curve over Time of Section A508.

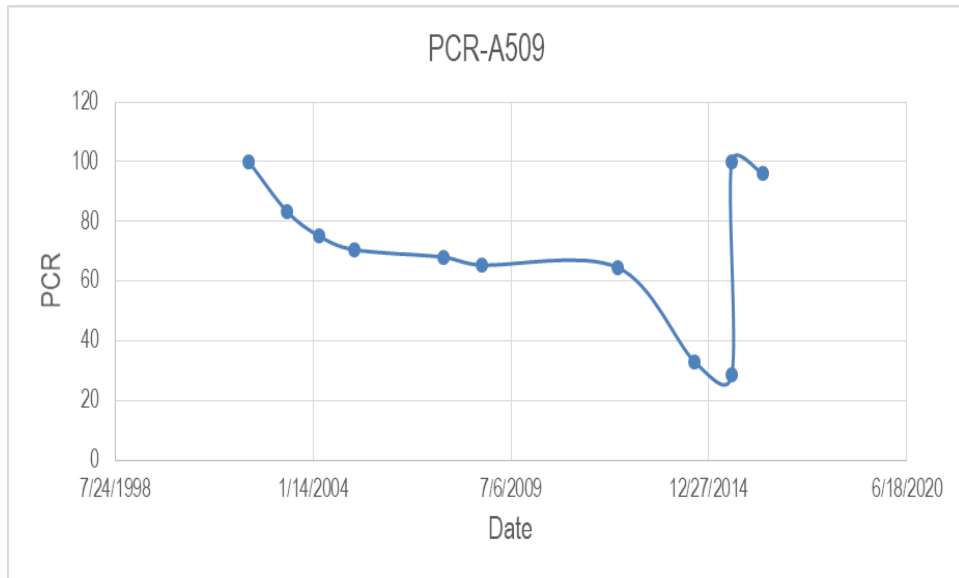


Figure B51 PCR Curve over Time of Section A509.

Vita

Cheng Zhu, was born in China. When he was studying in elementary school, he was curious about the construction works, such as buildings, roads, and tunnels, since his father is a construction engineer. In 2013, after finishing his study in China, he went to the graduate school of University of Nevada, Reno to do research in pavement engineering. His research was relevant to the rheological performance and aging mechanism of asphalt binder, including neat binder and several types of modified asphalt binder. After graduation, he decided to continue his study in a Ph.D. program in The University of Texas at El Paso. The main projects he has been involved included the Texas DOT project of evaluation of tack coat material by using laboratory testing, and a project of performance evaluation of the geocell in reinforcing subgrade. His desire career is to be a professional engineer in geotechnical and pavement engineering.

Permanent address: 2200 N Kansas St, Apt B
El Paso, Texas, 79902

This thesis/dissertation was typed by Cheng Zhu